

Exercise Dose Dependent Atrial Remodelling and Atrial Fibrillation

Simona Jakobov

A thesis submitted to the Faculty of Graduate Studies in Partial Fulfillment of the Requirements
for the Degree of Master of Science

Biology, York University, Toronto, Ontario

September 2020

© Simona Jakobov 2020

Abstract

The dependence of atrial fibrillation (AF) on exercise dose is U shaped. To assess the physiological basis for this relationship, we swam 3 groups of CD1 mice at variable daily durations (120, 180 and 240 minutes per day) while ensuring that all mice received similar amounts of total exercise. To do this, we measured O₂ consumption rates during swims and quantified exercise effort using volumes of O₂ consumed during swimming. Consistent with comparable total exercise effort, all 3 groups showed similar reductions in body weight and similar changes in most ventricular parameters, despite a trend towards lower heart rates with increased swim durations. AF vulnerability, atrial fibrosis, atrial hypertrophy, and P-wave duration were associated with exercise dose, and we suggest that increases in atrial pressure that occur with longer exercise durations promote this remodelling. Collectively, our data demonstrate that AF vulnerability and adverse atrial changes rise as exercise duration increases.

Acknowledgements

Foremost, I would like to thank my supervisor Dr. Peter Backx. His early recognition of my potential, and the limitless possibilities he has provided throughout my undergraduate and graduate studies. His patience, guidance and endless scientific knowledge were a major contribution to both my personal and professional development.

I would like to thank my wonderful committee members Dr. Robert Tsushima and Dr. Rolando Ceddia for their guidance and patience throughout my project.

I express my thanks to Dr. Robert Lakin for the continuous assistance, help with data analysis, willingness to teach me the surgical experiments, and conduction of the isolated atria experiments. This project would not have transpired without his work and dedication.

I am grateful to Nazari Polidovitch for the early assistance with the project, its development and execution. As well I would like to thank him for his expertise, guidance and willingness to teach me the techniques employed in this project.

I am thankful for the work of Ryan Debi, who has not only assisted me with the construction of the swimming tanks but also his expertise with the telemetric hemodynamic protocols.

I would like to thank my volunteers - Parashar Bhatt, Raghavan Vijayakumar, Eric Cerenzia, Jenna Baffa, Donovan Dev, Rushi Patel and Jin Shin for assistance with the swims. Many thanks to all the members of Dr. Back's lab for the support and the enjoyable experience they have created. Special thanks to Xiaodong Gao who has helped me with histology, immunohistochemistry and fluorescence measurements, as well as Michael Giggey for technical support and his engineering expertise.

I would like to acknowledge the continuous support of my friends and fellow graduate students - especially Nour Barazi. Her support and encouragement were enormous throughout my Master's Degree.

Finally, I would like to thank my family, parents and friends for their endless encouragement, inspiration, and personal support.

Copyright Acknowledgements

All Copyrights and Permissions for figures throughout the thesis were obtained through RightsLink® and the Copyright Clearance Center. All copyrights and permissions are available upon request.

Table of Contents

Abstract.....	ii
Acknowledgements	iii
Copyright Acknowledgements.....	iv
Table of Contents	v
List of Abbreviations	vii
List of Tables	ix
List of Figures.....	x
Chapter 1	1
1. Literature Review and Introduction.....	1
1.1 The electrophysiology of Atrial Conduction.....	3
1.2 The Electrophysiology of Atrial Fibrillation.....	8
1.3 Electrical, Cellular and Tissue Factors Predisposing to AF.....	14
1.4 Treatment of AF.....	24
1.5 Exercise, Cardiovascular Adaptations, and Atrial Fibrillation	26
1.6 Exercise Quantification in Humans.....	38
1.7 Exercise Quantification in Mice.....	44
1.8 Synopsis and Hypothesis.....	52
Chapter 2	53
2. Materials and Methods	53
2.1 Experimental Animals.....	53
2.2 Exercise Protocols and Exercise Quantification	53
2.3 Echocardiography.....	60

2.4	Surface ECGs in Anesthetized Mice	61
2.5	Intracardiac Measurements	62
2.6	Atrial Isolations and <i>Ex vivo</i> Electrophysiology	68
2.7	Heart Isolations and Histology	72
2.8	Telemetric Hemodynamics	76
2.9	Statistical Analysis	76
Chapter 3		78
3. Exercise Dose Dependent Atrial Remodelling and Atrial Fibrillation		78
3.1	Abstract	79
3.2	Introduction	80
3.3	Methods	82
3.4	Results	82
3.5	Discussion	99
3.6	Supplementary Figures.....	107
4. References.....		110
Appendices.....		123
5.1 Appendix A – Oxygen Consumption Quantification		123
5.2 Appendix B - The Integral Method, Theoretical Means of Calculating Oxygen Consumption		144

List of Abbreviations

(a-v)O₂D	Arteriovenous O ₂ Difference
Ach	Acetylcholine
AERP	Atrial Effective Refractory Period
AF	Atrial Fibrillation
ANP	Atrial Natriuretic Peptide
AP	Action Potential
APD	Action Potential Duration
BMR	Basal Metabolic Rate
BW	Body Weight
CICR	Calcium Induced Calcium Release
CO	Cardiac Output
CRF	Cardiorespiratory Fitness
CRP	C-reactive Protein
CSEP	Canadian Society for Exercise Physiology
CV	Conduction Velocity
CVD	Cardiovascular Disease
Cx40	Connexin 40
Cx43	Connexin 43
DADs	Delayed Afterdepolarizations
EADs	Early Afterdepolarizations
ECG	Electrocardiogram
ECM	Extracellular Matrix
EF	Ejection Fraction
ERP	Effective Refractory Period
FFM	Fat Free Mass
FS	Fractional Shortening
GP	Ganglionated Plexi
HR	Heart Rate

HRV	Heart Rate Variability
IL	Interleukin
LA	Left Atrium
LVDD	Left Ventricular End Diastolic Diameter
LVEDP	Left Ventricular End Diastolic Pressure
LVSP	Left Ventricular End Systolic Diameter
MET	Metabolic Equivalent
MMPs	Matrix Metalloproteinases
PA	Physical Activity
PMCA	Sarcolemmal/ plasma membrane Calcium ATPase
PNA	Parasympathetic Nerve Activity
RA	Right Atrium
RER	Respiratory Exchange Ratio
RMR	Resting Metabolic Rate
RP	Refractory Period
RYR	Ryanodine Receptor
SA node	Sinoatrial node
SAC	Stretch Activated Channel
SERCA	Sarco/endoplasmic reticulum Calcium ATPase
SNS	Sympathetic Nervous System
SR	Sarcoplasmic Reticulum
SV	Stroke Volume
TGFβ	Transforming Growth Factor Beta
TNFα	Tumor Necrosis Factor Alpha
VCO₂	Carbon Dioxide Production Rate
VF	Ventricular Fibrillation
V_{O₂}	Oxygen Consumption
V_{O₂ max}	Maximal Oxygen Consumption
WHO	World Health Organization

List of Tables

Table 2-1. Training Regimes of Mice Undergoing Three Different Swim Bout Duration Exercise Protocols	57
Table 3-1. Aerobic and Exercise Induced Physiological Adaptations in Exercising Mice	87
Table 3-2. Atrial Adaptations in Mice Swimming at Different Swim Doses	94
Table 3-3. Time-Dependent Hemodynamic Changes in Pressure Telemetry-Implanted Mice During an Acute Bout of Swim Exercise.....	98

List of Figures

Figure 1-1. U Shaped Curve of Exercise.	2
Figure 1-2. Ionic Currents in the Human Atrial Action Potential.....	6
Figure 1-3. Autonomic Regulation of the Ionic Channels in Cardiomyocytes.....	7
Figure 1-4. Mechanisms of Atrial Fibrillation.....	12
Figure 1-5. Reentry Mechanisms.....	13
Figure 1-6. Exercise Classification.....	30
Figure 1-7. The Consequences of Atrial Stretch.....	34
Figure 1-8. The Thermoneutral Zone of Mice and their Body Temperature.....	51
Figure 2-1. Mouse Swimming Exercise Apparatus and a Modified Oxygen Consumption Apparatus.....	54
Figure 2-2. Modified Oxymax Setup.....	58
Figure 2-3. Schematic Representation of Exercise Protocols.....	58
Figure 2-4. Typical Recording During VO_2 max Testing.....	59
Figure 2-5. Intracardiac 2F EP Catheter Placement in the Heart.....	64
Figure 2-6. Atrial Effective Refractory Period (AERP) Identification during Intracardiac Procedures.....	66
Figure 2-7. Atrial Arrhythmias Detection Using an Intracardiac 2F EP Catheter.....	67
Figure 2-8. Typical Setup for Isolated Atria Ex vivo Studies.....	72
Figure 2-9. Fibrosis Quantification using the Threshold Method.....	75
Figure 3-1. Self Regulation Behaviour During Swim.....	83
Figure 3-2. Exercise Quantification using Oxygen Consumption.....	85
Figure 3-3. Exercise Adaptations in Exercising Mice Relative to Control Mice.....	90
Figure 3-4. Atrial Fibrillation Inducibility in Response to Different Exercise Regimes.....	92
Figure 3-5. Atrial Fibrosis Increases with Swim Dose.....	96
Figure 3-6. Pressure and Heart Rate Changes with Swim Duration.....	98
Figure 3-7. Autonomic Remodelling Influences Heart Rates in CD1 Mice.....	107
Figure 3-8. Changes in Body Weight and Food Consumption over Exercise Protocol.....	108
Figure 3-9. Cumulative Exercise Dose and Atrial Fibrillation Preliminary Results.....	109
Figure 5.1-1. Oxygen Levels Do not Depend on Sampling Rate.....	126

Figure 5.1-2. Measured Oxygen Concentration Depends On Inflow Rate.....	127
Figure 5.1-3. Two Point Calibration Curve for the Oxymax System	128
Figure 5.1-4. Oxygen Measured by the Oxymax Unit is Intrinsically Dependent on Atmospheric and Partial Oxygen Pressures.....	129
Figure 5.1-5. Raw Swim Recording without Baselineing	130
Figure 5.1-6. Purpose of Baselineing Data.....	131
Figure 5.1-7. Calculating Baseline Points.....	133
Figure 5.1-8. Oxygen Consumption Raw Data and Data Extrapolation.....	142
Figure 5.2-1. Raw Data from a Singular 90 Minute Swim.....	145
Figure 5.2-2. Hypothetical Framework of Oxygen Content Changes during Exercise	146
Figure 5.2-3. Oxygen Consumption as an Integral	147

Chapter 1

1. Literature Review and Introduction

Cardiovascular disease (CVD) is the leading cause of death associated with old age and is responsible for 44% of non communicable diseases. The most common CVDs are ischemic heart disease and stroke, which can be potentially caused by arrhythmias – especially atrial fibrillation (AF), with AF leading to the most severe stroke cases [1].

AF is a supraventricular tachyarrhythmia characterized by unorganized atrial excitation and regular-irregular ventricular activation on an electrogram (ECG) [2, 3]. AF can be classified as either paroxysmal (self terminating, lasting no longer than a few weeks), persistent (non self terminating and requiring intervention) or permanent (AF that persists independent of any treatment) [3]. More than 33 million individuals worldwide are affected by AF, and this number is likely to double or triple within the next three decades. Unfortunately, due to its self perpetuating nature, AF is often fatal and the doubles death rates in affected individuals independently of other existing diseases [4]. AF is linked to aging [4], poor cardiovascular health such as hypertension, cardiac hypertrophy, heart failure and strokes [5] as well as sedentary lifestyle [4, 6, 7]. Fortunately, many of the risks pertain lifestyle changes [1], meaning CVD and AF are preventable. Physical exercise is one such attainable and important lifestyle change, and has tremendous benefits even at low doses [6]. In fact, endurance training at adequate doses is suggested to decrease AF risk and even benefit AF patients with symptom management [8]. Nevertheless, it seems that nothing done in excess is entirely beneficial and to this point high endurance training has been shown to increase AF susceptibility [7, 9]. Consequently, the

relationship between AF and the amount of exercise appears to be U-shaped [10] (**Figure 1-1**). Unfortunately, populations at both sides of the extreme seem to increase in the last 30 years – with a 30% increase in the sedentary lifestyle population and a 140% increase in marathon participation [11].

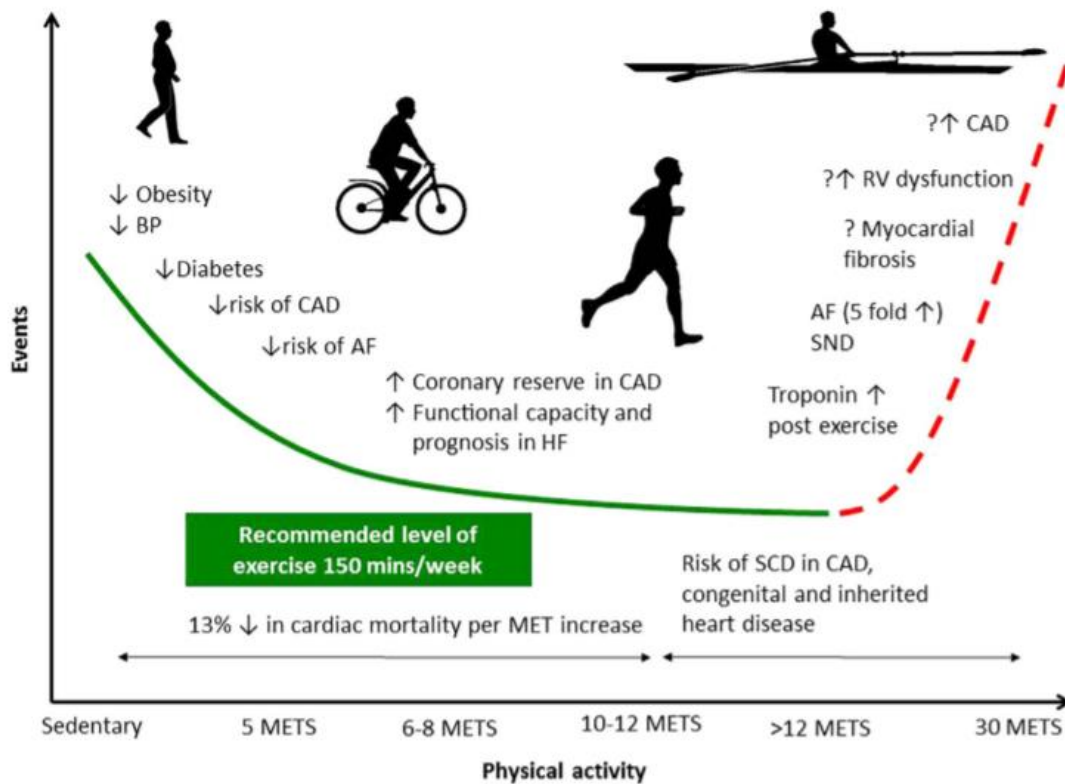


Figure 1-1. U Shaped Curve of Exercise - The U shaped curve of exercise versus events of cardiovascular disease risk. Exercise activity is measured by average metabolic equivalents. Note that an increase in risk is associated with both sedentary lifestyle and high endurance exercise, such as that seen in athletes. Copyright©2016, Trends in Cardiovascular Medicine [96].

1.1 The electrophysiology of Atrial Conduction

1.1.1 Normal Atrial Electrophysiology

In order to understand how excess endurance exercise triggers AF, it is useful to first introduce the concept of electrical activation of cardiomyocytes and the normal electrical activation pattern of the murine and human heart. The heart is equipped with a self activating group of pacemaker cells within the top of right atrium (RA) in a region called the sinoatrial node (SA). The signal travels from the RA to the left (LA) which leads to a contraction. The heart is composed a syncytium of electrically connected cells, coupled via connexin 40 and 43 gap junctions (Cx40 and Cx43) [4]. The signal then travels to the the atrioventricular node (AV), where it slows down. This allows a temporal gap to occur between atrial and ventricular contraction. The His bundle within the ventricular septal wall relays this electrical impulse towards to apex of the ventricles where the Purkinje fibers are located, from where conduction travels to the rest of the ventricles. Interestingly, conduction can travel bidirectionally and even initiate in the AV node, giving rise to retrograde conduction which is often arrhythmogenic [12].

The pattern of electrical conduction within each cell occurs through depolarization and repolarization which give rise to the action potential (AP). In humans, the resting membrane potential of cardiomyocytes sits at around -75 to -60 mV and is predominantly regulated by potassium (K^+) channels [13]. Once a depolarizing current reaches an atrial cell, an AP is initiated. Difference between atrial and ventricular action potentials can be attributed to differences in ion channel current densities and distribution of repolarizing currents [4, 13]. The atria AP is divided into 5 phases (0-4) (**Figure 1-2**). In phase 0, voltage gated, rapidly activating and inactivating sodium (Na^+) channels (I_{Na}) open, leading to depolarization and activation of

voltage gated L type calcium (Ca^{2+}) channels (I_{CaL}) at membrane potentials of -30 to -20 mV. Phase 1 is a rapid repolarizing current generated by K^+ channels [4, 13]. Voltage gated K^+ channels (I_{to}) open once the membrane potential reaches -30mV and quickly deactivate [13]. Ultrarapid delayed rectifier current (I_{kur}) also assist with phase 1 repolarization [4]. Phase 2 plateau is maintained by a balance between the repolarizing currents of I_{kur} and the slower rapid delayed rectifier currents (I_{kr}), as well as the depolarizing I_{CaL} current which lasts up to hundreds of milliseconds upon activation [4, 13]. Phase 2 ends with I_{CaL} inactivation which is both voltage dependent and calmodulin regulated [13]. Phase 3 is a repolarization back to the resting membrane potential which occurs with activation of more K^+ channels - namely, I_{Kr} , I_{Ks} (s=slow) and I_{K1} (inward rectifying K^+ channel) [13]. The function of I_{K1} is especially important in the atria compared to the ventricles during depolarization. Due to incomplete rectification as well as decreased density of I_{K1} smaller currents are required to achieve a depolarization threshold in the atria [4]. The final phase of the AP is Phase 4 – or the resting membrane potential at which the membrane potential is almost equal to the potential equilibrium of K^+ channels. The diastolic interval is regulated by the resting membrane potential [13]. During this time when Na^+ channels remain inactive, another AP cannot fire, a phase called effective refractory period (ERP) [14].

Two additional currents are active during the AP. The sodium calcium exchanger (I_{NCX}) provides a bidirectional current, as it exchanges 3 Na^+ ions for 1 Ca^{2+} ions. During the plateau phase (Phase 2) I_{NCX} leads to a net outflow of Ca^{2+} ions, resulting in a net depolarizing current; whereas as Ca^{2+} concentration decreases in the cell the current changes to repolarization due to a net inflow of Ca^{2+} ions [4]. Finally, an atrial specific K^+ channel ($I_{\text{K, Ach}}$) is an important regulator

of the plateau phases and therefore the action potential duration (APD) in the atria [4, 13]. As suggested by the name, these channels activate by regulation from acetylcholine (ACh), and therefore respond to parasympathetic regulation (**Figure 1-3A**). Effectively, $I_{K, ACh}$ reduce conductance in the SA node, induce bradycardia, and decrease the APD in the atria [13].

Atrial Electrophysiology in the Mouse

Differences between murine and human APs exist. APD is shorter in the mouse proportionally to their small body mass [4, 15]. Decreased SA node APD in mice is attributed to differences in delayed rectifier K^+ channels [15]. Five (5) K^+ channels have been previously identified in the adult mouse atrium: I_{to} , I_{Kur} , I_{K1} , as well as mouse unique I_{ss} (steady-state) and $I_{K, slow}$ ($I_{K, slow1}$ and $I_{K, slow2}$) [16, 17]. In humans, I_{Kur} is comprised of two K^+ currents - I_{Kr} and I_{Ks} , and has also been named I_{ss} [4, 13, 17]. In the mouse, I_{ss} is slow activating, non-activating current, involved in late repolarization. Finally, the distribution of all K^+ channels differs between species [17]. I_{Na} , I_{CaL} and I_{NCX} seem to have similar functions in the mouse and human atrial myocytes. Nonetheless, compared to humans where I_{NCX} is the dominant mechanism of Ca^{2+} removal, 90% of removal in mice is attributed to the sarcoplasmic reticulum (SR) [15]. Finally, the distribution of Cx40 and Cx43 in the mouse atrium is also well established [15].

Ion Channel Determinants of Reentry

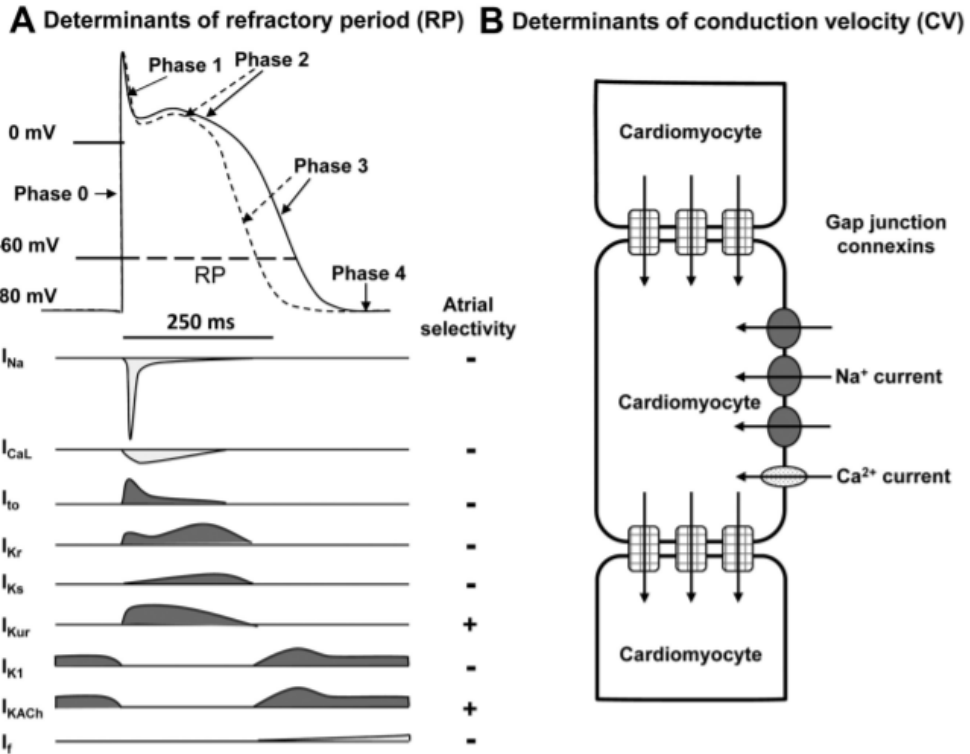


Figure 1-2. Ionic Currents in the Human Atrial Action Potential – The top left panel show the human atrial action potential. The panel below it shows the ionic currents as well as their temporal participation. Current inflow leads to a negative deflection, and current outflow leads to a positive deflection in the left panel. These ionic components regulate the refractory period length in the atrial myocytes. Atrial specific currents are indicated by +. The right panel shows channels whose remodelling leads to decreased conduction velocity during arrhythmia. Here, Na⁺ current represent the sodium calcium exchanger and the Ca²⁺ current represents the L-type calcium channels. Copyright©2011, Circulation [14].

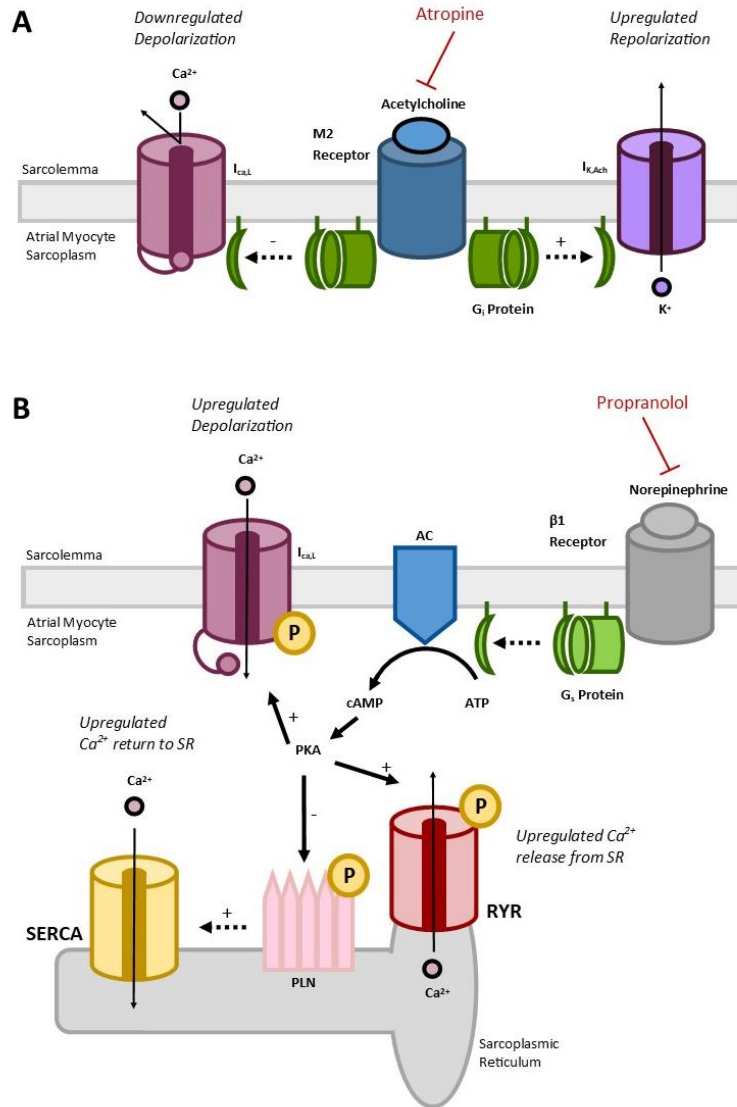


Figure 1-3. Autonomic Regulation of the Ionic Channels in Cardiomyocytes – A)

Parasympathetic regulation by Acetylcholine (via M2 receptors) leads to increase in hyperpolarization through potassium channels, such as $I_{K,Ach}$ in the atrial cardiomyocytes. This is blocked by pharmacological administration of Atropine. B) sympathetic stimulation leads to increased chronotropic and inotropic through activation of $\beta 1$ receptors and phosphorylation of various targets by Protein Kinase A. This is blocked by pharmacological administration of Propranolol. Calcium ion, Ca^{2+} ; L type Calcium Channel, $I_{Ca,L}$; Muscarinic Potassium Channels, $I_{K,Ach}$; Inhibitory G Protein, G_i ; Adenylyl Cyclase, AC; cyclic AMP; cAMP; Adenosine triphosphate, ATP; Stimulating G Protein, G_s ; Protein Kinase A, PKA; Ryanodine Receptor, RYR; Phospholamban, PLN; Sarcoplasmic Reticulum Calcium ATPase, SERCA. Figure generated using Microsoft Publisher.

1.1.1 Calcium Induced Calcium Released

During systole, Ca^{2+} enters the myoplasm from the sarcoplasmic reticulum (SR) and initiates a contraction. This process is therefore called excitation-contraction coupling [4, 18]. In the atria, Ca^{2+} enters the sarcolemma and cytoplasm and binds junctional ryanodine receptors (RYRs) on the SR which leads to further Ca^{2+} release from the SR reserve. This process is termed calcium induced calcium release (CICR). Differences between atrial and ventricular CICR exist and are described elsewhere [18]. In the atria, RYRs are clustered together, leading to Ca^{2+} sparks. Thereafter Ca^{2+} activates more non-junctional RYRs on Z-tubules and regulates contraction via the Troponin-Tropomyosin complexes [4, 18]. Finally, concentrations of Ca^{2+} are returned to normal via sarco/endoplasmic reticulum Ca^{2+} ATPase (SERCA), I_{NCX} and to a lesser extent a sarcolemmal/ plasma membrane Ca^{2+} ATPase (PMCA). The contribution of each varies between humans and mice [15]. Multiple factors can regulate contraction, one of which is the sympathetic nervous system (SNS) via β -adrenergic receptors which enhance the functions of I_{CaL} and SERCA (**Figure 1-3B**).

1.2 The Electrophysiology of Atrial Fibrillation

Although many patterns of tissue excitation occur in AF, they can generally be divided into either hierarchical or anarchical events. Hierarchical patterns generally involve "reentry" events and are classified as rotors, leading circle reentry, spiral wave reentry and circus movement; although these patterns include the events in which ectopic foci initiate(s) repeated activations [4, 19]. On the other hand, anarchical mechanisms involve multiple arrhythmogenic foci, as modeled by the multiple wavelet theory [4]. Reentry and multi-wavelets are invariably initiated by triggered arrhythmic events originating in tissue foci [4]. Several mechanisms are

believed to lead to the initiation of reentry and multi-wavelets events: 1) appropriately timed premature stimuli lead to non uniform depolarization-repolarization patterns (tissue foci), 2) non-uniformity of atrial conduction properties arising from electrical heterogeneity of tissue activation, typically associated structural changes (i.e. fibrosis) of the tissue, and 3) non-uniform (i.e. heterogeneous) repolarization events. Non-uniform conduction mentioned above is termed antistrophic conduction and usually occurs in very small tissue areas (i.e. at the microscopic level) [12]. In both uniform and non-uniform patterns, non-conductive, structural disturbances such as fibrosis vary the tissue conduction which can result in unidirectional block and non uniform conduction velocities (CVs) allowing for reentry from a slow pathway to a fast one [12]. In general, all of these mechanisms are favoured by two independent factors: CV and refractory period (RP). The product of these two factors gives a measure of the length of tissue that is depolarized (and therefore refractory) following tissue activation and is therefore referred to as the “wavelength”. When the amount of tissue present (called the pathlength) exceeds the wavelength, re-excitation of tissue following a single activation from the master pacemaker becomes more likely [5, 12]. This also becomes more likely when the frequency of triggers (i.e. irregular focal activity) increases. These mechanisms can be characterized as triggers, substrates, and modulators and categorized as structural, electrical, or autonomic remodelling, as will be described later (**Figure 1-4**).

1.2.1 A Brief History of Reentry and Atrial Fibrillation

Invariably, remodelling and triggered foci lead to various forms of reentry patterns. *Circus movement* was first described by Alfred Mayer in 1908 [12]. Mayer observed a circular movement of conduction in rings of tissue isolated from jellyfish [20]. In 1914, George Ralph

Mines used Mayer's concepts and described *circular excitation* in the cardiac tissue of dog-fish hearts. By stimulating on one end of the ring he was able to observe contractions that went around and circulated twice [21] (**Figure 1-5A**). In 1920, Thomas Lewis used these concepts to postulate the requirement of decreased refractoriness and increased atrial mass (i.e pathlength) for the perpetuation of AF but was nonetheless reluctant to prove such hypothesis without a clear definition of the "path by which reentry is affected" [22]. *Leading Circle Reentry* was introduced in 1976 by Maurits Allessie. Allessie was showed that circus movement does not require an anatomical obstacle, and could occur with unexcitable core within a ring of excitable tissue [23] (**Figure 1-5B**). Specifically, leading circle reentry requires a temporal excitable gap which exists due to a constant depolarization state, initiated from the circular wave of fibrillation around it [4]. In this model, the leading wave front re-excites the wave tail almost immediately, making the pathlength equal to the wavelength. As a consequence, the revolution time of the wave is determined by the RP and the shortest possible wavelength is assumed [4, 23]. *Spiral wave reentry* (also called rotors) was inspired from chemical reactions [24] and has been demonstrated in cells using imaging of intracellular Ca^{2+} waves [4] (**Figure 1-5C**). Such reentry occurs through a balance between source and sink cells. The "source" carry the depolarizing current, whereas the "sink" cells are downstream excitable cells. Usually, conduction is linear such that the number of source and sink cells is equivalent. Nonetheless, concave and convex wave fronts also exist. In a convex conduction, the number of sink cells exceeds the source, which decreases the conduction velocity as the source does not carry enough current to activate the downstream cells. The opposite holds for concave conduction (**Figure 1-5C**). In a spiral wave, the wave front are convex whereas the wave tail is concave – giving rise an unexcitable core which behaves as a block [4]. In cardiac tissue, a spiral wave may form through multiple mechanisms related to

APDs, refractoriness of previously excited tissue and abnormal ionic channel distribution and fibrosis – all of which are described in detail elsewhere [25]. Although never directly observed in AF patients [4], experimental work from animals and computational analyses encourages the presence of spiral waves/rotors in atrial models, and has been even demonstrated in ventricle fibrillation (VF) models [25]. Finally, *multiple wavelet theory* was postulated by Gordon Moe in 1959 based on the notion that AF must be self-perpetuating – it persists even after triggers ceased to occur [19, 26] (**Figure 1-5D**). According to this theory, fibrillatory wave fronts and tails collide leading to either block, fusion, or regeneration. If the number of fibrillatory waves remains above a critical number, AF will become sustained. For this purpose, decreased RP, increased RP heterogeneity, slowed CV and increased atrial mass are essential – maintaining the reentry course [4]. Although previously shown using computer models, Allesie was able to demonstrate the existence of multiple wavelets in dog atria exposed to Ach [4, 27].

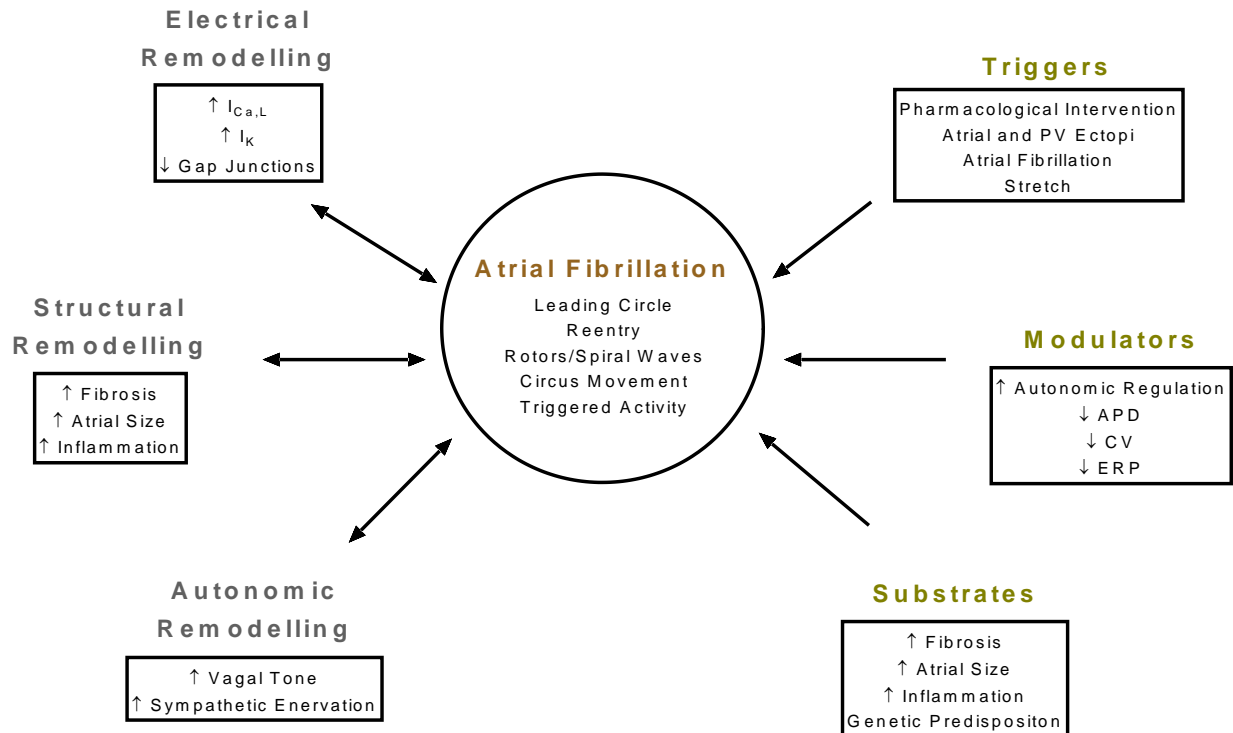


Figure 1-4. Mechanisms of Atrial Fibrillation - Remodelling refers to physiological and anatomical changes in cardiac tissue which lead to adverse function. Remodelling can be categorized as electrical or structural remodelling. Autonomic remodelling is sometimes considered separate from other forms of electrical remodelling. Remodelling promotes atrial fibrillation through enhancing reentry events such as re-entrant waves and rotors. Remodelling can also be characterized based on its function in atrial fibrillation perpetuation. The three categories are triggers which initiate the abnormal conduction, as well as substrates and modulators which assist with perpetuation and reentry of abnormal condition. Figure was created on Prism, based on the following: (Turagam et al. 2015 [9]; and Iwasaki et al. 2011 [14]; Pellman and Sheikh, 2015 [32]).

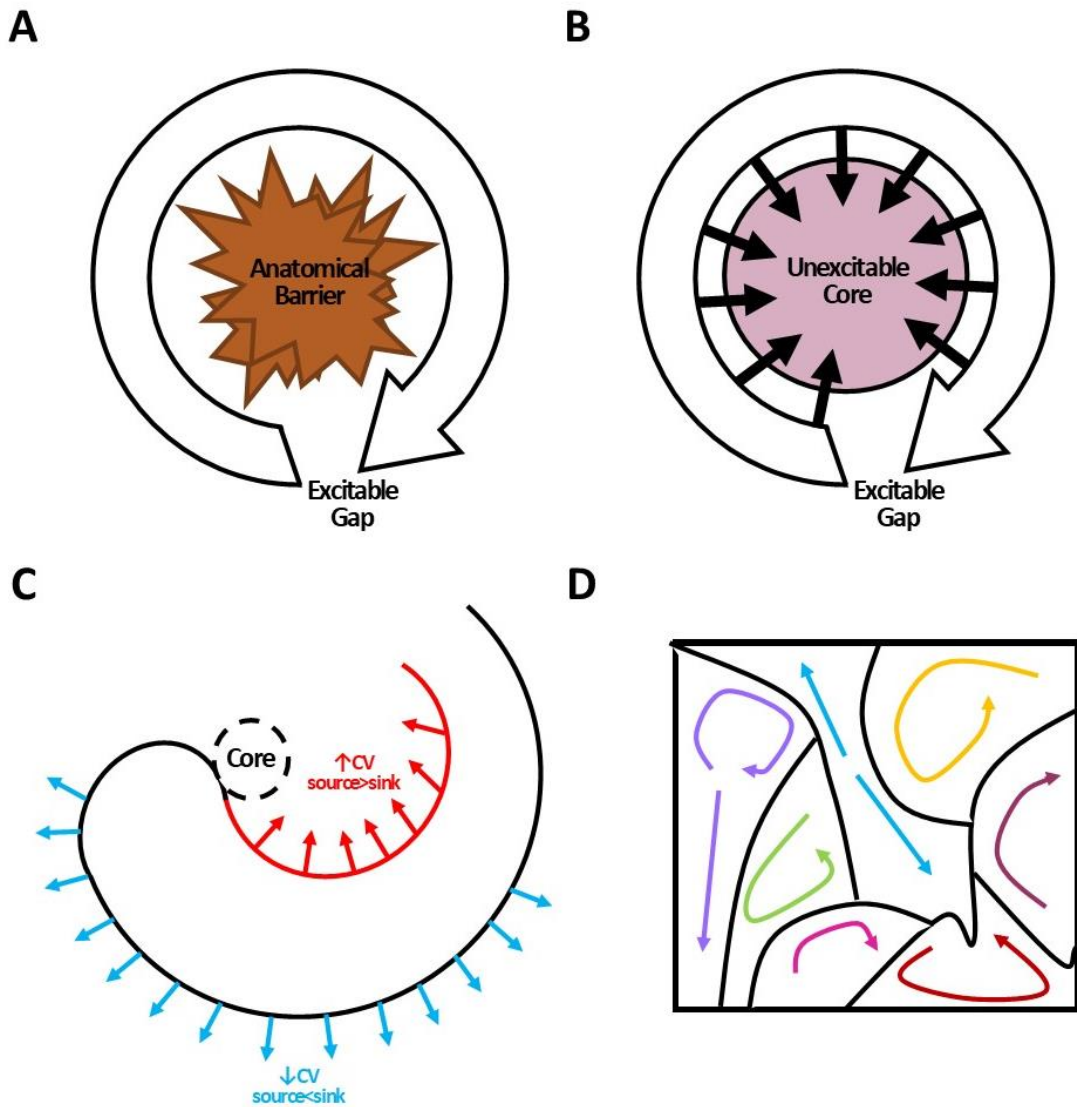


Figure 1-5. Reentry Mechanisms – A) circular excitation is the simplest form of reentry, which occurs with an anatomical barrier.; B) leading circle reentry is similar to circular excitation and occurs without a barrier but with a refractory core.; C) spiral wave reentry occurs due to mismatch between source and sink cells with concave conduction on the inner wave front and convex conduction on the outside of the wave front. the different types of conduction wave fronts are shown. CV= conduction velocity. Note the decrease in conduction velocity in convex waves, leading to reentry propagation.; D) Gordon Moe’s multiple wavelet theory. Figure created on Microsoft Published, based on Schotten et al. 2011 [4]

1.2.1 Reentry in Mice

As discussed above, if the wavelength is sufficiently small relative to the amount of tissue (called the critical mass of tissue) reentry and arrhythmias become far more likely [28]. It was widely believed that due to the small heart size in mice reentry is not possible [29]. Nonetheless, both AF and VF were shown in mouse models [2, 15, 19, 29]. In fact, the cheap cost, quick development, high genetic and phenotypical homology to humans, as well as the similar relationship between APD and diastole, makes mice a proper model organism to study cardiac arrhythmias and AF [29]. The susceptibility of mice to AF can be explained by the relationship between atrial circumference and wavelength. In fact, the ratio between the two is highly similar to humans at ~ 1 . As such, alterations in CV in both species increases probability of reentry arrhythmias and therefore AF [15]. In fact, even with a small surface area, the probability of AF is high as long as the RP is short enough [30].

1.3 Electrical, Cellular and Tissue Factors Predisposing to AF

Electrical changes leading to AF occur in association with and result from, changes in tissue properties which are referred to as *remodelling*. Remodeling is defined as changes in the molecular, electrical, cellular and tissues properties that clinically manifest as changes in size, shape, function, and regulation [31]. Increased parasympathetic nerve activity (PNA) and variability in ionic currents are examples of changes influencing electrical function, and consequently an example of *electrical remodeling* [14, 32]. Atrial hypertrophy and fibrosis, which commonly occur in association with AF, are examples of changes of tissue properties and are referred to as *structural remodeling* [32].

1.3.1 Electrical Remodelling

Autonomic Regulation

Autonomic regulation is a well established modulator of AF [9, 32]. The heart is innervated with intrinsic and extrinsic nervous tissue, and the regulation of electrophysiology of the heart by the autonomic system is very important [32]. The extrinsic nervous tissue originates from the brain and spinal cord, and innervates the heart is ganglia called Ganglionated Plexi (GP). Four of these ganglia are in the atria, in close association with the pulmonary veins (PVs) [33]. Multiple studies employed GP ablation to show that reduction of arrhythmia duration in AF patients [34]. Nonetheless, the success of GP ablation in AF is not as high as in other procedures, and becomes less effective in patients with persistent AF [32, 35]. Therefore autonomic regulation is deemed as a modulator of AF [32]. Autonomic regulation leads to triggered activity in the form of early afterdepolarizations (EADs) and delayed afterdepolarizations (DADs), which then provoke AF, as well as changes to ionic channel function that ultimately regulate APD and RP – all of which will be discussed below.

Automaticity and Triggered Activity

Arrhythmogenic increase in heart rate (HR) often arises from either enhanced automaticity whereby the pacemaker fires at irregular spontaneous rate or abnormal automaticity where cells activate easily due to decreased threshold (either in the pacemaker or elsewhere in the atria) [4, 28]. Nonetheless, there is little evidence that automaticity leads to AF and previous studies show that the pacemaker cells are protected from fibrillatory activation [36]. On the other hand some studies show that pharmacological manipulation of the SA node has been shown to reduce AF duration and incidence [36, 37]. The decreased CV within the SA node is believed to

maintain the arrhythmia, and therefore the dysfunction of SA node *per se* does not lead to AF [5]. Finally, SA node functional discrepancies seem to be related to paroxysmal AF, and not lone AF as found in athletes [19, 38].

A more common trigger of AF are EADs and DADs which occur during the repolarization phase of the AP in the atrial myocytes [4, 14, 19]. They are membrane oscillations that follow a normal AP and become self sustaining [4]. DADs occur due to spontaneous or abnormal release of Ca^{2+} from the SR when RYRs are defective or the SR is overloaded. Ca^{2+} is then released via I_{NCX} which causes a depolarizing current [4, 14]. Increased SR load and spontaneous release is often associated with enhanced SNS activity (β adrenergic stimulation) and therefore tachycardia [39] (**Figure 1-3B**). EADs can occur due to multiple mechanisms at either Phase 2 or 3. When APD is prolonged, such as with increased PNA, the inactivation and activation of I_{CaL} overlap – active Ca^{2+} channels can reactivate inactive Ca^{2+} channels leading to the perpetuation of the AP [4]. $\text{I}_{\text{K, Ach}}$ activation by the PNS leads to a decreased APD and return to a resting membrane potential (**Figure 1-3A**); nonetheless, the I_{CaL} window sits at -30 to 0 mV and reactivation of these channels leads to a repeated depolarization [40]. As such, EADs are favored during bradycardia [4, 39]. Late Phase III EADs occur during simultaneous increases of PNS and SNS functions. In this case, Ca^{2+} SR loads are increased via β -adrenergic stimulation and APD is decreased by $\text{I}_{\text{K, Ach}}$. Although the concentration of Ca^{2+} released are strong, their concentration remains relatively normal which differentiates them from DADs [4].

Triggered activity must prevail by depolarizing neighbouring cells – the sink, source match must support conduction propagation which occurs when the chaotic irregular conduction dependent on the HR propagates to neighbouring cells via decreased gap junction numbers (and

therefore CV) as well as structural block (such as fibrosis). Furthermore, conduction coupling leads to synchronization of APDs and therefore irregular behaviour in neighbouring cells which continues propagating in the syncytium. The outcome are islands of cells with similar conductive properties. Reentry to these islands can then cause fibrillatory conduction by local conduction blocks and similar refractory properties [40].

Ionic Changes and Gap Junctions

Electrical remodelling primarily occurs through changes in ionic channels and gap junction function which has been shown to occur through both altered expression and regulation [4, 41]. Increased I_{Na} and I_{CaL} depolarizing currents increase APD and therefore hinder arrhythmia propagation. On the other hand, decreased I_{Na} hinder conduction propagation (decrease CV) as well as alter the RP, thereby increasing the probability of reentry [4]. Increased K^+ flux, such as during increased vagal tone, decrease the APD and promotes reentry by decreased refractoriness as well as promotion of EADs [4, 28, 42]. Likewise, downregulation of I_{to} has been shown in chronic AF patients and shown to occurs within 24 hours of tachycardia in animal models [4, 41]. I_{K1} and $I_{K,Ach}$ have been shown increased at both the mRNA and protein expression levels, which significantly decreases APD and therefore promotes AF [41, 43, 44]. Finally, tachycardia induced Ca^{2+} loading to the SR is well known and promotes DADs as well as EADs, as previously discussed [4].

As previously mentioned, both Cx40 and Cx43 are expressed in the atrial syncytium [4]. As predicted, decreases in gap junction expression leads to decreased CV thereby increasing the possibility of reentry [28]. Nonetheless, studies seem conflicting with regards to Cx40 and Cx43 expression in AF patients and animal models – some report increase, decrease or even no change

in expression [4, 5, 41]. Thomas et al. suggest that these discrepancies could be partially explained by different functional specificities of Cx40 and Cx43 in atria [45]. As such, gap junction remodelling might explain the underlying differences in AF pathologies and direct treatments [41].

Unfortunately both tachycardia and AF promote electrical changes [5], one means by which AF becomes self perpetuating – it is well known that “AF begets AF” [4], a concept introduced in 1995 [46]. Wijffels et al. showed that atrial pacing leads to atrial ERP (AERP) shortening and enhanced AF susceptibility in goats, which was supported by similar data found in dogs by Morillo et al. [47, 48]. As such, rapid pacing is an often employed experimental technique to induce AF and assess AF susceptibility [4]. One explanation lays in the reduction of the APD is associated with a decrease in I_{CaL} , which leads to a decreased wavelength and subsequent susceptibility of reentry [5]. It is no surprise that such reductions in I_{CaL} also lead to contractile dysfunction in the atria as given excitation-contraction coupling is Ca^{2+} dependent [46]. Despite a decrease in I_{CaL} in AF patients, the recurrence of EADs and DADs can be attributed to enhanced expression of I_{NCX} as well as I_{K1} function [44, 49, 50]. Finally, similarly to discrepancies related to the function of gap junction in AF, the effects of AF on gap junctions was also appears conflicting [46]. Fortunately, electrical remodelling has been shown reversible and AERP restoration was achievable, even after years of AF in patients, as well as in animal models [48, 51, 52]. On the other hand, electrical remodelling is closely linked to structural remodelling which was regrettably shown irreversible in multiple studies, as will be discussed later [2, 46].

1.3.2 Structural Remodelling

Fibrosis

The cells in the heart are surrounded by an extracellular matrix (ECM) composed of Type I and Type III collagen, as well as other signal molecules. The ECM possess important functions in the heart as it contains components that regulate apoptosis, it partakes in the regulation of contractile function and strength transmission during fiber shortening as well as contains signal molecules such as cytokines and growth factors [53]. In a typical myocardium the cell bundles are separate by perimysial fibrous tissue which runs perpendicular to the long axis of the myocyte bundle. Individual cells are separated and supported by endomysial fibrous tissue which runs parallel to the myocyte bundle [4]. An imbalance of fibrosis degradation and formation leads to irreversible damage, and ample of CVDs such as congestive heart failure and AF [4, 31]. Furthermore, the interrelation between AF and other CVDs is amplified when fibrosis is the underlying cause of either one and all three behave as risk factors for each other [4].

On a cellular level, collagen deposition is completed by fibroblasts, which constitute the majority of cells found in the heart [54]. On a molecular level, fibrosis has been shown modulated by multiple signalling pathways including transforming growth factor beta (TGF β), Angiotensin II, and various growth factors [4, 31, 55]. The TGF β cytokine family are a group of multifunctional proteins playing a role in growth, inflammation and repair and are potent activators of fibroblasts [19, 56]. Upon binding of TGF β , the serine/threonine receptor dimerizes leading to the phosphorylation of Smad transcription factors. Dimerization of Smad 2 and 4 allows for translocation into the nucleus and subsequent upregulation of the *COL1A1* and *COL1A2* genes, which encode Collagen I subunits [57] (). Angiotensin II is a response molecule

to increased arterial pressure through the renin-angiotensin pathway and increases fibrosis production through increased fibroblast proliferation, and upregulation of TGF β as well as plasminogen activator inhibitor-1 – a protease inhibitor responsible for collagen degradation [58].

Fibrosis is an important AF substrate as it interferes with electrical conduction and decreases CV [59]. Conduction in healthy atria exhibits uniform anisotropy where conduction occurs fast in the longitudinal direction and slower in the transverse [12, 60]. Fibrosis leads to non-uniform anisotropic conduction by increasing the resistance between conductive cells, leading to unidirectional block to the longitudinal direction [12, 59]. Such decrease in CV in the transverse direction due to enhanced resistance, predisposes reentry into the longitudinal pathways thereby enhancing AF, specifically through *leading circle reentry* [12]. Furthermore, fibroblasts can connect electrically to cardiomyocytes and act as sinks however given their inability to depolarize they promote reentry by behaving as conduction block [14, 59].

Finally, fibrosis is self perpetuating and facilitates the notion that “AF begets AF”, leading to permanent AF forms [14]. One proposed mechanism suggests that constant atrial stretch during AF leads to a decrease expression of matrix metalloproteinases (MMPs) that break down the ECM and increased function of their inhibitors [4]. Another explanation suggests that increased ECM leads to decreased energetic supply increasing cell death and therefore enhanced fibrosis formation, as well as inflammation which is intrinsically correlated with fibrosis formation [55]. Unfortunately, fibrosis formation is irreversible making it a therapeutic as well as preventative goal [14].

Inflammation

Post operative AF was the most frequent complication after open heart surgery, which served as the basis for the correlation between inflammation and AF [61]. Several studies were able to show the link between the two later in patients with lone AF. For example, inflammatory lesions were identified in 8/12 patients by Frustaci et al. and T cells and macrophage infiltration was shown in biopsies of left atrial appendages in 7/7 patients, by Nakamura et al. [62, 63]. On a cellular level, inflammation was shown correlated tumor necrosis factor alpha (TNF α), IL-6 and IL-1 β , IL-1 receptor antagonist, soluble TNF α receptor and C-reactive protein (CRP) [61]. CRP received attention as a marker of inflammation and several studies have shown correlation between CRP and AF, AF duration as well as LA dimensions [64-66]. TNF α has also been at the centre of attention and is known to promote contractile dysfunction, increased fibroblast function, and cardiac hypertrophy [4, 61]. TNF α was showed increased in AF patients, and serum and left atrial tissue TNF α were directly correlated with LA size in these patients [67]. Moreover, we were able to show that pharmaceutical and genetic manipulation of TNF α and its downstream signalling molecule p38 eliminated exercise induced AF in swim exercised mice [2, 68] and Saba et al. was able to show that overexpression of TNF α leads to increased atrial arrhythmia inducibility in mice as well [69].

Finally, inflammation seems to both be caused by AF and participates in its pathogenesis. The prevalence of AF is higher in post operative patients and those with pro-inflammatory conditions such as myocarditis and pericarditis [70, 71]. Additionally, administration of anti-inflammatory even at low doses, seems to decrease post operative AF, which coincided with marked decrease in CRP and IL-6 [72]. Conversely, AF patients with restored rhythm post

cardioversion had lower levels of CRP compared to those with recurred AF – suggesting the AF in itself is proinflammatory [70].

Fibrosis and Inflammation Coordination

Inflammation and fibrosis seem to be intrinsically correlated with each other – further amplifying the causative effect of inflammation on AF [55]. Galea et al. suggests that fibrosis may be the link between inflammation and AF [70]. Indeed proinflammatory markers and fibrosis were shown colocalized in left atria of AF patients [73]. Therefore, it is possible to conclude that one mechanism by which AF becomes self perpetuating is by increased inflammation, which induces structural and electrical change which further promote AF [14, 70].

Atrial Dilation and Atrial Stretch

Dilation or enlargement of the atria occurs due to either volume or pressure overload and atria respond faster and stronger to wall stress than ventricles [2, 4]. Left atrial size is a predictor for AF, with AF increasing at LA size of >40mm even after adjustments for other factors such as age, sex and CVD. In fact, with atrial size >45mm cardioversion, although seems successful at first, had no effect on restoring sinus rhythm after 6 months [74]. Elevated atrial size invariably increases the pathlength, thereby increasing the probability of reentry and promoting multiple wavelets [5, 75].

On a cellular level, atrial dilation and AF are interrelated acutely and chronically. Acute atrial dilation leads to changes in the activity of several strain-dependent/stretch activated membrane currents, which respond to deformation of the plasma membrane. Alterations in their activity cause reductions in APD, ERP, CV, as well as increases conduction heterogeneity, all of which predispose the atria to reentry [19, 76, 77]. These data are supported in Langendorff-

perfused rabbit hearts. Here, a strong correlation between introduced pressure and arrhythmia susceptibility was found, which was explained by a strong correlation with decreased APD and ERP. Furthermore, the study also suggested that all parameters returned to normal 3 minutes post release of atrial stretch – suggesting that acute responses are reversible [78]. Stretch activated channels (SACs) have been implicated the mechanism between atrial dilation and electrical remodelling [19]. Many types of SACs have been demonstrated in the mammalian heart. For example, SAC K^+ channels responsible for repolarization in the atria [79]. Another mechanism has been suggested by Iribe et al. whereby SACs seem to increase the probability of spontaneous Ca^{2+} release and therefore DADs [80, 81]. Finally, administration the atrial SAC inhibitors, GsMtx4 peptide [82] and gadolinium [83] suppressed AF.

Chronic atrial dilation was shown to lead to structural remodelling such as fibrosis, and loss of myofilaments and degeneration [4] which appears to enhance arrhythmia even in the absence of electrical remodelling [84]. Verheule et al. used a mitral valve regurgitation model in dogs and noted increases in AF vulnerability despite ERP elevations, with AF attributed to increased interstitial fibrosis and connexin remodelling as opposed to electrical remodelling [85]. Finally, chronic atrial stretch is associated with decreased MMP expression, which was previously shown in persistent AF patients, suggesting decreased ECM and fibrotic degradation [4].

Finally, AF seems to perpetuate atrial dilation. For example, Sanfilippo et al. monitored 15 AF patients and found that after a follow up of ~20 months these patients showed right and left atrial dilation [86].

1.3.3. Pulmonary Vein Ectopy and the Left Atrium

The left atrium and PVs received special attention. Haïssaguerre et al. found that the PVs were the main source of ectopic foci in AF patients, and ablation of these foci lead to attenuation of AF episodes in these patients [87]. Automaticity, triggered activity and microreentry have been suggested as mechanisms underlying PV triggered AF [4, 19]. Nonetheless, the discovery of automaticity in PVs predates the description of their involvement in AF, and was initially described by Brunton and Fayrer in 1876 [4]. Since then, differences between PV cells and atrial myocytes with regards ionic channel distribution and electrophysiological properties have been described [5]. On top of that, structural differences have also been identified by an increased interstitial fibrosis and inflammation in the PVs, predisposing the tissue to reentry [88, 89]. Given the proximity of the LA to the PVs it often has increased fibrillatory behaviour [4, 14]. Notwithstanding, both the LA and RA exhibit increased fibrillatory behaviour compared to the ventricles [4]. These observations are the basis for PV ablation procedures where scar tissue around fibrillatory foci is created to isolate reentry events and PV denervation procedures to prevent increased vagal tone in these susceptible areas [32].

1.4 Treatment of AF

AF is a debilitating disease given its self perpetuating nature and causative relationship with fatal outcomes such as thrombopoiesis, stroke, heart failure and ventricular arrhythmias [4, 5, 90, 91]. Treatment options are available for AF but prevention remains most adequate. Treatment includes either *rate control* or *rhythm control*.

In rate control, the impact of AF is minimized. Here, the symptoms of AF as well as the prevention of tachycardia associated cardiomyopathy and stroke are targeted [92]. In rate control,

pharmacological blockade of conduction through the AV node is employed to improve ventricular activity and contraction [32, 92]. Pharmacological agents include β -adrenergic receptor blockers, calcium channel blockers, as well as other drugs that reduce the conduction but enhance the ERP in the AV node and minimize effects of autonomic regulation [32, 91]. Nonetheless, because rate control does not target AF directly and aims to minimize ventricular contraction, risks of thrombopoiesis remain high, exercise capacity is not really enhanced and often a combination of different drugs is required [19, 32, 91]. Furthermore, such pharmacological agents often induce unfavorable complications such as reduced sinus bradycardia and heart block [32].

Rhythm control strategies seek to restore sinus rhythm (cardioversion). It can be divided into two categories – non-invasive rate control which employs pharmacological agents and invasive rate control such as ablation [32]. Such strategies are often employed in younger AF patients (<65 years old) for paroxysmal AF and their use is often inadequate for patients with structural heart disease, and permanent or persistent AF. The use of rhythm control for persistent AF patients can be achieved through a combination of interventions and only if the risk of recurrence is low [91, 92]. Non-invasive rhythm control employs class Ic (Na^+ inhibiting) or class III (K^+ inhibiting) pharmacological antiarrhythmics [19, 92]. Nonetheless, such agents often produce unfavorable proarrhythmic side effects like ventricular tachyarrhythmias [5] such as Torsade des pointes [92]. Invasive rhythm control strategies such as ablation include direct current shock and cardiac surgery where specific areas of atrial muscle are destroyed [19]. Such procedures aim to eliminate ectopic foci, especially in the PVs, or remove scar tissue to prevent recurrence of reentry [32]. Unfortunately, recurrence occurs in most cases, are more likely in

persistent AF patients [93], and repeat ablation procedure are often required, which may also prove unsuccessful in some cases [94].

Taken together with the self-perpetuating nature of AF, the persistence of structural remodelling and the inadequacies of AF management and treatment, AF prevention becomes the best long-term goal for those at risk. This is especially important for athletes, as detraining and decreased physical activity are the primary prescribed means to relieve AF related symptoms and pharmacological interventions often employed in regular AF patients may decrease performance and should therefore be avoided in professional athletes [9]. The relationship between exercise and AF will be discussed now.

1.5 Exercise, Cardiovascular Adaptations, and Atrial Fibrillation

The most ancient, but nonetheless extremely accurate, description of the effects of exercise on health is that of Hippocrates: “All parts of the body... if used in *moderation* and exercised in labors to which each is accustomed, become thereby healthy and well developed and age slowly...” [95]. It is now a well accepted notion that this description directly relates to cardiovascular health. The benefits of exercise on the overall and cardiovascular health are well known [96]. Exercise has been shown protective of coronary heart disease [97], cardiac death, nonfatal myocardial infarction, congestive heart failure [98], diabetes, hypertension, and ischemic heart disease [99]. Such benefits are apparent even with other concurrent conditions and characteristics, such as elevated cholesterol, smoking, obesity and other CVDs [98, 100]. Nonetheless, many other studies suggest that the relationship between exercise and cardiovascular health is not linear – but rather U shaped [96]. A frequently mentioned metaanalysis by Lee et al. found an increased CVD risk is elevated in those running at longer

durations and distances, more frequently and higher speeds – all of which were directly correlated with a higher cardiorespiratory fitness (CRF) [101]. Similar to other CVDs, AF and exercise also show a U shaped relationship, independent of age [10]. Sex related differences affect AF prevalence with exercise, with mostly male athletes suffering from the condition [102]. Nonetheless, a U shaped curve has also been shown for women [10].

Multiple studies identified an increased prevalence of AF with extreme endurance exercise. The first documented evidence of elevated AF prevalence in athletes was published by Coehlo et al. who identified 5/19 athletes with sudden AF episodes initiated during exercise activity. Furthermore, these episodes were reproducible by both programmed stimulation and exercise [103]. Data from 146 young (<25 year old) athletes found 9% AF prevalence, which also reproducible in controlled settings [102]. The risk of exercise induced AF since then has been shown by multiple longitudinal, observational, retrospective and prospective case studies; reviews of these exist elsewhere [11]. More specifically, lone AF was significantly more prevalent in athletes than the general population, and occurred in the general population under the circumstances of vigorous exercise [102, 104]. As such, vigorous exercise has since then been identified as a risk factor for lone AF. Mont et al. found that of 70 AF patients seen at the arrhythmia outpatient clinic, 32 were sportsmen with 63% of these suffering from lone AF specifically [105]. Data from these same patients suggests that 1500 lifetime hours of endurance sport behave as a threshold risk for lone AF [105, 106]. On the other side of the U shape, lone AF is also caused by unhealthy lifestyle patterns such as obesity, abnormal sleep patterns, excessive alcohol consumption, caffeine and nicotine use, as well as stress [107].

It is worth highlighting that these relationships are dependent on variable exercise dose quantities such as intensity, duration, and frequency. Andersen et al. assessed the prevalence of arrhythmias in in cross-country skiers. Arrhythmias risk increased with total number of races (cumulative “dose”) and had a tendency to increase with race time (exercise “duration”) [108]. Furthermore, Lavie et al. suggest that although walking decreases all cause mortality less than vigorous exercise, it can be done for longer durations without such risks increasing again, thereby differentiating between exercise intensity and duration [6]. Similarly, Lee et al. identified that running 1-20 miles per week, at 6-7 miles/hour, 2-5 times a week reduces all-cause-mortality while longer, faster and more frequent runs did not [101, 109]. AF specifically was shown to have the same relationship with exercise by Andersen et al., with AF being the most common arrhythmia identified among the cross country skiers [108]. Elousa et al. identified that a total threshold dose of 1500 lifetime hours of sport practice a risk factor for AF [106]. Finally, exercise frequency of jogging bouts per week has been shown correlated with AF risk by Aizer et al. [110]. Therefore, a close relationship between physical activity (PA) duration, cumulative dose, frequency *and* intensity, and AF, exists.

Finally, exercise dose has also been showed directly related to cardiac damage. Specifically, high amount of work done per exercise bout, such as during marathon running, leads to increases in serological levels of cardiac damage biomarkers, such as Troponin and CRP [109]. The mechanisms underlying exercise induced AF will now be discussed.

1.5.1 Pathophysiological Mechanisms of Exercise and Atrial Fibrillation

Ventricular and atrial structural changes occur with exercise which lead to the increased risk of AF in high endurance athletes. The functional and structural adaptations of the ventricles

are well established and are collectively termed “athlete’s heart” [111, 112]. These changes depend on the type of exercise which can be either classified as isotonic/dynamic or isometric/static (**Figure 1-6**). Running and swimming are examples of dynamic exercise and increase oxygen consumption, and are therefore deemed as aerobic exercises [113]. One of the parameters effecting oxygen consumption (as will be discussed more in depth in the next section) is cardiac output (CO), which is determined by the stroke volume (SV) and HR [6, 113]. Modulation of SV and HR lead to structural and functional adaptations in the heart. These effect both atria and ventricles and include the following modifications which lead to AF: 1) chamber dilation, 2) electrical remodelling, 3) structural remodelling including fibrosis, 4) increased vagal tone which leads to APD heterogeneity, 5) gap junction remodelling and 6) inflammation. The mechanisms are similar to those found in regular AF pathology.

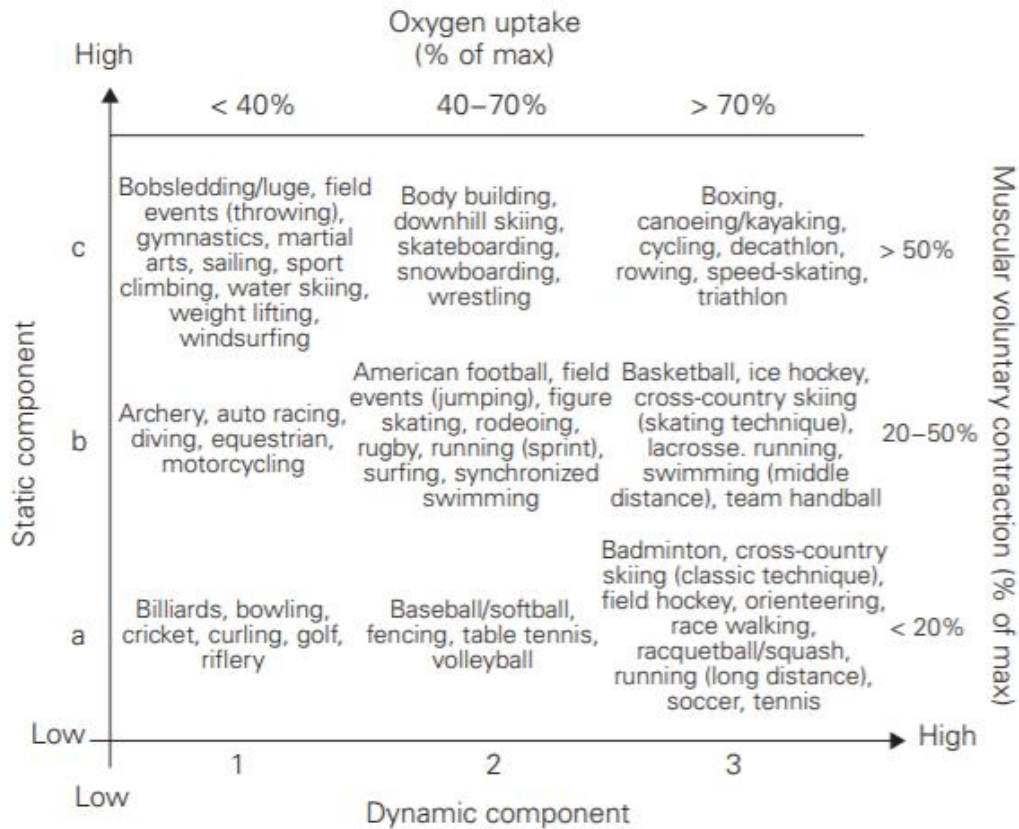


Figure 1-6. Exercise Classification – Exercise can be classified as either dynamic/endurance (involves changes in muscle length and joint movement with rhythmic contractions that develop a small muscular force) or static (involves no changes in muscle length or joint movement but develop a large muscular force). Dynamic exercise is also termed aerobic exercise and leads to increases in oxygen consumption. Swimming and running are examples of endurance exercise. Copyright©2006, Herz [113].

Acute and Chronic Ventricular Adaptations with Endurance Exercise

Increased cardiac dimensions in athletes were first mentioned in the 1890s – and confirmed later on with the introduction of the ECG [114]. Since then, multiple studies have noted increased ventricular hypertrophy and dilation in endurance exercise athletes and early works can be dated to the 1960s [114-119]. Increased voltages in ECGs are indicative of ventricular hypertrophy and dilation can be identified with echocardiographic measurements by

increased internal diameter. In fact, ECG pre-screening of athletes is practiced in some countries [120], especially because hypertrophic cardiomyopathy leads to sudden cardiac death in many athletes [121]. Nonetheless differentiation between adaptive or pathological changes is complex and beyond discussion here [120].

In athletes, cardiomyocytes respond the hemodynamic loads by stretching, leading to increased production of contractile proteins and subsequent hypertrophy. During dynamic exercise (i.e acutely), elevations in SV lead to increases in volume load (hypervolemia) and increases in CO cause higher pressure load [113, 122]. Fargard et al. employed cycling ergometry to assess LV adaptations and function during exercise in runners and non athlete controls. Increased ventricular dilation, ventricular diameter and contraction velocity occurred in athletes but remained unchanged in controls [123]. Such adaptations serve to contribute to increased SV in athletes [2]. Nonetheless, increases in ejections fraction (EFs) and fractional shortening (FS) during exercise are similar between athletes and non-athletes [123, 124]. Bar-Shlomo et al. suggest that untrained individuals attain increased ejection fraction through increases LV diastolic volume whereas trained individuals have decreases systolic LV volumes [124].

Chronic pressure and volume overload (such as with endurance exercise) leads to irreversible damage in the ventricles in the form of collagen deposition, cardiomyocyte apoptosis, contractile dysfunction and dilated cardiomyopathy [122]. Specifically, endurance athletes undergo eccentric ventricular hypertrophy where new sarcomeres are predominantly added in parallel, as opposed to in series [122, 125]. These adaptations appear as early as after 9 weeks of swimming exercise, and has been shown to decrease upon detraining [126-128]. These

changes can be monitored through echocardiographic evaluations as the left ventricular diastolic diameter (LVDd), left ventricular wall thickness, FS - the percentage change in the LV diameter with each contraction, and ejection fraction EF – the fraction of blood volume ejected at each beat relative to diastolic volume [129]. Specifically, athlete’s heart is characterized by a normal or below normal EF at rest [126], and similar trends for FS are described [130]. Finally, although the LV was more studied than the RV, RV dilation and hypertrophy has also been mentioned in endurance athletes and pertains the same changes associated with the LV [113].

Here, echocardiography will be used to assess ventricular dimensions and function during rest in anesthetized mice. In our previous swim models, we found a significant reduction in both FS and EF compared to control sedentary mice – which sets the expectations for this study as well [2, 19, 131].

Chronic Atrial Dilation and Stretch

Atrial dilation promotes AF through reentry mechanisms, by increasing the pathlength and promoting multiple wavelets [5, 75]. Nonetheless, some studies suggest that atrial dilation alone cannot promote AF, and is therefore only a substrate [132, 133]. Atrial stretch also leads to upregulation of other remodelling pathways including the renin-angiotensin pathway which leads to further atrial dilation, inflammation and oxidative stress, as well as apoptosis and de-differentiation – all of which have the potential to perpetuate AF (**Figure 1-7**) [4, 134]. These mechanisms are described in detail elsewhere [134].

Similarly to the ventricles, atrial volume and pressure loads occurring *during* dynamic exercise lead to increased stretch (elongation of the cardiomyocytes) as well as enhanced contraction. Overtime, these lead to dilation and increased wall thickness *chronically* [134, 135].

Both the RA and LA are effected by exercise and dilation has been shown in both [136]. LA dilation has been noted in 14% of bicyclists [137]. Mont et al. found interesting results from lone AF patients all of whom had LA dilation, whether they engaged in sports or not, when compared to sedentary controls [105]. Finally, Wilhelm et al. found a correlation with total lifetime exercise dose and atrial dilation [138]. Markers of atrial stretch, such as atrial natriuretic peptide (ANP), are directly correlated with atrial dilation coefficients and their elevations even appear to be associate with cumulative lifetime exercise dose [139]. Therefore, atrial enlargement is highly involved in AF pathogenesis in athletes [9].

It is possible to assess left atrial and PV adaptations via echocardiography in mice. Nonetheless, due to the small size, it requires high attention [140]. Our laboratory has attempted to assess atrial size, however we found that assessing atrial hypertrophy provides more consistent results by weighing. As such, in this study, atrial dilation will be assessed by weighing dry isolated atria, as we previously done [2].

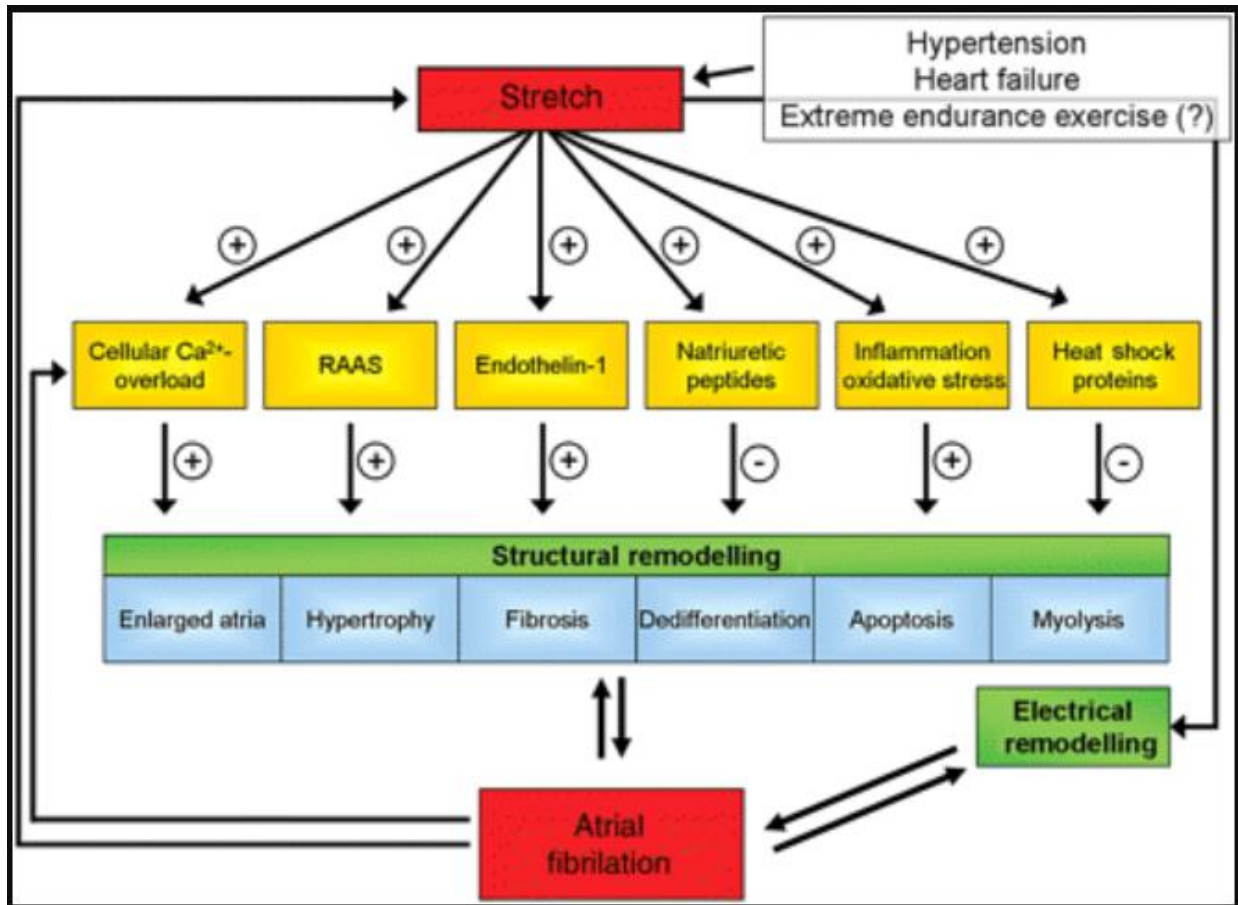


Figure 1-7. The Consequences of Atrial Stretch – During endurance exercise, atrial stretch occurs due to the volume and hemodynamic load increases in response to the increased cardiac output requirement. Extreme endurance exercise leads to high degrees of atrial stretch which activates multiple pathways leading to structural remodelling. Consequently, atrial fibrillation becomes more likely, especially with the electrical remodelling that accompanies high endurance exercise. Enlarged atria and hypertrophy leads to increased pathlength thereby enhancing reentry; fibrosis and apoptosis are related to inflammation and all of these lead to conduction blocks as well as increased pathlength; dedifferentiation occurs through expression of fetal genes, which lead to downstream activation of fibrillatory mechanisms; finally myolysis is the loss of contractile machinery in the cardiomyocytes which leads to contractile dysfunction. Copyright©2010, Cardiovascular Research [134].

Autonomic and Electrical Remodelling in Response to Exercise

During exercise, CO increases through both alterations in SV and HR [113]. In fact, HRs range from 40 bpm at rest, to 200 bpm at maximal exercise intensity [126]. During exercise, HR first increases by withdrawal of the PNS and at higher exercise levels due to further increase in by enhance SNS. Both of these responses increase in magnitude with the progression of exercise [141]. This is reflected in chronic autonomic remodelling in athletes. The hallmark of observation is decreased resting heart rate and HRs at submaximal exercise intensity levels, compared to non exercising controls [142]. Sinus bradycardia was first noted by White in long distance runners [114, 143] and since then, it was proposed that up to 90% of endurance athletes will have sinus bradycardia, with HR of <60 beats/min [144]. Although it is well accepted that sinus bradycardia results from autonomic remodelling in athletes [145], decreased HRs have also been attributed to intrinsic changes in the SA node [146, 147]. It appears that autonomic remodelling in athletes is dependant on cumulative exercise dose [138].

Such electrical and autonomic remodelling increases the prevalence of AF in athletes. Although vagal tone is not a common cause of AF pathology in the general population, it is extremely common in lone AF patients and athletes [19, 148]. Mont et al. found that 57% of lone AF episodes in endurance athletes were vagal stemmed, compared with only 18% in lone AF patients from the general population [105]. In fact, vagal stemmed AF is most common in endurance athletes [149]. Nonetheless, increases in stress level and enhanced sympathetic activation *during* exercise can also induce AF in athletes [148, 150]. Furthermore, Morseth et al. identified that individuals with sinus bradycardia and therefore vigorous physical activities, had the highest AF risk [10].

Functionally, vagal remodelling in athletes leads to decreased APDs and ERPs as well as increased APD heterogeneity [146, 148]. On a molecular level, autonomic remodelling predispose athletes to AF through enhanced Ca^{2+} loads [39], EADs and late phase III EADs [4, 42] during exercise. Whereas elevated vagal tone at rest leads to APD heterogeneity and reductions through $\text{I}_{\text{K ACh}}$ which predisposes to reentry [4, 9, 39, 146]. Alongside electrical and autonomic remodelling, gap junction remodelling has also been associated with exercise – however the data seems to be confounding. For example, Cx40 remodelling has been previously shown in running, but not swim exercised mice [2, 19].

In this study, sECGs will be used to assess RHRs. Concurrently, autonomic remodelling will be assessed during sECG studies through pharmacological blockade of the parasympathetic branch with intraperitoneal injections of atropine (an M2 receptor inhibitor) and the sympathetic branch with propranolol injections – as done in humans [145]. Furthermore, the influence of vagal tone on AF will be assess through administration of atropine which increases refractoriness and subsequently prevents vagal stemmed AF. Finally, APD will be quantified in isolated atrial experiments.

Inflammation and Fibrosis

Unlike the physiological responses of autonomic remodelling, dilation and hypertrophy (athlete's heart)– atrial fibrosis and inflammation are considered pathological responses [151]. Despite being generally accepted, research of increased fibrosis in athletes is lacking. Fibrosis is a proposed substrate of AF with exercise, but it is mostly identified using animal models [146, 149]. We were able to show that increased collagen deposition in atria behaved as a substrate for AF in swimming mice, which was abolished with either genetic ablation of $\text{TNF}\alpha$ or

administration of Etanercept (a TNF α inhibitor) – suggesting a causative relationship [2, 68]. Similarly, introduction of TNF α lead to mice increased fibrosis deposition without exercise as well as inflammation, demonstrated by expression of proinflammatory markers [152]. Finally, meta-analyses from human athletes suggests that cumulative exercise dose influences fibrosis deposition [153-155].

In accordance with fibrosis, atrial inflammation is also found in athletes but no direct correlation between inflammation, exercise and AF exists in human studies [149, 156]. Increases in IL-6, IL-1, and CRP post endurance exercise are known [149, 157] and meta-analyses indicate variable inflammatory responses to running doses [157]. Nonetheless, we previously observed increased macrophage infiltration with intense swimming exercise in mice, which was also associated with the TNF α cytokine and increased AF inducibility [2].

The relationship between exercise, inflammation and fibrosis is well established in skeletal muscle [19]. At the onset of exercise, neutrophil levels increase in response to the stretching of the muscle. This process is mediated by cytokines such as IL-1 and TNF α . Macrophages follow as well, and both types of inflammatory cells deposit in the ECM around the myocytes. Macrophages release IL-1 which further recruits more neutrophils. As previously discussed, macrophages release TGF β which upregulates collagen deposition in the myocytes as well as perpetuate the inflammatory response [158]. Despite being less characterized in cardiac muscle post exercise, the relationship between fibrosis, inflammation and arrhythmia is known and has been extensively demonstrated in myocardial infarction models [159].

Therefore, despite the lack of direct evidence, the link between inflammation, fibrosis, exercise, and AF is well accepted and it appears the exercise dose influences both

pathophysiological responses. Here, fibrosis will be quantified using the histochemical approach by staining sliced tissue slices for collagen using picrosirius red.

1.6 Exercise Quantification in Humans

Exercise quantification is important for training programs of elite athletes as well as for the health guidelines of the general population [7, 160]. Furthermore, the U shaped curve suggests that AF and the pathological mechanisms underlying it depend on exercise “dose” (i.e. intensity, frequency, total exercise dose and duration). To identify an accurate relationship between exercise and CVD risk, exercise amount should be quantified, a task dependent on the type of exercise conducted. Exercise can be divided into static and dynamic categories – depending on the involvement and activity of the skeletal muscles during exercise as well as based on the aerobic demands of the body during exercise [113]. As such, exercise activity can be characterized by two definitions and endurance training often has a high dynamic and a high aerobic component (**Figure 1-6**). Endurance/aerobic workload can be quantified externally - planning and questionnaires, or internally - through physiological measurements such as oxygen consumption (V_{O_2}), maximal oxygen consumption ($V_{O_2 \max}$), and metabolic equivalents (METs) [160]. These variables will be discussed in depth now. It is worth highlighting that other quantification methods include measurements of HR and Lactate production during exercise [160]. For example, HR or ~130 beats/min during exercise corresponds to the minimal exercise intensity which enhances CRF [161]. Nonetheless, such quantification methods are beyond discussion here.

1.6.1 Endurance Exercise Quantification – Oxygen Consumption

A more uniform means of quantifying endurance exercise is V_{O_2} as aerobic exercise poses an increased demand in oxygen supply [113]. V_{O_2} is expressed in the units of volume of oxygen consumed per unit time normalized by weight ($\text{mL O}_2 \text{ h}^{-1} \text{ kg}^{-1}$) often at standard temperature and pressure conditions. Aerobic exercise quantification is based on oxidative respiration whereby glucose and other molecules are converted to energy in the form of adenosine triphosphate (ATP), through a reaction with oxygen [162] (**Equation 1**).



The equation for V_{O_2} is termed Fick's principle, and is the product of the arteriovenous oxygen difference ($(a-v)\text{O}_2\text{D}$) and CO , both of which change as training progresses [113]. The increase in V_{O_2} during exercise can be divided into three phases. Phase 1 occurs during the first 15-25 seconds of exercise onset; here, increases in V_{O_2} can be attributed to CO modulation [113, 163] which can be ascribed to increases in both HR and SV. SV changes by 1) an increase in end diastolic volume, as per the Frank Sterling mechanism, and 2) decrease in the end systolic volume, due to enhanced contraction of the myocardium [113]. Phase 2 is an exponential increase in V_{O_2} related to work rate conducted by the skeletal muscles [163]. As such, $(a-v)\text{O}_2\text{D}$ is a predominant factor during this phase [113, 142]. Phase 3 is a steady state V_{O_2} , whose absolute value is dependent on the exercise intensity. This steady state is not $V_{O_2 \text{ max}}$, but rather the steady state V_{O_2} supplementing the oxygen deficit - the differences between resting V_{O_2} and the steady state exercise V_{O_2} . Oxygen deficit represents the amount of the oxygen demand supplied by other anaerobic processes until the increased oxygen uptake can supplement this oxygen demand again [163]. Severe and extreme endurance exercise increase the threshold

steady state of V_{O_2} . The modulation of the threshold at increased exercise intensities is dependent on the anaerobic threshold – the limit at which aerobic respiration in the muscles is also supplemented by energy from other sources, such as lactate metabolism, as well as fatigue at which point $V_{O_2 \max}$ is attained [163, 164].

1.6.2 Endurance Exercise Quantification – Maximal Oxygen Consumption

Chronic training leads to increased $V_{O_2 \max}$, a measurement of CRF, through modification in the training induced adaptations of the heart, modifications of the peripheral circulatory structures, the function of the skeletal muscles and the regulation by the autonomic system [113, 142]. For example, one of the limiting factors of $V_{O_2 \max}$ has been postulated as the skeletal muscle mitochondrial volume numbers and mitochondrial enzymes levels – the rate of cellular oxidative respiration [142, 165]. Furthermore, the increased fiber density in the skeletal muscles decreases the velocity of blood in the capillary beds and enhances O_2 exchange [165]. In fact, $(a-v)O_2D$ is often increased due to decreased venous O_2 concentrations [142]. Interestingly, SV reaches a threshold at 40-50% of $V_{O_2 \max}$ suggesting that HR modulation is extremely important for increases in CO [163]. Consequently, maximal HR plays a dominant role in attainment of $V_{O_2 \max}$ [166]. Nonetheless, SV and ventricular size are also increased in individuals with higher CRF ($V_{O_2 \max}$) [167].

1.6.3 Endurance Exercise Quantification – Metabolic Equivalents

Relative exercise quantification is completed via the METs [101, 113, 168]. A MET in human studies is defined as energy costs associated with aerobic exercise divided by the basal metabolic rate (BMR, can also be referred to as resting metabolic rate (RMR)), measured during sitting calmly [168]. This BMR has been estimated for a 70kg person as a V_{O_2} of

3.5 mL O₂/kg/min [113, 168]. METs have been quantified for many activities, ranging from household movements to extreme endurance exercise and were published in a collective report in 1983 by Bouchard et al. for the Canada Fitness Survey [168, 169]. METs of aerobic exercise, such as swimming or running, depend on the speed of movement, the resistance and/or the mass lifted (i.e load). For example, the MET value of swimming vary from 4.3 to 13.6, with speeds ranging from 2 to 4 km/h [168]. METs are extremely useful to prescribe activities based on persons V_{O₂ max}, which could also be measured in METs. Maximal MET is directly correlated with the PA levels preformed, meaning that PA and CRF are intrinsically related and either one can be used to assess exercise capacities [113, 168]. For example, a person whose maximal capacity is 6 METs can be assigned a range of activities with METs of 1-6, with such recommendations often adjusted for sex and age [168].

Nonetheless, the METs method has its setbacks. For example, BMR is not a set value and varies depending on sex, age and body fat composition [168]. Furthermore, exercise has the potential to alter BMR. Ample of studies have shown conflicting findings of changes of BMR with endurance exercise [170]. For example, Gilliat-Wimberly et al. suggests that BMR increased in women participating in 9 hours of activity per week, compared to sedentary [171]. In fact, Sullo et al. showed that BMR increases are associated with higher CRF in elite athletes, supported by another study by Bryne and Wilmore [172, 173]. On the other hand, studies also suggest a decrease in BMR younger individuals [174] or no overall significant changes in athletes [173]. Such differences could potentially be attributed to sex, age, genetics as well as exercise mode [175]. Nonetheless, METs provide an easy and quick guideline which could be used with caution [168, 175].

1.6.4 Current Recommendations – Exercise Quantity and Health

Exercise recommendations on the quantity and intensity for the general population exist and have been published a while ago. For example, the World Health Organization (WHO) recommend at least of 150 minutes of moderate intensity or 75 minutes of high intensity aerobic exercise a week – or an equivalent combination of both [101]. To compile these recommendations the WHO collected data from various reviews and included considerations of all cause mortality, musculoskeletal, metabolic and cardiovascular health as well as epidemiological outcomes. The Canadian Society for Exercise Physiology (CSEP) even suggest performing such activity in 10-minute bouts. Interestingly, they explicitly state that “more physical activity provides greater health benefits” despite the now known U shaped curve [176]. Pollock suggests that such guidelines should not be prescribed in general and different guidelines should fit unique predispositions such as sex, age, and other underlying health related conditions [161].

1.6.5 Exercise Quantification and Atrial Fibrillation

Nonetheless, the recommendations above are well below that of endurance athletes’ performance and AF prevalence increases at higher exercise doses. Many studies depend on external means of exercise quantification – specifically using surveys of PA [160]. For example, Lee et al. quantified heavy running dose as >6 hours a week whereas Schnohr et al. provided an upper limit of 4 hours or more [101, 177]. La Gerche, suggests that elite athletes exercise 15-40 hours a week [178], way above the limits collected from the two former studies. Nonetheless, all studies identified increased CVD risk at the provided higher limits. La Gerche and Schmied attempted to “guesstimate” the relationship between exercise intensity and AF through data

reconstruction from three separate studies. They suggest that questionnaires are biased given that individuals with higher fitness will rate exercise intensity differently from less fit individuals [179]. Here, data was summarized from Mozaffarian et al. (pace of leisure time walking) [180], Aizer et al. (jogging frequency) [110], and Andersen et al. (frequency and pace of cross country skiing competitions) [108] – all of which employed questionnaires to collect their data. La Gerche and Schmied concluded that low intensity exercise decreased AF risk whereas moderated and high intensity exercise lead to a gradual increase in AF prevalence [179]. Khan et al. also suggests that questionnaires are often biased and employed $V_{O_2 \max}$ (CRF) to assess the correlation between AF and exercise. Here, AF risks increased with maximal METs above 9.3 [181]. Interestingly, a review by Merghani et al. describes increases in AF risks above 12 METs, with most athletes exercising at 15 METs or above [96]. Even though CRF is known to be correlated with exercise dose [101, 182-184], such studies do not directly assess PA which in itself is also an important factor, especially for AF pathogenesis [185].

Therefore, it appears that AF depends on multiple variables of exercise such as intensity, duration, and frequency. Nonetheless no study quantified PA in a controlled manner (internally) to identify its' association with AF risk, and therefore empirical data suggesting how exercise dose parameters influence AF independently is lacking. Finally, suggested mechanisms underlying the relationship between exercise dose and AF in athletes is lacking. Here PA will be adjusted by varying swim durations from 60 to 120 minutes, while maintaining the total cumulative dose, the exercise frequency and intensities identical between groups. Quantification of exercise will be derived from V_{O_2} as described in **Appendix A and B**.

1.7 Exercise Quantification in Mice

Dogs, pigs, mice and rats are employed for exercise models, the most common being the latter two [186]. The model organism, exercise and measured parameters should all be considered when animals are used to model human exercise.

Mice are commonly used in experimental settings due to the high similarity in physiology, metabolism and genome to humans – without the higher cost associated with rats [162]. Various exercise models can be employed in the mouse model and CD1 mice specifically are internally motivated to exercise in both voluntary (freewheel running) and involuntary exercise (treadmill running and swimming) [131, 162, 187]. Age is an important consideration with mice where maturation starts to slow around 42 weeks, and weight increases relatively slowly thereafter [188]. Exercise abilities appear to be dependent on age. For example, Chappell et al. identified 22% decreased in CRF (measured in $V_{O_2 \max}$) between 100 day old and 5 year old mice, despite no significant differences in BMR [189]. Similarly, Schefer and Talan found that adult (12 month old) mice and old (24 month old) mice had different CRF, V_{O_2} (physical abilities), as well as running speeds [162, 190]. Here, swimming duration was varied to alter exercise dose in mice starting at an age of 42 weeks (6 weeks).

The exercise protocols in the animal should mirror that of exercise in humans when assessing CVD and other cardiovascular parameters. As such, duration, intensity, frequency and exercise modality should be carefully considered. Exercise in mice has 3 phases: exercise training (acclimatization), the appropriate exercise protocol and finally rest prior to phenotypical assessment [186]. Exercise is usually completed at $\sim 75\% V_{O_2 \max}$ with many of the mice models employing treadmill running and swimming [186]. Many different models of exercise were

conducted in mice with short term periods (<4 weeks) and long term periods (>9 weeks), with swimming bout durations from 30 minutes and up to 3 hours [2, 68, 131, 186, 191, 192]. In fact, swimming duration is the most commonly employed parameter to vary exercise capacity in mice [186, 191], with cardiovascular adaptations appearing as early as 2 weeks [2]. Although swimming could be considered stressful for the animal, we were previously able to show that no such stress related response was found in either our running or swimming mice [131] and that CD1 mice are intrinsically motivated to swim against a steady water current [2, 19]. On top of preventing simulation of drowning which occurs with attaching tail weights to the swimming animals or bubbling the water, this mode of exercise also averted inadequate swimming behaviours such as bobbing and diving [19, 193, 194]. Bernstein suggests that disadvantages of swimming exercise in mice are related to the difficulty in measuring cardiovascular parameters, the difficulty in exercise intensity quantification, and the lack of graded workload protocols [191]. Nonetheless, a custom-built quantification apparatus was prepared here and quantification was also previously used by Kaplan et al. [195]. Additionally, cardiovascular parameters can be assessed using implanted telemetry units *during* exercise and abundant protocols *post* exercise [2, 68, 191]. As such, swimming is an appropriate model for endurance exercise in mice and will be also implemented here.

1.7.1 Oxygen Consumption in Mice

As previously discussed, exercise quantification can be done externally (planning and questionnaires) or internally (through physiological measurements) [160]. In animal models internal exercise quantification is completed via either direct or indirect calorimetry methods (respirometry), given the outcome of all metabolic activity is either heat or work [162, 191, 196].

Direct calorimetry measures the heat produced by the animal during metabolic activity whereas respirometry measures the component that generate heat according to **Equation 1** [162, 196] similarly to V_{O_2} measurements in humans [113, 162, 197]. In direct calorimetry, heat produced during activity can be quantified according to **Equation 2** [196].

$$\text{Heat} = Q_w + Q_a + Q_m \quad \text{Equation 2}$$

Where, Q_m denotes heat detected by the direct calorimetry equipment, Q_a denotes heat of dry air, and Q_w denotes heat carried by water vapor. The extensive calculations for each can be found elsewhere and are beyond discussion here [196].

Respirometry uses the principle of oxidative respiration and can be completed in either open or closed calorimetry systems [198]. Similarly to humans, V_{O_2} is effected by CO, SV, HR and (a-v) O_2D in mice [191]. For example, HR has been measured in swimming mice before, and seems to peak and plateau quickly after 3-10 minutes [2, 191, 195]. The hypothesized maintenance of constant HR during longer periods of swimming exercise suggests that it is a constant workload exercise, resulting in submaximal levels of intensity [191] however measurements of HRs during prolonged swimming exercise in mice is not well characterized.

V_{O_2} is then converted to heat using either the stoichiometry provided in **Equation 1**, or through employment of the respiratory exchange ratio (RER) – the ratio between carbon dioxide produced and oxygen consumed – which changes based on the primary energy molecule used (i.e fats, carbohydrates, fats). For example, energy production associated with 1 gram of glucose is 15.7kJ whereas 1 gram of fat produces 37.7kJ, suggesting a correction to V_{O_2} could be necessary [199]. Four studies found an agreeable increase from 81 kJ/L oxygen to 87 kJ/L oxygen when the RER is increased from 0.7 to 1.0 [199-203]. Specifically, RER is employed to calculate heat production from V_{O_2} according to **Equation 3** [196] or correct V_{O_2} according to

Equation 4 [204]. Although RER can be calculated through the simultaneous measurement of carbon dioxide production rate (V_{CO_2}) or by an assumption of an RER value of 0.85, it is not necessary. Chappell et al. found that RER values from 0.7 to 1.0 produce no significant differences in calculations with only 3% error [204]. In fact, 0.85 is the exact median between the RER of active (0.88) and anesthetized mice (0.83), found by Burnett et al. - values that are similar to humans as well as other larger animals [191, 196, 204, 205].

$$\text{Heat} = V_{O_2} * (1.232 \text{ RER} + 3.815) \quad \text{Equation 3}$$

$$V_{O_2} = F * \left(\frac{\%O_{2in}}{100} - \frac{\%O_{2out}}{100} \right) / \left(1 - \frac{\%O_{2out}}{100} * (1 - \text{RER}) \right) \quad \text{Equation 4}$$

Where, F is the inflow rate in the units of volume per unit time, and %O_{2in} and %O_{2out} are the percent values of oxygen measured inflowing and outflowing from the measuring chamber.

Other exact calculations employed in respirometry have been previously derived and modified, and were employed to calculate V_{O_2} here, as discussed in **Appendix A and B** [162, 198, 199, 206].

1.7.2 Direct vs. Indirect Calorimetry (Respirometry)

There are disadvantages and advantages to each method. Although there is only one assumption associated with direct calorimetry, it is a significant one – heat storage by animal is assumed negligible [162, 196]. There is a 10% error associated with even 1 degree Celsius for a mice weighing 30g due to the innate nature of heat retention [162]. Furthermore, the method is very tedious and quantification of measuring small heat quantities is extremely challenging [162]. And finally, the method does not provide any information with regards to the oxidized substrate [207].

Respirometry on the other hand is only associated with assumptions that can be corrected mathematically, despite their abundance [196]. Three of these assumptions are related to molecular mechanisms - CO₂ production, macromolecule utilization and protein digestion. All of these can be corrected by RER [162, 196, 204]. RER is known to be effected by diet, which also effects the thermic cost of absorption and digestion, as well as the body fat composition [199]. Nonetheless, Tschop et al. suggests even when chow differs in composition, dietary effects are minimal if the mice consume the same diet and are stored within the same facility [207]; and Speakman mentions that protein oxidation is negligible, inducing only small errors [162]. To refute food consumption as a confounding variable, food weight normalized by body weight, daily food consumption rate and diets were monitored in this study. Furthermore, the method assumes anaerobic metabolism is negligible [196], however the kinetics of V_{O2} during exercise intrinsically reflect oxygen deficits and anerobic thresholds [163, 208]. Additionally, the weight of the animals can be variable and body composition directly effects V_{O2} as different organs have different metabolic rates [199]. This was empirically measured in a famous study by Elia et. al in 1992 [209]. For example, at rest, skeletal muscles utilizes 13kcal/kg whereas adipose tissue utilizes 4.5kcal/kg, but these vary with the amount of adipose tissue in the body, the gender and age [209]. Nonetheless, such differences can be accounted for in mice if weights are measured at the post-absorptive stage of digestion, after rest and at a thermoneutral environment [199]. To this end, Speakman suggests than V_{O2} can be calculated for lean body mass through a division by the mass to the power 0.75 [162]. In this study all the mice are age matched, housed in identical environments, weighed at identical time points of the day and are age matched – therefore such setbacks can be considered negligible. Finally, many environmental conditions must be controlled and measured [162, 199]. These include pressure, humidity and temperature [162,

196, 199]. Temperature does not only effect the measured V_{O_2} , but, as suggested by Speakman, also alters the contribution of heat to warm or cool the mice if they are not in their thermoneutral zone – the environmental temperature most preferred by the animal. In fact V_{O_2} has a strong relationship with ambient temperature to maintain the body temperature of mice constant at $\sim 37^\circ\text{C}$, similarly to other homeotherms with a body temperature of $37\text{-}39^\circ\text{C}$ [162, 199]. The thermoneutral zone for mice has been previously identified as $26\text{-}32^\circ\text{C}$ [162] (**Figure 1-8**), which is the temperature range employed during swim exercise here. Furthermore, many systems –such as the Oxymax by Columbus Instruments which is used in our study - are equipped with hardware that corrects for environmental conditions and corrects them to standard pressure and temperature (STP) conditions [162] and data can be corrected for these conditions manually as well [196].

As such, respirometry remains the most frequent exercise quantification method in mice. It is worthwhile to mention that both direct and indirect calorimetry yield very similar results and allow for accurate comparisons between different groups of mice if the *same* method is employed across all study groups [196].

1.7.3 Metabolic Equivalents in Mice and Basal Metabolic Rates

Technically, METs can be also calculated for mice, given the availability to measure BMR in mice. This approach is often employed and is considered a normalization for energy expenditure measurements in the mice, and therefore, corrects for any differences related to size, gender or body composition [199]. Nonetheless, there is no set value for BMR in mice such as in humans. BMR in mice reflects energy expenditure on the maintain minimum vital bodily functions and the thermic effects of food [210]. Nonetheless, BMR does not fluctuate with body

mass for rodents of the same age, gender and strain – suggesting that such correction is not necessary for all types of studies [199]. Furthermore, Speakman suggests that a temporal resolution is of high importance for correct V_{O_2} measurements – especially when V_{O_2} is measured for BMR [162, 210]. For example, if the time frame for data collection is too low, noise associated with the equipment may interfere with the results but if the time frame is too large, PA may interfere with BMR quantification [162]. Temporal resolution is reflected in the time constant of the apparatus – the response time of the equipment. Even et al. suggests a rule of thumb: “the time required by a system to respond to 95% of the change in %O₂ and %CO₂ is equal to three times the cage volume divided by the flow rate through the chamber” but can also be found empirically [199]. For example, by varying sampling rate and inflow rates as was completed previously [210]. BMR could however change with exercise as was suggested by an ample of human studies, previously discussed [170]. Nonetheless, BMR will not be measured here because only male CD1 mice (identical strain) are employed and environmental conditions are identical for exercise groups. Furthermore, PA, and not only METs, is related to CVD risk and AF suggesting quantification of exercise is sufficient for our conclusions [7, 10, 101, 178, 211].

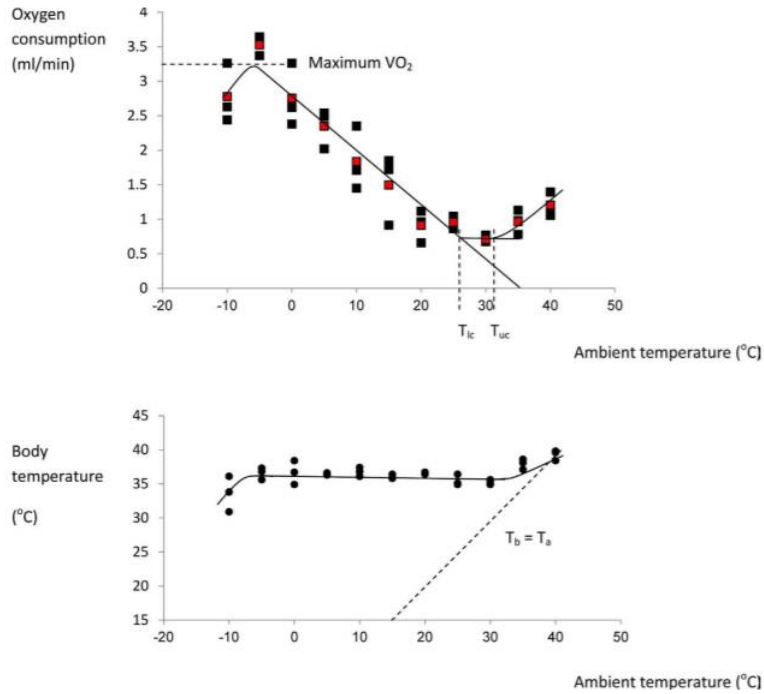


Figure 1-8. The Thermoneutral Zone of Mice and their Body Temperature – Top panel shows the thermoneutral zone of mice as between the lower critical (T_{lc}) and upper critical temperatures (T_{uc}). Basal oxygen consumption was collected from multiple mice, at different ambient temperatures. A thermoneutral zone of 26-32°C was identified – at this range mice do not use energy to heat or cool their body. The bottom panel shows the body temperature of the mice at different ambient temperatures. As endotherms, mice tend to keep their body temperature at 37-39°C. Copyright©2013, Frontiers in Physiology [162].

1.8 Synopsis and Hypothesis

The adverse effects of exercise on the heart are now well accepted and the number of individuals participating in endurance exercise is only rising. Even though exercise is generally beneficial, there is a dose-dependent relationship between exercise and its influence on AF perpetuation and manifestation. Furthermore, even though there are widely accepted adaptations that occur with exercise that lead to AF (such as increased vagal tone and atrial enlargement), their dose dependent relationship of these with AF on exercise is weakly characterized.

I hypothesize that i) Atrial remodeling and AF will follow a dose dependent relationship with exercise dose *and* ii) the pathophysiological mechanisms underlying AF will differ depending on exercise dose. Based on this hypothesis, the objectives of this study were:

- 1) Develop a means to quantify exercise in swimming mice,
- 2) Characterize the dose response relationship between exercise dose and AF
- 3) Identify the pathophysiological mechanisms underlying AF at different exercise doses

Chapter 2

2. Materials and Methods

2.1 Experimental Animals

CD1 mice were ordered from Charles River at 5 weeks of age and allowed to acclimate in the Farquharson Life Sciences Animal Facility at York University for 1 week. Thereafter, mice were randomized into two groups: swim exercise and control sedentary, as described in greater detail below. After completing the swim exercise, mice were phenotypically assessed over the next 7 days. All sedentary control mice were 14 weeks old during phenotypical assessments. All experimental protocols conformed to the standards of the Canadian Council on Animal Care.

2.2 Exercise Protocols and Exercise Quantification

We previously established that CD1 mice swim vigorously against water current (20L/min) when placed into swim tanks [2, 19] and employed a similar approach here. The water currents were supplied by a submersible pump (Everbilt Submersible Utility Water Pump, Home Depot Product Authority, Atlanta, GA, U.S.A or 12V Shoreline Bilge Pump 800 Gallon Per Hour, Rule Industries, Gloucester, MA, U.S.A) placed into the swim tanks (**Figure 2-1A and 2-1B**) with flow rates controlled by a speed controller (DC Motor Speed Controller (PWM) Speed Adjustable Stepless Governor Regulator, Walfront Electronics) (**Figure 2-1C**). Swimming in the presence of water currents avoids behaviours such as bobbing and diving [19, 193, 194] and complications associated with attaching weights to mouse tails which is used to simulate drowning conditions [194]. The swim tanks were either “open air” or enclosed by a transparent top to allow oxygen consumption rates to be quantified (**Figure 2-1**). At all points of the swim exercise temperature was maintained at the thermoneutral zone of mice (30-32°C) [162].

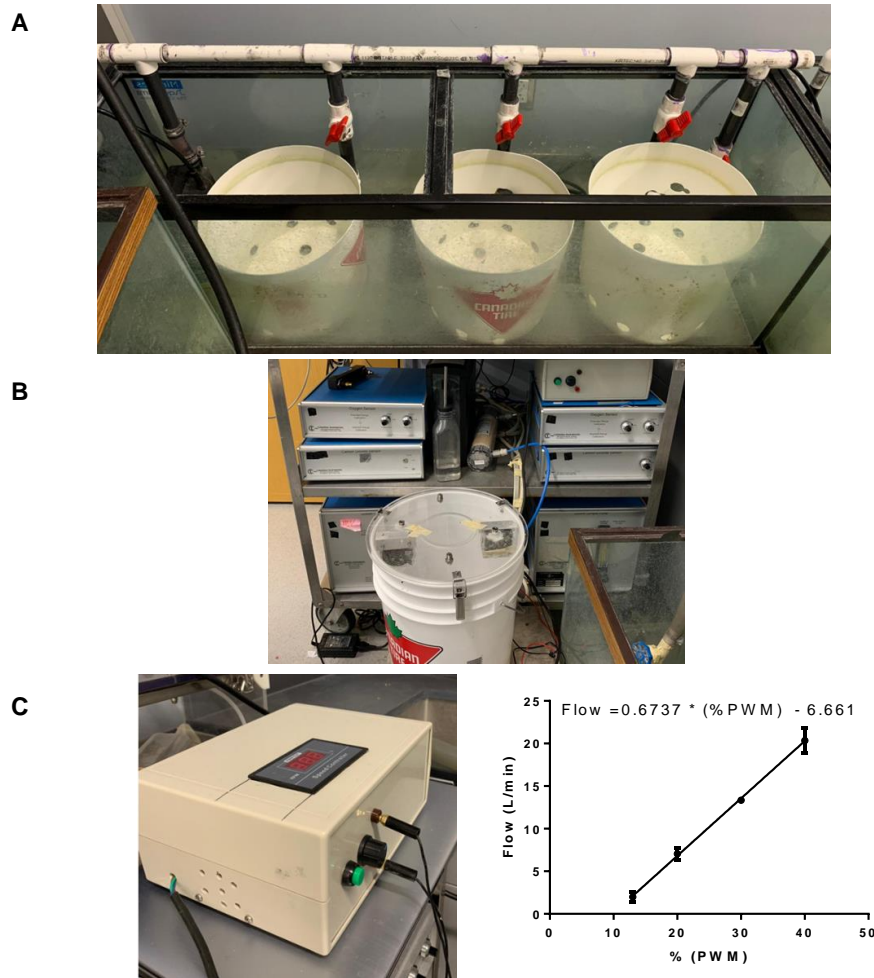


Figure 2-1. Mouse Swimming Exercise Apparatus and a Modified Oxygen Consumption Apparatus – A) Mice were usually swam against a current generated by a water pump (Everbilt Submersible Utility Water Pump, Home Depot Product Authority, Atlanta, GA, U.S.A) in round tanks within custom designed frameworks at 30-32°C water temperatures. The current prevented floating behaviour and promoted swimming exercise behaviour. B) A modified swimming apparatus was connected to a calorimetry system for oxygen consumption measurements (Oxymax, Columbus Instruments, Columbus, OH, U.S.A). C) Current to the modified swimming apparatus was generated in this apparatus using an individual water pump (12V Shoreline Bilge Pump 800 Gallon Per Hour, Rule Industries, Gloucester, MA, U.S.A). The pump was connected to a speed controller in a custom designed protective box (DC Motor Speed Controller (PWM) Speed Adjustable Stepless Governor Regulator, Walfront Electronics). A calibration curve was generated for the PWM.

Exercise protocols were designed to study the influences of exercise durations while maintaining total exercise effort, frequency, and intensity of exercise similar. Acclimatization was initiated at 10 minutes a day, for 1 swim and increased by 10 minutes every day until the required swim bout duration was reached. For mice swimming at 120-minute swim bout durations, two swims were completed on the second week with an increase of 10 minutes per swim bout (**Table 2-1**). Variable swim durations (from 60 minutes and up to 3 hours) were previously employed in swimming mice models [186, 192] and 90 minute swim bouts were previously employed in our swim model . Therefore, we swam mice at 60-, 90- and 120-minute bout durations. Exercise was quantified by first measuring oxygen consumption (V_{O_2}) which were then used to calculate daily energy expenditure (volume of O_2 consumed per day during swim) and total exercise effort (total consumed O_2 during swimming) as described in **Appendix A and B**. Shortly, aerobic exercise, such as swimming, increases energy production from oxidative respiration. Consequently, respirometry employs calculations of energy expenditure during exercise from V_{O_2} [196]. Although respirometry is not often used to quantify energy expenditure in swimming mice [191], a modified respirometry Oxymax system was used here for V_{O_2} quantification (Oxymax, Columbus Instruments, Columbus, OH, U.S.A) (**Figure 2-1** and **Figure 2-2**). Preliminary assessments revealed accuracy and reproducibility of data with such hardware modifications which allowed us to quantify swimming exercise. Mice underwent swimming exercise twice a day at the assigned swim bout durations with swims numbers titrated to maintain equivalent integrated doses/effort relative to the reference, 6 weeks, 90-minute swim group (**Figure 2-3**). Therefore, we had mice swimming for 120 minutes/day, 180 minutes/day or 240 minutes/day for a variable number of weeks.

Maximal oxygen consumption ($\text{VO}_{2 \text{ max}}$) was assessed by selecting random mice (minimum 6) from each exercise regime. Forty-eight (48) hours after the final swim bout, these mice underwent testing in a modified swimming apparatus equipped with a column which promoted swimming at the periphery (where the current is the highest). Mice were swam individually starting at 15 L/min and water current was increased by 5% using a speed controlled (**Figure 2-1C**) until exhaustion marked by inability to swim and progressive decreased in measured VO_2 . $\text{VO}_{2 \text{ max}}$ was quantified using data from peak performance.

Table 2-1. Training Regimes of Mice Undergoing Three Different Swim Bout Duration Exercise Protocols – Three final swim bout durations were employed depending on the exercise protocol: 60 minutes, 90 minutes and 120 minutes swim bouts. Three different acclimatization protocols were employed within 2 weeks. For the 120 minutes swim bouts, two acclimation swims were completed a day: one in the morning (9am) and one the in afternoon (3pm). The training regimes are outlined below in increasing order. Exercise protocols were initiated the following day and carried to the required weekly duration, depending on the exercise regime.

Final: 120 minutes/day	Day 1	Day 2	Day 3	Day 4	Day 5	Day 6	Day 7
Week 1	10 min	20 min	30 min	40 min	50 min		
Week 2	60 min						

Final: 180 minutes/day	Day 1	Day 2	Day 3	Day 4	Day 5	Day 6	Day 7
Week 1	10 min	20 min	30 min	40 min	50 min		
Week 2	60 min	70 min	80 min	90 min			

Final: 240 minutes/day	Day 1	Day 2	Day 3	Day 4	Day 5	Day 6	Day 7
Week 1	10 min	20 min	30 min	40 min	50 min		
Week 2	60 min	80 min	100 min	120 min			
	70 min	90 min	110 min				

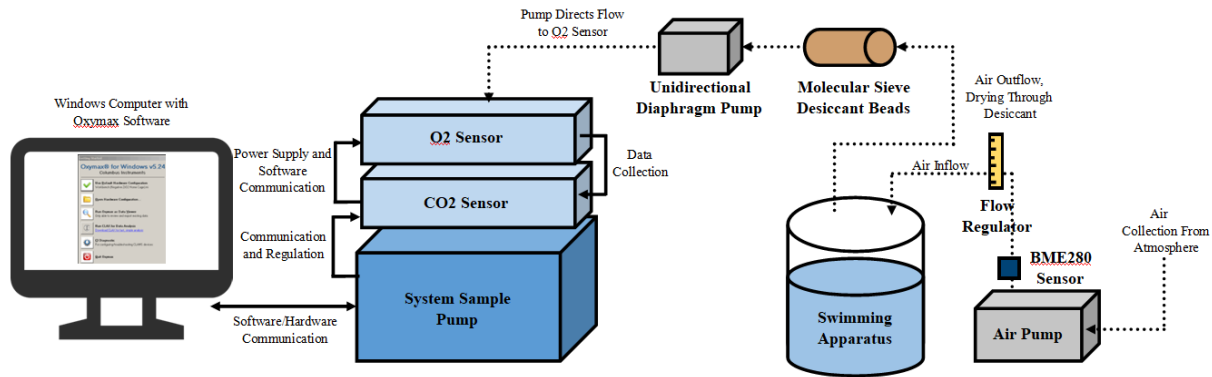


Figure 2-2. Modified Oxymax Setup – To allow for independent oxygen sensor function the calorimetry system (Oxymax, Columbus Instruments, Columbus, OH, U.S.A) was adapted and modified as shown above. Gas collection was directed immediately to the “O2 Sensor”. This way, excess flow through the CO2 sensor and the system sample pump were averted. Shorter air distance allows for a shorter response time and higher temporal resolution. This arrangement also allowed for continuous control of inflow rate regulation, as well as monitoring of environmental conditions of temperature, humidity and pressure by a BME280 sensor (Adafruit Industries, New York, NY, U.S.A). If carbon dioxide monitoring is required in the future, the CO2 sensor could be connected in line with the O2 sensor. Dashed lines indicate gas flow, bold lines indicate electrical communication.

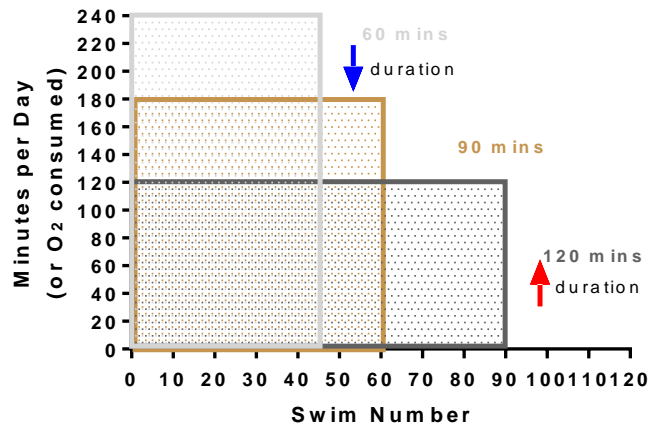


Figure 2-3. Schematic Representation of Exercise Protocols – A) Mice were swam according to three different regimes to assure exercise duration was varied as either 60, 90 or 120 minutes/swim (120, 180 and 240 minutes/day) but cumulative exercise work was maintained identical. modules of swimming exercise. The theoretical approach is presented. The areas under the curve are identical.

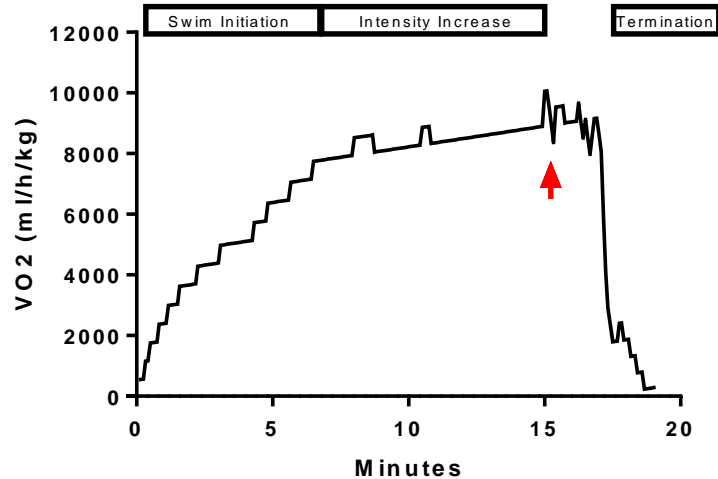


Figure 2-4. Typical Recording During VO₂ max Testing – Six to nine (n=6-9) mice were randomly selected from each group and subjected to VO₂ max testing. Each mouse was placed individually within a modified swimming apparatus equipped with a column promoting swimming at the periphery where water current was the highest. This prevented self regulatory behaviour such as bobbing and floating which occur in areas with low water currents (such as the middle of the swimming apparatus). Swims were initiated at 15 L/min water currents (for the first 5-10 minutes of the swims) and increased thereafter incrementally using a speed controller, as shown in the figure with a progressive increase in oxygen consumption (VO₂). Maximal oxygen consumption (VO₂ max) was marked by a sudden peak in VO₂ with a decrease thereafter. The VO₂ max is marked with a vertical arrow. The data within 15 seconds before and after peak performance were employed as the VO₂ max of the mouse.

2.3 Echocardiography

Functional and anatomical changes associated with endurance exercise are collectively termed “athletes’ heart” and include ventricular enlargement and reduced ejection fractions at rest [212]. Echocardiography provides non-invasive means to assess these parameters. Dilation is assessed through ventricular diameter measurements (LVDd), and hypertrophy is assessed through left ventricular wall width (LVPWWth) [129] or weighting dry ventricular weights (VW) [2]. Functional parameters such as ejection fraction (EF) and fractional shortening (FS) provide information on the systolic function. Fractional shortening (FS) is the percentage change in the LV diameter with each contraction, and ejection fraction (EF) is the fraction of blood volume ejected at each beat relative to diastolic volume [129]. Echocardiography was used to assess these parameters.

Control and exercised mice were anesthetized using a 3% isoflurane/oxygen mixture and placed on a heated pad in the supine position. Body temperature was maintained at 36.9-37.2°C and monitored using a rectal temperature probe. The pad also contained Lead II surface ECG probes which were connected to the echocardiography equipment (VisualSonics Vevo 770, VisualSonics Inc. Toronto, ON, Canada). Chest fur was removed using depilatory (Veet, Reckitt Benckiser, Slough, United Kingdom or Nair, Church & Dwight, Princeton, NJ, U.S.A). A layer of ultrasound, acoustic coupling gel was applied to the chest wall and re-applied as needed (Aquasonic 100, Parker Laboratories Inc. Fairfield, NJ, U.S.A). B Mode (two-dimensional) examinations were used to position the probe parallel to the long axis of the left ventricle (LV). Once the probe was positioned as necessary, isoflurane concentration was decreased to 1.5%. LV diastolic and systolic diameters (LVDd and LVDs) as well as LVPWWth were measured in

M-Mode and confirmed using the ECG screen. EF and FS were also measured in M-Mode. EF was calculated from $(EDV-ESV)/EDV*100$ whereby volumes were derived from ventricular diameter measurements assuming an ellipsoid shape of the ventricle [129]. All M-Mode examinations were measured twice, and the average of the data was used for analysis, for each mouse. A minimum of 10 randomly selected mice from each exercise regime group were used for echocardiographic analysis.

2.4 Surface ECGs in Anesthetized Mice

Exercise induced sinus bradycardia is a hallmark observation in endurance athletes [142] and therefore we assessed whether swimming induced decreases in resting HRs in anaesthetized mice. Adaptations leading to decreased heart rate have been proposed as autonomically modulated. Therefore we employed pharmacological blockade by atropine sulphate and propranolol hydrochloride to block the parasympathetic and sympathetic branches, respectively, as commonly done in humans [145].

Mice were placed in a sealed chamber connected to an isoflurane vaporizer (EZ-155KF Key Fill Isoflurane Vaporizer, E-Z Systems, PA, U.S.A). Isoflurane was kept at 3% until mice were immobilized which took approximately 1 minute. Subsequently, mice were placed on a custom-built heating pad supplied by heated water from a laboratory water bath. Mice were kept in the supine position and temperature was monitored using a rectal probe (THM 150, VisualSonics Inc. Toronto, ON, Canada). Body temperature was maintained at 36.9-37.2°C. Isoflurane was lowered, and ideal anaesthesia was achieved at approximately 1.5% isoflurane and a leg-twitch reflex was used to assure minimal anaesthesia [19]. Lead II surface ECG (sECG) was conducted using platinum subdermal needle electrodes (Genuine Grass® Reusable Subdermal Needle

Electrodes, Natus Medical Incorporated, Pleasanton, CA, U.S.A) connected to an amplifier (Gould ACQ-7700 amplifier, Data Science International, New Brighton, MN, U.S.A). Data was collected using Ponemah Physiology Platform acquisition software on a Windows XD operation system (Data Science International, New Brighton, MN, U.S.A). A stable HR and temperature were recorded for a minimum of 20 minutes. The R-R intervals in the last 5 minutes of this recording were used to find the average baseline HR of each mouse and P-wave durations were also quantified during this period.

Pharmacological blockade of the parasympathetic and sympathetic branches of the autonomic nervous system were completed using intraperitoneal injections of 1 mg/kg body weight of atropine sulphate and 10 mg/kg body weight propranolol hydrochloride, respectively (Sigma-Aldrich, Oakville, ON, Canada). Specifically, after baseline HR was recorded, atropine injection was completed, and a minimum of 20 minutes was recorded. The R-R intervals in the last 5 minutes of this recording were used to find the average HR post parasympathetic blockade. Thereafter, propranolol injection followed a minimum of 15 minutes was recorded. The R-R intervals in the last 5 minutes of this recording were used to find the average HR post complete autonomic blockade.

2.5 Intracardiac Measurements

Although exercise possess various health benefits, especially on the cardiovascular system, a paradox exists whereby high endurance training leads to increased risks to CVD, and especially AF [10]. Intracardiac investigations offer an invasive means to pace the heart, which is known to initiate AF episodes [4]. During intracardiac experiments the RP can also be studied through delivery of timed stimulations [213].

To prepare for the procedure, mice were placed in a sealed chamber connected to an isoflurane vaporizer (EZ-155KF Key Fill Isoflurane Vaporizer, E-Z Systems, PA, U.S.A) which was kept at 3% until mice were immobilized. Mice were placed on a heating pad supplied by heated water from a laboratory water bath and kept at 3% isoflurane until experimental analysis of electrophysiology began. Temperature was monitored using a rectal probe and maintained at 36.9-37.2°C. While in the supine position with the caudal direction away from the researcher, a small incision to the right of the midline was made, and the jugular vein was isolated and cannulated with an a 2F octapolar catheter (CI'BER Mouse, Numed, Hopkinton, NY, U.S.A). The catheter was directed into the right atrium and ventricle and positioned using the His bundle as a reference point, such that the His bundle has the largest amplitude in Lead 34 (**Figure 2-5**) [19]. Bipolar electrograms were generated whereby atrial procedures were observed best in Leads 78 and 56, whereas ventricular procedures were observed best in Lead 12 and 34. Once the positioning was ideal, isoflurane concentration was lowered to 1.5-1.75%. Stimulations were adjusted by a cycle controller (Pulsar 6i, Frederick Haer Co (FHC), Bowdoin, ME, U.S.A) connected to an amplifier (Gould ACQ-7700 amplifier, Data Science International, New Brighton, MN, U.S.A). Ponemah Physiology Platform acquisition software on a Windows XD operation system was employed to acquire and analyze data and Lead II sECG data was obtained using the same subdermal needles were used as previously described.

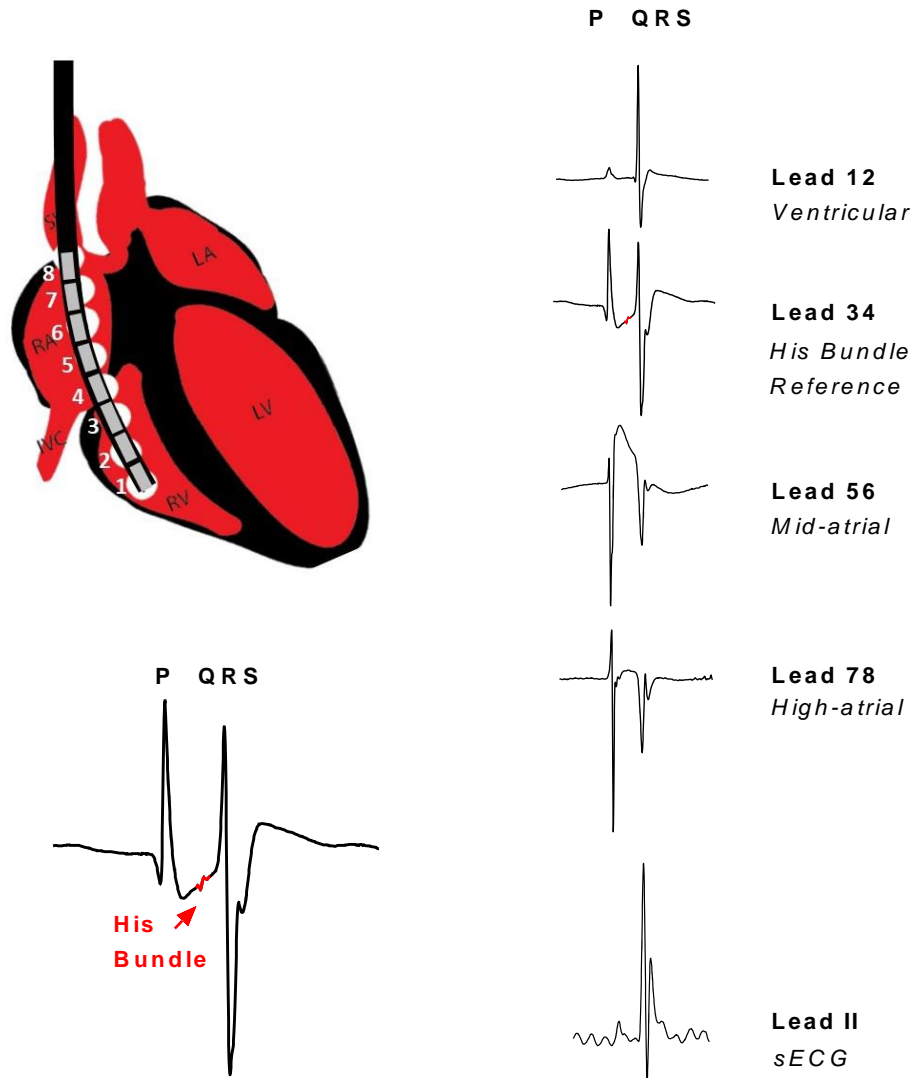


Figure 2-5. Intracardiac 2F EP Catheter Placement in the Heart – The 2F EP Catheter (CI'BER Mouse, Numbed, Hopkinton, NY, U.S.A) was introduced through the right jugular vein, directed to the right atrium and positioned within the right ventricle as shown above. The ventricular signal (QRS) is progressively decreasing from the distal (12) to the proximal (78) leads; whereas the atrial signal (P wave) progressively increases. Leads 78 and 56 were used to stimulate the high and mid right atrium whereas Lead 12 was used to stimulate the right ventricle. Correct positioning was confirmed through observation of the His bundle in Lead 34 as shown on the right. Lead II represents a simultaneous surface ECG recording. Figure was adapted from Copyright©2015, Nature Communications [2]. LA, Left Atrium; RA, Right Atrium; LV, Left Ventricle; RV, Right Ventricle; IVC, Inferior Vena Cava

The capture voltage was determined first. Seven (7) stimulations were applied at an interval of 20 ms below the R-R interval. Threshold voltage was increased from 0V in 0.05V increments until capture was observed. This was repeated for high atria (Lead 78), mid atria (Lead 56) and right ventricle (Lead 12). All stimulations used thereafter were applied at 1.5x the capture threshold.

Atrial refractory period was determined by field stimulating the most anterior (high) regions of the right atrium (HAERP) and the middle (mid) region of the right atrium (MAERP) by selecting the appropriate leads of the intracardiac catheter to apply high voltages (i.e. leads 78 for the HAERP and 56 for MAERP). Seven (7) premature stimulations (called S1) at 20 ms intervals below the R-R interval were applied (7XS1) followed by a single (extra) stimulation (called S2) applied after varied times, starting at an interval of 20 ms from the final S1 stimulus. An ineffective S2 stimulation was apparent by a QRS generated by the last final S1 premature stimulation (QRS_{S1}) but lack of S2 generated P-wave (P_{S2}) (**Figure 2-6**). The S2 interval was increased by 1 ms until capture was achieved observed by the presence of a QRS_{S1} and P_{S2} , followed by a QRS generated by the S2 extrastimulation (QRS_{S1}) (**Figure 2-6**). If capture was effective at a 20ms S2, this interval was decreased by 1 ms until capture was no longer observed. A similar protocol was repeated in Lead 12 for ventricular effective refractory period (VERP). Atrioventricular node effective refractory period (AVERP) was identified with a similar protocol in Lead 78 but the extrastimulation (S2) followed after 7xS1 starting at 40 ms after the last S1 stimulation. AV block was evident by the presence of a P_{S2} followed by a sinus rhythm P, without ventricular activation in between. The interval was increased from 40 ms by 1 ms until QRS was again captured (QRS_{S2}). All data was confirmed minimum twice.

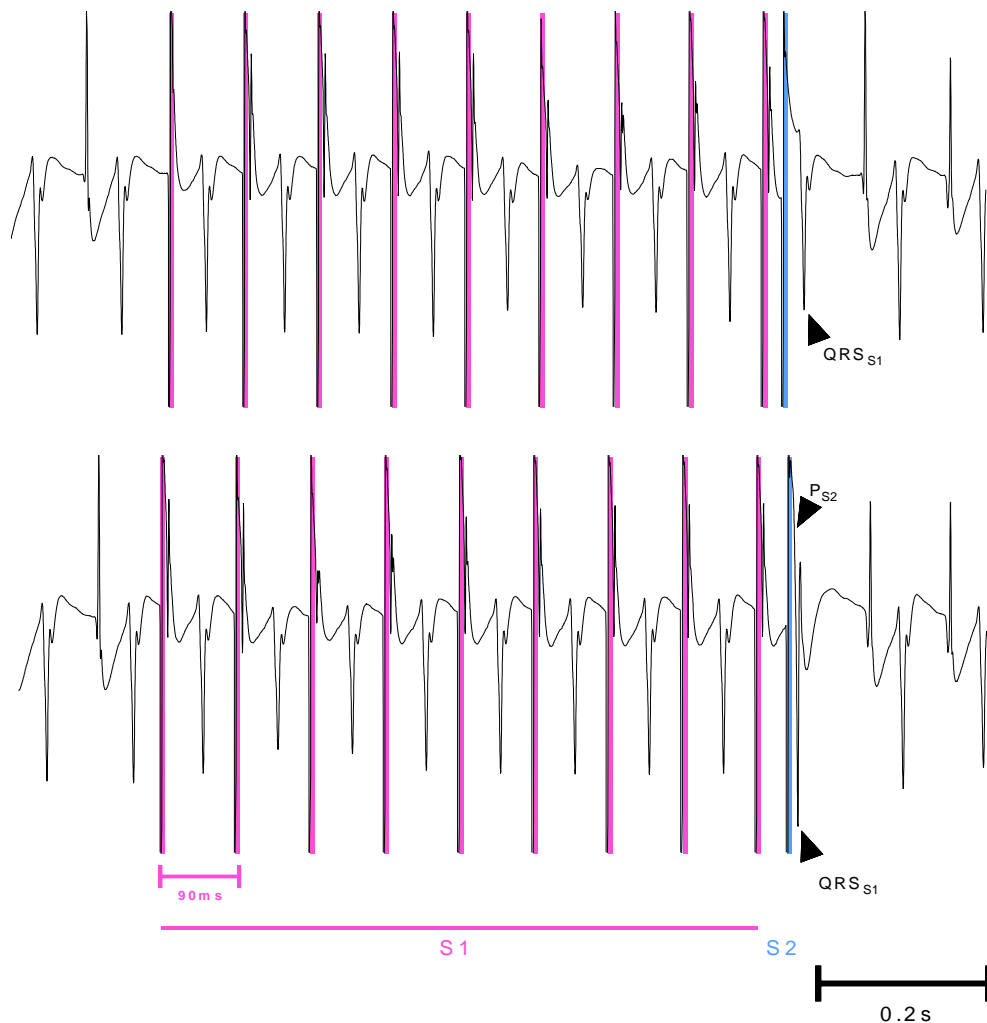


Figure 2-6. Atrial Effective Refractory Period (AERP) Identification during Intracardiac Procedures – AERP was determined in both mid and high right atria using Leads 56 and 78, respectively. All stimulations were carried out at 1.5x voltage capture to assure stimulation. A sequence of 7 premature stimulations at 20 ms below the R-R interval were delivered as indicated by Stimulation 1 (S1). A secondary premature stimulation (S2) was initially delivered 20 ms after S1 and further increased by 2 ms until recapture of the S2 stimulation. Adjustments of 1 ms were completed until capture was again abolished. If capture was observed at 20 ms, S2 stimulation was decreased by 1 ms until capture was abolished. Capture was confirmed by the presence of a P wave (PS2) right before the QRS generated by the final S1 stimulation (QRSS1) as shown in the bottom panel. Capture failure was confirmed by the lack of PS2 as shown in the top panel.

To assess AF and ventricular arrhythmia susceptibility, two protocols were used. First, programmed stimulation was applied as follows: 27 pulses, at 40 ms intervals decreased to 20 ms by 2 ms reductions [213, 214]. This was repeated 3 times. A second overdrive pacing protocol was applied as follows: 20 pulses at 20 ms intervals repeated 20 times at 1 second breaks. If the AERP was lower than 20 ms, the interval was decreased from 20 ms [214]. This was repeated 3 times. All protocols were applied to the high atria (Lead 78) and mid atria (Lead 56) in sequential order. AF was defined as a reproducible bout of chaotic atrial activation for a minimum of 10 seconds. AF was visible through the absence of clear P-waves in Leads 78 or 56, chaotic atrial activity in sECGs (Lead II) and regular-irregular ventricular activation (QRS complexes) in Lead 12 and II (**Figure 2-7**).

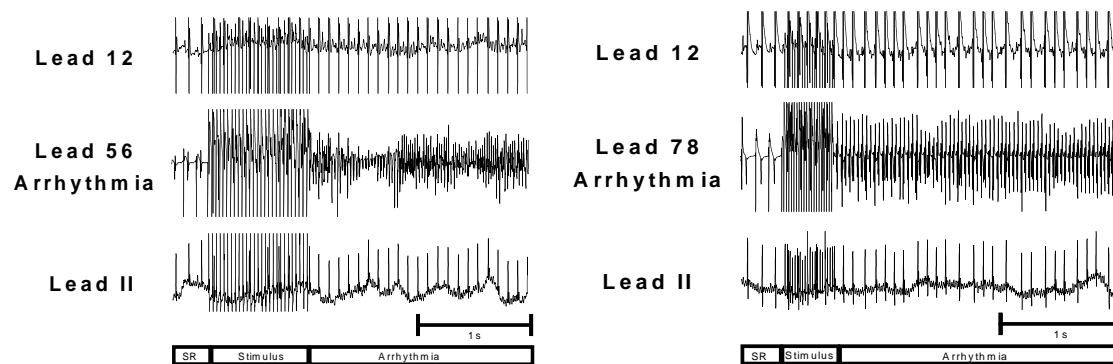


Figure 2-7. Atrial Arrhythmias Detection Using an Intracardiac 2F EP Catheter – Atrial Arrhythmias were observed in the mid (Lead 56) and high right atria (Lead 78). With stimulation at the other respective atrial electrode. Atrial fibrillation was confirmed by the absence of regular P-waves in atrial tracings at Leads 56 and 78, as well as abolishment of P-wave in the surface ECG (Lead II) and Lead 34. The presence of regular-irregular QRS complexes in Lead II sECGs confirmed the presence of Atrial Fibrillation.

2.6 Atrial Isolations and *Ex vivo* Electrophysiology

Increased vagal and sympathetic tone are causative of lone AF in athletes [148]. Nonetheless, AF perpetuation is enhanced through structural remodelling such as fibrosis, which is also hypothesized in athletes [2, 9, 148]. To assess the pathophysiological mechanisms of AF in the exercised mice, AF nature was visualized in *ex vivo* denervated hearts. Furthermore, it is known that APD and CV vary with exercise, behaving as modulators of AF when decreased [4]. Therefore, optical mapping was employed to quantify CV and APD in denervated hearts.

2.6.1 Atrial Isolations

Mice were injected intraperitoneally with 0.2mL of heparin (1000IU/ml, Leo Pharma, Thornhill, ON, Canada) and given 5 minutes for absorption. Thereafter, mice were anesthetized (as described above) and kept under anesthesia (~3% isoflurane). Lack of response was identified using the toe-pinch method. The thorax was opened using a midline incision starting from the abdomen and terminated at the top of the chest. The diaphragm was cut opened to reveal the heart. The heart was excised into Tyrode's solution (35°C), in mmol/L: 140 NaCl, 5.4 KCl, 1.2 KH₂PO₄, 1 MgCl₂, 1.8 CaCl₂, 5.55 D-glucose, 5 HEPES, and 10 IU/ml heparin with 7.4 pH. The heart was pinned to a Sylgaard filled petri dish using insect pins and any residual pericardial, connective or lung tissue was excised. The atria were separated from the ventricles via an incision along the atrioventricular connective tissue between the two chambers and pinned to reveal the mitral and tricuspid valves. Fine scissors were inserted into the superior and inferior vena cava and incisions were made and the atria were cut open. The atria were turned to reveal the pulmonary vein and any residual non cardiac tissue was removed. The ventricles were dried

with a paper towel and weighed. Atria were dried with a paper towel and weighed at the end of *ex vivo* analyses.

2.6.2 Isolated Atrial (*Ex vivo*) Electrophysiology

Following isolation, atria were superfused with 10mM AminoNaphthylEthenylPyridinium (Di-4-ANEPPS) in Tyrode's solution for 10 minutes. Di-4-ANEPPS is a fluorescent voltage sensitive dye, also called potentiometric dye [215]. The dye inserts itself in the plasma membrane of cell using two hydrophobic carbon chains and aligns perpendicularly to the membrane surface. The dye undergoes electronic redistribution of charge upon membrane depolarization [216]. Such changes lead to shifts in the emission spectra of the potentiometric dyes which alters the the amount of quantity of light recorded. Using this method, voltage changes can be quantified and tracked in isolated cardiac cells [215]. When bound, Di-4-ANEPPS has an absorption wavelength of 540 nm and its emission spectrum varies around 680 nm with 10% decrease in sensitivity with 100mV and these properties diminish in aqueous solution [216]. Optical mapping employs the qualities of potentiometric dyes to trace spatiotemporal changes in electrical activity within various tissues including the heart [215, 217].

Atria were then transferred and continuously superfused using carbogenized (95% O₂ & 5% CO₂) Krebs solution; in mmol/L: 118 NaCl, 4.2KCl, 1.2 KH₂PO₄, 1.5 CaCl₂, 1.2 MgSO₄, 2.3 NaHCO₃, 20 D-glucose, 2 Na-pyruvate, pH at 7.35-7.4 (**Figure 2-8A**). Solution flow rate, volume and temperature (35°C) were kept constant throughout the experiment. Atrial appendages were illuminated using a mercury light (Mightex, Pleasanton, CA, U.S.A) with a 543±22nm band-pass filter. Fluorescence light was collected using a 645±75 nm band-pass filter.

Images were captured using a high speed camera (MiCAM Ultima-L, SciMedia, CA, U.S.A) connected to an Olympus MVX-10 upright microscope (Center Valley, PA, U.S.A) equipped with a 0.63x c-mount adapter and a 0.38x lens relay. Frames were captured at 1000 fps, at 3x3 binning and 100x100 pixels resolution, using Ultima Acquisition (Brainvision, Tokyo, Japan) software.

To assess AF inducibility *ex vivo*, platinum needle electrodes (Genuine Grass® Reusable Subdermal Needle Electrodes, Natus Medical Incorporated, Pleasanton, CA, U.S.A) were inserted in the Sylgard petri-dish to the left of the left atrial appendage and below the inferior vena cava to replicate the lead II arrangement during sECGs. Field electrograms were collected using an acquisition system with Acknowledge software (Biopac MP150, BIOPAC Systems, Inc., CA, U.S.A). First, the capture voltage was determined. Continuous stimulations were applied at an interval of 20 ms below sinus rhythm. Threshold voltage was increased from 0V in 0.05V increments until capture was observed. The same stimulation protocols as *in vivo* intracardiac experiments were employed to assess AF vulnerability. Here, stimulation was delivered to both the left and right atrial appendages. AF was characterized as reproducible chaotic activation lasting longer than 10 seconds.

Thereafter, Rhythm GUI MATLAB based software (Efimov Lab, Washington University, MO, U.S.A) was used to analyze optical mapping data. To visualize re-entrant behaviour, frames during fibrillatory activity were subjected to phase mapping [217]. Shortly, phase describes the progression of the action potential in a specific region of the myocardium through a cycle between $-\Pi$ and $+\Pi$ [192, 217]. The phase is found using a Hilbert Transform plotted against the real optical action potential data [217]. In depth descriptions of this analysis are available

elsewhere [192, 217]. Using the phase map, reentry activity was observed and noted using curved arrows pointing in the direction of reentry.

Conduction velocity (CV) was identified by pacing the left atrial appendage at 90 ms cycle lengths. Here the data was masked to isolate background pixels from tissue pixels, filtered to remove high frequency noise ($<100\text{Hz}$), adjusted for drift and normalized. Exact functions of each correction can be review elsewhere [215, 217]. Activation maps were generated to calculate CV. Activation was defined as the steepest segment (highest first derivative of fluorescence signal for each pixel, dF/dt) of the optical action potential [215] (**Figure 2-8B**). Local conduction velocity vectors in the horizontal and vertical directions between two neighbouring areas were identified and their sum vector was identified [19, 215]. A conduction velocity map was generated and 3 regions of interest with uniform conduction were selected and averaged.

Finally, Action potential duration (APD) was also calculated using Rhythm software. APD was identified as 90% completion of the optical action potential for each pixel starting activation (APD_{90}), also defined as the time duration from activation to the first point less than 10% of the maximum value after the peak of the optical action potential [215]. The median APD_{90} from 3 regions of the left atrial appendage were averaged for each heart.

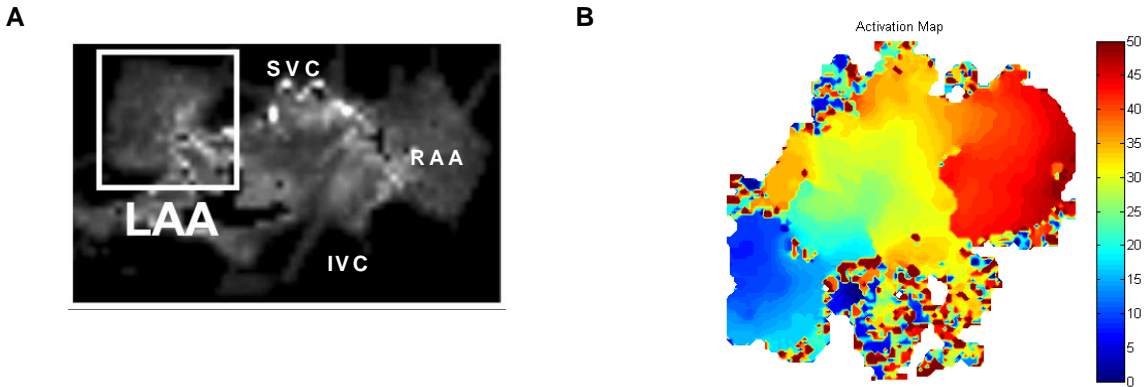


Figure 2-8. Typical Setup for Isolated Atria Ex Vivo Studies - A) an example of isolated atrial tissue pinned to a sylgrad dish. Red circles are positioned in where platinum needles were placed to simulate lead II arrangement during in vivo ECG analysis. Figure was adapted from Copyright©2015, Nature Communications [2]. B) An activation map from isolated atrial appendages of a swim exercised mouse. Pulses were delivered to the atrial appendage (in this case blue) and the time to activation was measured using temporal patterns of activation of the action potential measured with Di-4-ANEPPS dye. Longer activations are marked by colors, with blue being the quickest and red being the longest activation time (as labeled by the scale on the right). LAA, Left Atrial Appendage; IVC, Inferior Vena Cava; RAA, Right Atrial Appendage; SVC, Superior Vena Cava.

2.7 Heart Isolations and Histology

As previously discussed, structural remodelling in the form of fibrosis deposition and inflammation are theoretical but well accepted substrates of AF in athletes. Increased Collagen I deposition behaves as the mechanism for increased fibrosis, which can be detected using a picrosirius red stain during histological analysis [2].

2.7.1 Heart Isolations

Mice were anesthetized as described prior and kept under anesthesia. Lack of response was identified using the toe-pinch method. The thorax was opened using a midline incision starting from the abdomen and terminated at the top of the chest. The diaphragm was cut opened and the

heart was identified. The inferior vana cava was cut and the heart was perfused from the apex using a 30G needle with 1% KCL in 0.01M PBS to arrest the heart at diastole (PBS buffer tablets (pH7.4 - 100mL), Genaxxon bioscience GmbH, Ulm, Germany). Perfusion of minimum 5 mL was complete until all blood was washed through. A direct perfusion of 20 mL of 4% paraformaldehyde (PFA) in 0.01M PBS followed. The hearts were excised and placed within 35mL of 4% PFA in 0.01M PBS overnight. Thereafter, the hearts were washed in tap water for 30 minutes and stored in 70% ethanol solution until further use.

2.7.2 Tissue Preparation

Hearts were cleaned under the microscope of any non cardiac tissue in 70% ethanol solution. The hearts were cut in half, along the midline of the short axis to reveal an opened 4 chamber view. Half of the heart was dehydrated using a series of 1-hour alcohol washes (70%, 80%, 95%, 100% x2) and subsequent 45-minute xylene washes (Xylene-Ethanol, Xylene x2), each for 1 hour. The hearts were placed in paraffin at 60-70°C overnight and then tissues were embedded in paraffin blocks using an embedding station (HistoStar™ Embedding Workstation, Thermo Fisher Scientific, Waltham, MA, U.S.A). Three (3) layers, 100 µm apart, with 3 slides per layer were prepared for each heart where the presence of the left atrium prioritizing other tissues. This was done using a microtome (Thermo Scientific™ HM 325 Rotary Microtome, Thermo Fisher Scientific, Waltham, MA, U.S.A) and a heated water bath (Standard Lighted Tissue Floatation Bath, Boekel Industries, Inc., PA, U.S.A). Slides were left in 30-40°C overnight to dry.

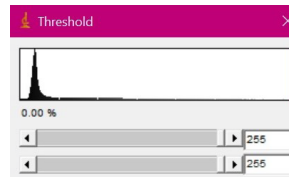
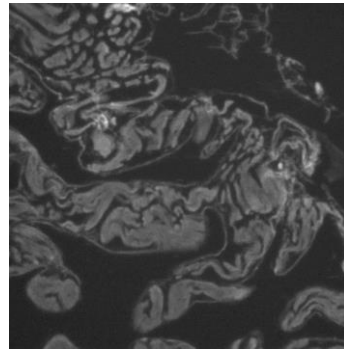
2.7.3 Histology

Deparaffinization of slides for histology was completed using a series of 3-minute washes with xylene (xylene x2, Xylene-Ethanol) and subsequent 3-minute ethanol washes (100% x2,

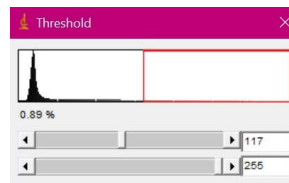
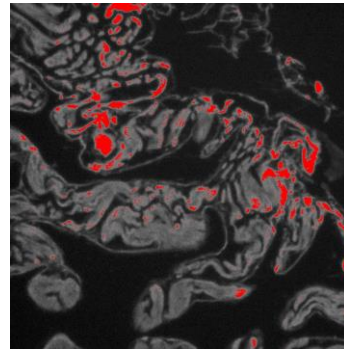
95%, 70% and 50%). Slides were then washed with tap water for 10 minutes and placed in a picosirius red (PSR) solution for collagen staining for 45 minutes to 1 hour. Thereafter, slides were washed in 0.5% acetic acid solution, twice. Tissue was again dehydrated using a series of ethanol washes (95% x2 and 100% x2) as well as xylene washes (Xylene x3). Slides were mounted with cover slips using Toluene (Fisher Scientific, Waltham, MA, U.S.A).

One (1) slide per tissue layer was imaged for a total of 3 layers, for each heart, using the EVOS™ FL Auto 2 Imaging System (Thermo Scientific™ AMAFD2000, Waltham, MA, U.S.A) with a Texas Red filter. Texas Red and PSR have very similar fluorescence properties whereby absorption and emission occur at 550 nm and 610 nm, respectively, for Texas red and at 550 nm and 635 nm for PSR [218, 219]. Data was analyzed using ImageJ software with the threshold method which exploits the brightness of pixels for collagen stained tissue relative to background tissue [19, 220]. Collagen stained pixel counts were expressed as percentages relative to total tissue pixel counts (**Figure 2-9**). The average percentage of the 3 layers was used as the measurement for each heart left atrium, with the whole left atrium selected for analysis. A similar size area for the free left ventricular wall was also analyzed similarly for each slide. Quantification was completed using a blinded experiment, whereby a third-party researcher measured collagen contents without knowing which image belonged to which mouse or exercise group.

**No Tissue
Selected**



**Collagen
Selected**



**Whole Tissue
Selected**

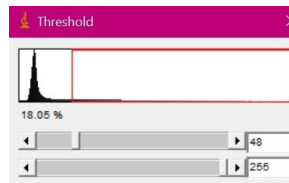
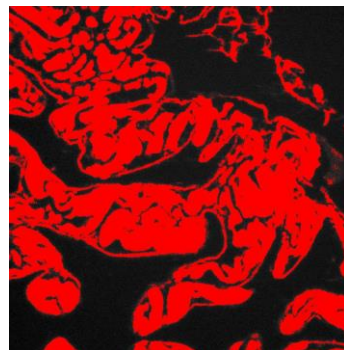


Figure 2-9. Fibrosis Quantification using the Threshold Method – Paraffin embedded, sliced tissue slides were stained with Picrosirius Red (PSR) and imaged using EVOS™ FL Auto 2 Imaging System (Thermo Scientific™ AMAFD2000, Waltham, MA, U.S.A) using fluorescence microscopy with a Texas Red filter. ImageJ software was used to quantify collagen by selecting pixels of variable intensities. Manual adjustments of the threshold allowed selection of either collagen (middle panel) or whole tissue (bottom panel) pixels. Fibrosis content was quantified by calculating the collagen pixels as a percent of total tissue pixels. Threshold adjustments are illustrated on the right.

2.8 Telemetric Hemodynamics

To assess ventricular and atrial hemodynamic function over the swim course, 3 naïve mice (aged 8 weeks) were employed. Radiofrequency emitting hemodynamic telemetry devices (PA-C10, Data Sciences International) were implanted as described in (Aschar-Sobbi et al. 2015) [2]. Shortly, mice were anesthetized with 3% isoflurane until mice were immobilized which was assessed with the toe-pinch reflex. Mice were given a loading dose of Metacam (2mg/kg) and placed on a heating pad to maintain temperature at 36.9-37.2°C. Respiration was maintained at 1.5-2Hz. Under aseptic conditions, the ventral thoracic region was shaved and cleared with depilatory. A ventral midline incision was made and the right common carotid artery was isolated with blunt dissection, ligated (5-0 silk), and bathed in 2% lidocaine solution. The catheter was introduced into the carotid artery, advanced into the left ventricle, and secured with suture. Mice were monitored over a 10-day recovery period, with additional doses of Metacam (1mg/kg) given if necessary. After recovery, mice underwent acclimatization swims (10 minutes/day for 2 days). Thereafter, mice underwent exhaustive swim sessions (up to 120 minutes/swim). For exhaustive swim sessions, a 30-minute baseline recording was performed prior to and following the exhaustive swim. Data analysis was performed using Ponemah P3 Plus software (v6.4, Data Sciences International). Systolic and diastolic blood pressures, heart rate, and the derivative of the pressure recording over time (dP/dt) were determined on a beat-to-beat basis.

2.9 Statistical Analysis

All analyses were completed using Prism software or Microsoft Excel. Summary data are presented as mean \pm SEM, unless otherwise stated. Normality was assessed using the

D'Agostino-Pearson omnibus normality test. $P \leq 0.05$ was used for significance. Significance was identified either using a one-way multiple comparisons ANOVA using Sidak multiple comparisons or a similar nonparametric test (Dunn's multiple comparisons) if normality in sample groups was absent. Alternatively, two-way ANOVA analysis was completed using multiple comparisons with Sidak multiple comparisons. Pearson's r was calculated for correlational studies. Contingency tables were used to assess arrhythmia inducibility. All significance relative to control are shown by *, unless otherwise stated.

Chapter 3

To present the conclusions of the thesis in collaborative manner with the objectives of this project, I chose to present my results and discussion as would be presented in a journal article.

3. Exercise Dose Dependent Atrial Remodelling and Atrial Fibrillation

Simona Yakobov^{1,2}, Robert Lakin¹, Nazari Polidovitch¹, Xiao Dong Gao¹ and Peter H. Backx¹

¹Department of Biology, York University, 4700 Keele St, Toronto, ON M3J 1P3,

²Muscle Health Research Centre, York University, 4700 Keele St, Toronto, ON M3J 1P3,

3.1 Abstract

The incidence of atrial fibrillation (AF) is strongly linked sedentary lifestyle and cardiovascular disease, and accordingly mild to moderate exercise effectively reduces AF risk. On the other hand, high-end endurance athletes have an AF risk rivaling that seen in CVD, suggesting a U-shaped dependence of AF on exercise. We sought to assess this relationship with emphasis on atrial responses, using CD1 mice which were swam 120, 180 or 240 minutes per day (divided into 2 sessions per day). We measured oxygen (O_2) consumption rates (V_{O_2}) to estimate work performed during swimming. The number of swimming days was tailored for each group of mice to ensure that all mice performed similar amounts of total work during swimming (i.e. O_2 consumed with swimming ~ 500 L O_2 /Kg). Consistent with comparable total exercise effort, all 3 groups showed similar reductions in body weight and changes in most ventricular parameters compared to sedentary mice (that were handled, but not swam). On the other hand, there were trends towards lower heart rates with higher exercise doses. By contrast, AF vulnerability in mice as well as atrial fibrosis, atrial enlargement and P-wave duration correlated positively with daily exercise dose (i.e. O_2 consumed with exercise per day) while AF duration correlated with amount of atrial fibrosis. In conclusion, we found for the first time that when exercise dose exceeds a threshold O_2 consumption value of ~ 15 L/kg per day for swimming mice, atria undergo fibrosis and hypertrophy, which leads to increased AF vulnerability and duration.

3.2 Introduction

Atrial fibrillation (AF) is the most common arrhythmia, affecting approximately 1% of the population [4]. AF is a condition linked to strongly with aging [4] as well as heart disease and poor cardiovascular health [5] associated with sedentary lifestyle such as obesity, diabetes and metabolic syndrome [4, 6, 7]. On the other hand, physical exercise even at low doses reduces the AF incidence [6] and can reduce symptoms associated with AF [8]. Nevertheless, high intensity endurance training also paradoxically increases AF risk. Consequently, AF incidence appears to show a U-shaped dependence on exercise [10].

Despite many decades of investigations, the pathogenesis of AF remains unclear. A common feature of most conditions linked to AF is elevated preload (i.e. venous filling pressures) which are commonly associated with impaired diastolic ventricular function often combined with reduced cardiac contractility [4]. AF is associated with electrical and structural changes (called remodeling) in the atria [31]. Structural atrial remodeling consists primarily of atrial fibrosis and hypertrophy. Atrial fibrosis slows conduction by creating microscopy barriers to electrical AP propagation while also increasing tissue anisotropy and promoting myocardial depolarization [12, 59]. Fibrosis combined with atrial hypertrophy strongly increase AF vulnerability by promoting and supporting reentry electrical events, which are hallmarks of AF [4]. Although electrical remodeling in AF patients is controversial, the most common relevant electrical changes in the atria appear to be increased heterogeneity of repolarization [149] arising from regional alterations in K^+ channel expression as well as heterogeneous innervation and activity of parasympathetic nerves [4]. Decreases in gap junction expression in AF resulting in decreased CV have also been suggested, although the results are conflicting [2, 4].

It is important to appreciate that virtually all the previous publications examining the atrial changes in AF patients have studied aging patients with underlying CVDs, since this is by large the bulk of the AF patients. There is accordingly a paucity of data in athletes and the factors contributing to AF in endurance athletes are far less certain. Nonetheless, a few mechanisms (remodelling) have been linked to AF in athletes [9, 148], albeit in an older population [9]. For example, athletes invariably have increased vagal tone, which not only leads to sinus bradycardia [142, 148] but also promotes electrical changes (reduced refractoriness) leading to AF [138]. Endurance athletes also have enlarged atria, probably related to high exercise volumes [9, 148]. Consistent with rodent studies [146, 149], a recent study in endurance athletes found evidence for atrial fibrosis [221], although this is controversial [146].

Several studies attempted to determine the dependence of AF on exercise dose by quantifying exercise frequency [101, 110, 177], intensity [108, 179], duration [96, 177] and cumulative lifetime dose [133], as well as cardiorespiratory fitness [181]. A major limitation of these studies is the reliance on subjective self reporting to estimate exercise dose, which makes the results controversial [179, 181]. Thus, the purpose of our studies is to identify how exercise dose influences atrial remodelling and AF susceptibility. We varied the dose of exercise by altering the duration that mice swam each day. The work performed with exercise was quantified by measuring oxygen consumption rates (V_{O_2}) during swimming. Our results show that V_{O_2} cannot be reliably varied with swimming intensity in mice. On the other hand, when mice performed equivalent amount of work during swimming (~ 500 L O_2 /Kg), adverse atrial changes and AF vulnerability become increasingly detectable when the duration of swimming per day exceeds around 180 minutes per day for our swimming mice (~ 15 L O_2 /Kg per day).

3.3 Methods

After we swam mice at the appropriate exercise regimes and quantified exercise dose, we studied selected atrial and ventricular parameters to 1) confirm exercise promoted aerobic remodelling known to occur in athletes, 2) assess AF vulnerability and all mice (exercise and control) and 3) explore which pathophysiological mechanisms underlie AF inducibility. Detailed methodologies are described in **Chapter 2 – Methods**.

3.4 Results

3.4.1 *Exercise Quantification in Swimming Mice*

We showed earlier that CD1 mice are intrinsically motivated to swim against a steady water current [2, 19]. To assess the dependence of AF on the amount of swim exercise in mice (i.e. dose), we initially attempted to alter the intensity of exercise by varying the magnitude of the flow velocities of water currents while simultaneously measuring O₂ consumption rates (V_{O₂}) to quantify exercise effort, as done routinely in human exercise studies [160]. Three groups (n=3 mice per group) were swam together in swim tanks with currents generated by water pumps supplying between 5-20 L/min. Unexpectedly, as summarized in **Figure 3-1**, V_{O₂} varied only marginally (P=0.99) with water flow rates. This observation suggests that mice self-regulate their swimming effort when flow rates change, as concluded previously [191]. Anecdotally, it was observed that the mice regularly interrupt their swimming by intermittent immobility, floating and riding the water currents, which has been described previously as “inappropriate swimming behaviour” in rodents [193, 194], suggesting a self regulatory behaviour which was shown an innate characteristics in rodents [187].

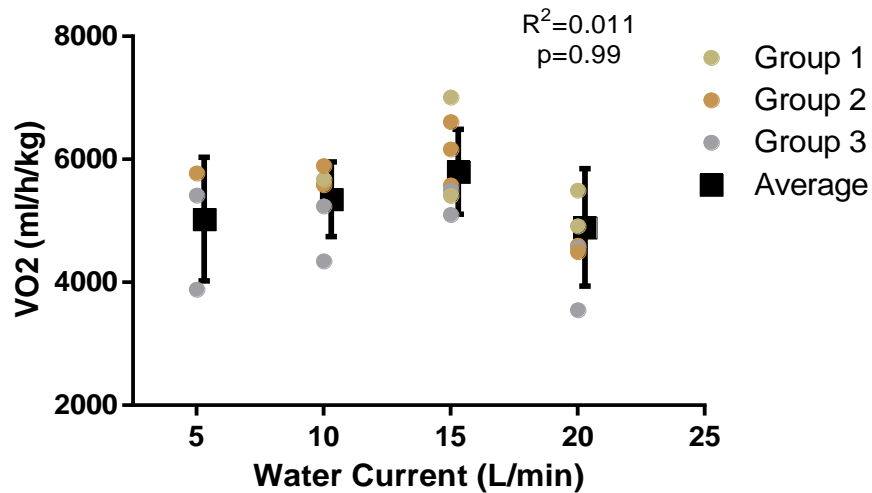


Figure 3-1. Self Regulation Behaviour During Swim – Three (n=3) mice were placed in a swim apparatus together and consumption (V_{O_2}) was measured using a modified calorimetry system (Oxymax, Columbus Instruments, Columbus, OH, U.S.A). This was repeated for three groups of mice. Swimming behaviour was monitored, and mice were forced to swim against a water current provided by a submerged pump. The mice were swam for 90 minutes at currents of either 0, 5, 10, 15, or 20L/min and V_{O_2} was quantified as describe in Appendix A and B. Mean V_{O_2} at each water current was found and plotted. No correlation between water current and V_{O_2} was identified ($p=0.86$). Data are mean \pm SD, * $p\leq 0.05$.

Armed with this information, we elected to alter exercise effort (dose) between mice by varying the amount of time spent swimming each day (i.e. 60, 90 or 120 minutes twice per day), with all mice swimming with identical water currents generated at 20L/min, as used previously [2]. The number of weeks that each group swam was tailored so that each group consumed approximately the same total O_2 during the study (**Figure 3-2A and 3-2B**). Although we expected that the number of swimming weeks needed to ensure that all the mice performed the same work during swimming would scale (inversely) with swim durations, this was not the case. In fact, the mice swimming 120 minute per day (swimming twice/day) consumed about the same amount of O_2 after ~7 weeks as did the 180 minute group after 6 weeks and as did 240 minute

group after ~4.5 weeks (**Figure 3-2A**). This lack of scaling between the weeks needed to ensure all mice consumed about the same amount of O₂ with exercise and the duration of each swim bout could be traced to systematic declines in V_{O₂} over time during a typical bout of swimming, as illustrated in **Figure 3-2C**. As a result, the 120 minute group had higher (P<0.0001, Sidak post hoc analysis) average V_{O₂} (7282±13 mL O₂/hour/kg) during each swim than the 180 minutes group (6054±70 mL O₂/hour/kg), which in turn had higher average V_{O₂} than the 240 minute group (5865±23 mL O₂/hour/kg) (P=0.038, Sidak post hoc analysis). Accordingly, we observed a decrease in relative exercise effort, measured in percent work relative to maximal oxygen consumption (VO_{2 max}), throughout swimming (**Figure 3-2D**). As discussed later, the time-dependent changes in V_{O₂} during swimming may have important implications on the mechanisms underlying adverse atrial remodeling with exercise.

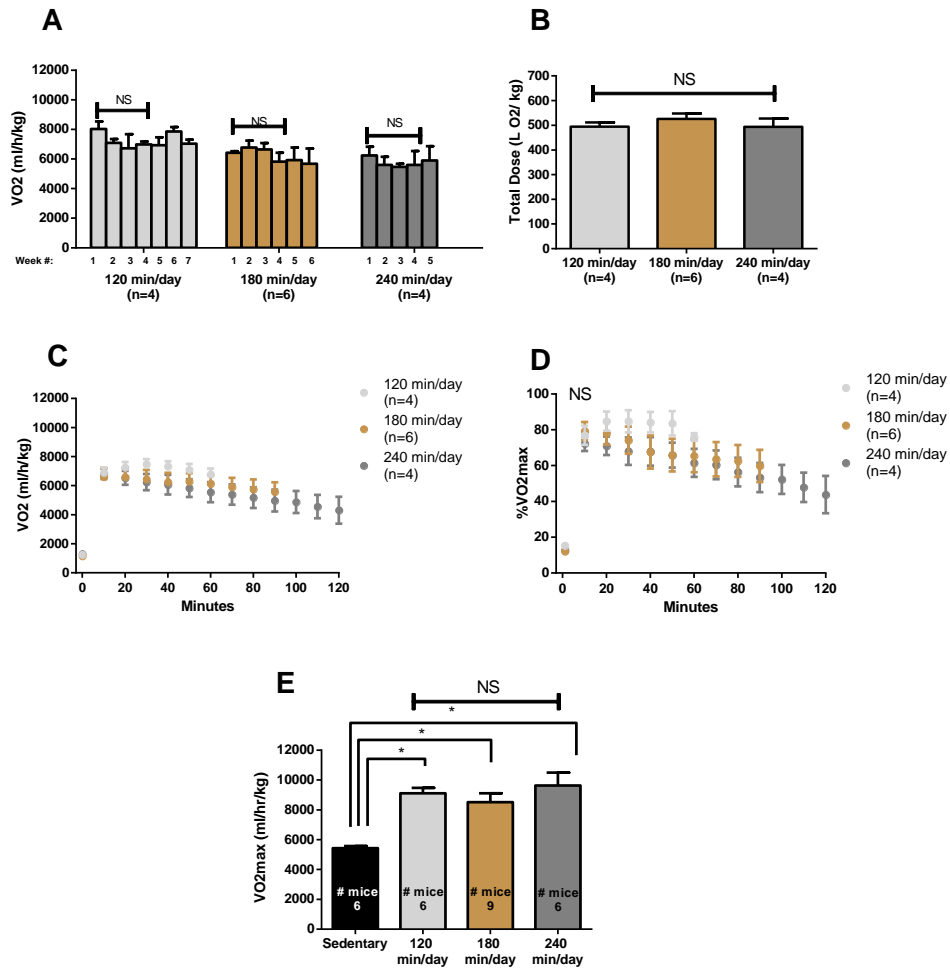


Figure 3-2. Exercise Quantification using Oxygen Consumption – Mice were swam in groups of 3 for either 60, 90 or 120 minutes per swim. Exercise was terminated such that all mice preformed identical total exercise doses (view Appendix A and B). Occasionally each group was swam in a modified swimming apparatus capable of oxygen consumption (V_{O_2}) measurements. A) average V_{O_2} was plotted for each week for all groups (two-way ANOVA). B) All exercise groups had similar total work loads (measured as total volume of oxygen consumed over the whole exercise regime, normalized by body weight). C) Progressive changes in V_{O_2} as a function of time of swim bout for all groups. Mean V_{O_2} represents average V_{O_2} for that time point from the recorded swims of that group. D) To assess relative exercise intensity in swimming mice, we quantified maximal oxygen consumption ($V_{O_2\max}$) (as described in panel E), and identified the percent (%) ratio between V_{O_2} throughout the last bout of swimming and $V_{O_2\max}$. E) To assure proper endurance exercise is completed during swims, maximal oxygen consumption ($V_{O_2\max}$) was found 48 hours after the last swim bout for mice (n=6-9) randomly selected from each exercise regime using a modified swimming apparatus. There were no differences in $V_{O_2\max}$ in mice exercising for different daily doses (one-way ANOVA). Data are mean \pm SEM, * relative to sedentary mice, * p <0.05 ** p <0.01 *** p <0.001. Sample sizes are shown.

3.4.2 Aerobic Conditioning in Swimming Mice

As might be expected, all exercised groups of mice had lower ($P < 0.001$) body weights than 14 week old sedentary mice (that were handled twice a day but were not swam). Despite these differences in body weights, *ad libitum* food intake did not differ between the groups (**Table 3-1**) (**Supplementary Figure 3-8**). On the other hand, although no differences in ventricular weights (VW) were observed between the exercised and sedentary mice, the VW normalized to body weight (BW) was slightly elevated ($P < 0.01$, one-way ANOVA) in all the exercise groups (**Table 3-1**) compared to sedentary mice. The increases in VW/BW ratios were accompanied by trends towards increases ($P < 0.05$, one-way ANOVA) in diastolic and systolic diameters and by reductions ($P < 0.01$, one-way ANOVA) ejections fractions (EF), relative to the sedentary mice (**Table 3-1**), with significance observed in mice swimming for the longest durations (240 minutes/day) ($P < 0.012$, Sidak post hoc analysis). These changes indicate mild ventricular hypertrophy and dilation in conjunction with reduced ejection fraction in exercised mice, as typically seen in athletes [111, 112] and exercised mice [2, 222] (**Table 3-1**). The similarities in ventricular adaptations observed between exercise groups were accompanied by lack of differences in total integrated effort and similar cardiorespiratory fitness measured by $V_{O_2 \max}$ ($P > 0.999$, nonparametric test) (**Figure 3-2E**). Finally, these adaptations were also supported by the increased $V_{O_2 \max}$ in all exercise groups compared to the sedentary mice ($P < 0.01$, nonparametric test) (**Figure 3-2E**).

Table 3-1. Aerobic and Exercise Induced Physiological Adaptations in Exercising Mice.

	Sedentary (age- 14 weeks)	120 min/day	180 min/day	240 min/day	P value
<i>Number of Mice</i>	18	12	9	11	
Weight (g)	42.43±0.93	36.32±0.53** *	35.38±0.87** **	35.07±1.02** **	<0.0001
Food Intake (g food /g mouse)	0.151±0.02	0.121±0.02	0.144±0.01	0.145±0.02	0.67
Ventricle (<i>Number of mice</i>)	3	4	3	5	
VW (mg)	152.8.8±10.7	161.5±5.5	138.5±3.5	142.6±5.9	0.18
VW/BW (mg g⁻¹)	2.84±0.15	3.99±0.17***	3.90±0.14**	3.82±0.24**	0.0006
Echocardiograph <i>y (Number of mice)</i>	15	8	14	10	
LVDD (mm)	4.139±0.09	4.402±0.14	4.351±0.24	4.485±0.04*	0.036
LVDs (mm)	2.462±0.11	2.795±0.21	2.604±0.07	3.022±0.06*	0.0045
FS(%)	40.78±1.72	36.91±2.98	40.59±1.44	32.07±1.03**	0.0076
EF(%)	71.42±2.10	65.82±3.86	71.19±1.80	60.56±1.47*	0.0078
LVPWWth(m m)	0.67±0.03	0.70±0.04	0.71±0.04	0.70±0.02	0.62

VW, ventricular weight; VW/BW, ventricular weight/ body weight; LVDD, left ventricular diastolic diameter; LVDs, left ventricular systolic diameter; FS, fractional shortening; EF, ejection fraction; SV, stroke volume; CO, cardiac output; LVPWWth, left ventricular posterior wall thickness; Data are mean±SEM, sample sizes (number of mice) are shown, *p≤0.05, **p<0.01, ***p<0.001, with the right column showing P values for nonparametric test or one-way ANOVA as appropriate.

Despite the similar ventricular changes between the exercise groups, **Figure 3-3** shows that baseline HRs (beats per minute) were not reduced in the 120 minute group ($P=0.97$, Sidak post hoc analysis), but were reduced ($P<0.01$, Sidak post hoc analysis) in the 180 minute and 240 minutes group, compared to sedentary mice (**Figure 3-3B**). This dependence of HR on daily swim duration is consistent with human studies showing that the degree of sinus bradycardia requires a threshold dose of exercise, which was linked to changes in autonomic control of HR [141]. The bradycardia seen in our mice was also dependent on changes in the autonomic nervous system (**Supplementary Figure 3-7A**). The evidence for this is summarized in **Figure 3-3B** which shows that reduced HRs seen in the 180 and 240 minute groups were abolished following full autonomic blockade (i.e. after atropine and propranolol treatment) ($P>0.05$, two-way ANOVA). Moreover, no differences ($P=0.16$, one-way ANOVA) in beating rates were observed in isolated atrial preparations, which lack autonomic regulation (**Figure 3-3C**). **Figure 3-3B** also shows that when the parasympathetic nervous system is blocked with atropine, HRs were lower in the 240 minute group ($P=0.012$, Sidak post hoc analysis), with clear trends towards lower HRs in the 180 minute group ($P=0.22$, Sidak post hoc analysis), compared to sedentary mice. Considering that no HR differences existed between the groups after full autonomic blockade, these observation support the conclusion that cardiac sympathetic nerve activity is lowered by increasing amount of daily exercise, which can be also appreciated by inspection of **Supplementary Figure 3-7B** which shows the change in HR seen after propranolol treatment (in the presence of atropine). On the other hand, **Supplementary Figure 3-7B** shows that the HR changes in the 180 and 240 groups following atropine treatment were ~1.5 fold greater larger then the response in the 120 and sedentary groups, although this did not quite reach significance ($P=0.052$, two-way ANOVA). An increase in cardiac parasympathetic

nerve activity was expected as exercise dose increased based on previous studies in humans showing increased vagal tone with fitness levels [138]. It is important to note that atropine administration also increased HRs in sedentary mice as well (**Figure 3-3B**), demonstrating that the dose of pharmacological agent administration was appropriate in our approach.

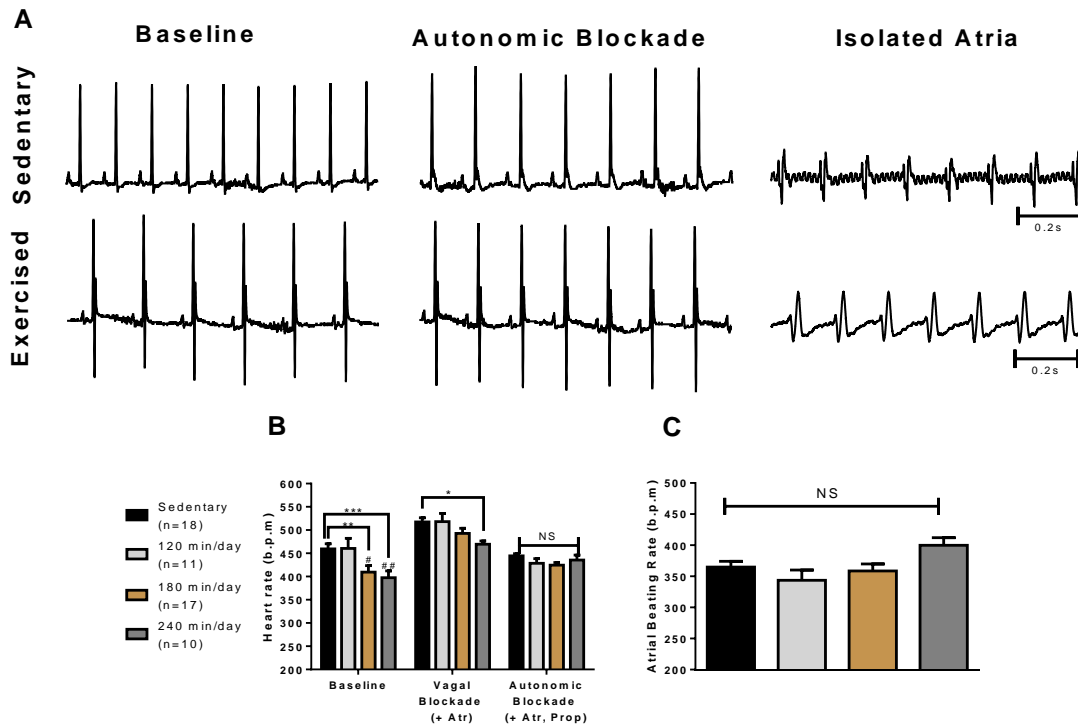


Figure 3-3. Exercise Adaptations in Exercising Mice Relative to Control Mice – To investigate whether exercise induced bradycardia occurred in mice undergoing swimming exercise [142], heart rates (HRs) were assessed using surface ECG (sECG) recordings (Data Sciences International, New Brighton, MN, U.S.A) in mice under minimal anaesthesia, before and after pharmacological complete autonomic blockade by using Atropine (2mg kg⁻¹) and Propranolol (10mg kg⁻¹). A) Exemplary 1 second sECG tracings are shown. Decreased HRs are evident by an increased R-R interval in exercised mice. Decreased HRs were abolished upon complete autonomic blockade. Electrograms of beating isolated atria are shown on the right most panel with lack of differences between intrinsic beating rates in exercised and control mice. All electrograms were taken from the same mouse for either the exercised or control. B) HR decreased significantly in mice that swam at for 180 and 240 minutes/day, which are abolished upon autonomic blockade. Decreased HRs are apparent even with parasympathetic blockade in mice swimming for 120-minute bouts. Sample sizes shown. C) Beating rates were not significantly different among groups or compared to the control sedentary group (n=14 sedentary, n=4 120 minutes/day, n=12 180 minutes/day, n=4 240 minutes/day). Data are mean±SEM, sample sizes are shown, *p≤0.05, **p<0.01, ***p<0.001, ****p<0.0001.

3.4.3 Dose Dependent Atrial Fibrillation

We next examined whether daily exercise duration (i.e. daily exercise dose) affected AF vulnerability. In these studies AF was defined as arrhythmic event characterized in ECG recordings by highly irregular activity, similar to the pattern seen in typically AF patients and animal models [2] lasting for >10 seconds following overdrive pacing of the atria (**Figure 3-4A**). The ECG pattern measured in intact mice is consistent with the AF events seen in isolated atria using optical mapping which show the presence of dynamic rotors coupled with complex regional blocking patterns (**Figure 3-4C**). The incidence of AF inducibility was greater ($P=0.0087$, χ^2 test for trend) in mice exercising for 180 (2/25) or 240 minutes/day (3/10) (**Figure 3-4B**), with the incidence of AF being ~3-fold greater in the 240 minute/day group compared to the 180 minute/day group. Importantly, the durations of atrial arrhythmias correlated strongly ($p=0.045$, $r=0.9975$) with total O_2 consumed each day during swimming (i.e work associated with swimming per day) establishing that AF vulnerability is profoundly affected by exercise per day (**Figure 3-4D**). It is worth recalling that the mice who swam for the shortest period per day showed the highest average rate O_2 consumption (i.e. V_{O_2} of 7282 ± 13 mL O_2 /hour/kg), indicating a higher exercise intensity with shorter swims. Thus, while AF vulnerability tracks with the time spent swimming each day, a role for exercise intensity during swimming in promoting AF vulnerability could not be identified in our experimental conditions.

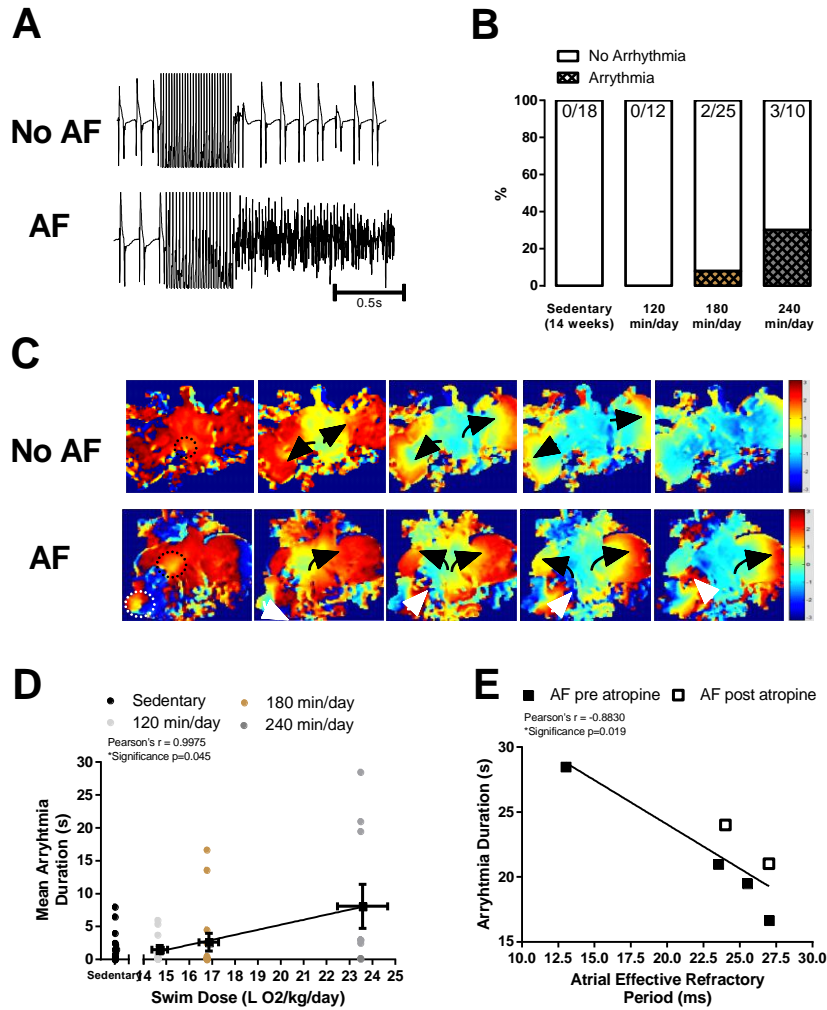


Figure 3-4. Atrial Fibrillation Inducibility in Response to Different Exercise Regimes – Rapid stimulations were delivered either to the high atria (Lead 78), mid (Lead 56) atria *in vivo*. A) Representative electrograms are shown for atrial fibrillation and lack thereof. B) Percentages of mice with arrhythmias sustained longer than 10 seconds were considered inducible. Atrial Fibrillation was elevated in mice swimming for 180 and 240 minutes/day (χ^2 -test for a trend) C) Isolated atrial appendages were subjected to identical stimulation protocols as *in vivo* hearts, and stained with Di-4-ANEPPS. Phase maps were generated to observe reentry events. D) Atrial arrhythmia durations are illustrated in color and a correlation between daily exercise dose (volume of O₂ consumed per day) is shown. E) Atrial effective refractory period was measured in the mid (lead 56 - MAERP) and high (lead 78 - HAERP) atria *in vivo* and their average was plotted against AF duration for each mouse. There was a significant correlation between the two values. Data are mean \pm SEM, sample sizes shown in the top panel contingency table. * $p\leq 0.05$, ** $p<0.01$, **** $p<0.0001$.

3.4.4 Electrical Remodelling and Atrial Fibrillation Inducibility

Previous studies have established that atrial refractoriness strongly influences arrhythmias including AF vulnerability [30], largely by facilitating reentry-type arrhythmias [4, 28]. Consistent with this, the duration of the induced AF events correlated strongly with the AERP before and after atropine treatment ($P=0.019$, $r=-0.8830$) (**Figure 3-4E**). Moreover, atropine administration, which prolonged atrial refractoriness (**Supplementary Figure 3-7C**), probably by reducing M2-mediated activation of $I_{K,Ach}$ as well as possibly reducing of I_{Ca} [4], reduced the AF incidence by 2/3 in the 240 group as well as by 1/2 in the 180 minutes/day mice. Despite the the observed relationship between AERP and AF, no differences ($P>0.05$, one-way ANOVA) were observed in the AERP between the groups (**Table 3-2**), regardless of the atrial region (high atria: $P=0.28$, mid atria: $P=0.07$). Furthermore, the amount of prolongation in atrial refractoriness after atropine administration did not differ between the groups (**Supplementary Figure 3-7D**), even though the 180- and 240-minute groups showed greater vagal-dependent effects on HR (**Supplementary Figure 3-7B**). This absence of differences in AERP is not unexpected, since very few mice went into AF and suggests that AERP is not the primary determinant of AF vulnerability.

Table 3-2. Atrial Adaptations in Mice Swimming at Different Swim Doses

	Sedentary (age- 14 weeks)	120 min/day	180 min/day	240 min/day	P value
<i>In vivo</i>	16	12	13	10	
Electrophysiology (<i>Number of Mice</i>)					
HAERP	28.03±2.12	30.25±1.67	30.23±1.28	27.22±0.83	0.28
MAERP	24.78±1.57	28.00±1.54	28.08±0.94	23.56±1.43	0.07
AVERP	48.74±1.92	51.21±1.42	54.27±2.20	51.11±2.50	0.19
P Wave (ms)	15.17±0.52	16.75±0.79	18.38±1.39*	19.18±0.91**	0.0055
<i>Ex vivo</i>	3	4	3	4	
Electrophysiology (<i>Number of Mice</i>)					
APD₉₀	27.27±1.42	29.87±2.35	30.26±1.50	29.38±1.83	0.75
CV	0.59 ±0.04	0.39 ±0.02*	0.42 ±0.02	0.47 ±0.03	0.0052
Atrial (<i>Number of Mice</i>)	3	4	3	5	
AW (mg)	17.67±0.28	18.55±0.70	18.80±1.03	18.54±0.49	0.67
AW/VW (mg g⁻¹)	102.9.6±0.72	114.9±2.94	135.6±6.03*	130.8±5.25*	0.0017
AW/BW (mg g⁻¹)	0.29±0.02	0.46±0.02	0.53±0.02*	0.52±0.02*	0.0039

HAERP, High Atrial Effective Refractory Period (ms); MAERP, Mid Atria Effective Refractory Period (ms); AVERP, Atrioventricular Effective Refractory Period (ms); APD₉₀, 90% Action Potential Duration Completion (ms); CV, Conduction Velocity (m/s); AW, atrial weight; AW/VW, atrial weight/ ventricular weight; AW/BW, atrial weight/ body weight. Data are mean±SEM. *p≤0.05, **p<0.01, with the right column showing P values for nonparametric test or one-way ANOVA as appropriate.

3.4.5 Structural Remodelling and Atrial Fibrillation Inducibility

As already mentioned, the lack of AERP between the groups despite the higher increased AF susceptibility in the 180- and 240-minute groups suggests that other factors are influencing AF inducibility. In this regard, previous studies have established that AF is invariably linked to atrial fibrosis [2, 68]. Thus, we measured atrial collagen levels using picrosirius red staining in histological sections (**Figure 3-5A**). These studies revealed that collagen levels were elevated ($p < 0.01$, two-way ANOVA) with the mice swimming 240 minutes per day show higher fibrosis deposition relative to mice swimming for 180 ($p = 0.0004$, Sidak post hoc analysis) or 120 minutes/day ($p = 0.0002$, Sidak post hoc analysis) (**Figure 3-5B**). Furthermore, the amount of atrial collagen levels correlated ($p = 0.036$, Pearson $r = 0.9984$) with the work performed (integrated O_2) per swim as well as with the AF durations ($p = 0.037$, Pearson $r = 0.5431$) (**Figure 3-5C and 3-5D**). Consistent with the fibrosis results, we observed slowed atrial conduction velocities in exercised mice relative to sedentary mice ($P < 0.05$, nonparametric test) as well as elongation in P wave durations ($P < 0.01$, one-way ANOVA) (**Table 3-2**). These observations establish that elevated AF susceptibility is linked to the amount of atrial fibrosis which in turn is driven by the work associated with exercise per day.

Additionally, endurance athletes frequently display atrial dilation, enlargement and hypertrophy which promote arrhythmias and AF [9, 148]. Although absolute atrial weights (AW) of exercised mice were not increased ($P = 0.036$, nonparametric test) relative to sedentary mice, AW normalized by VW as well as BW were elevated in exercised groups ($P < 0.01$, nonparametric test) (**Table 3-2**), suggesting mild atrial hypertrophy as typically observed in endurance athletes [134, 135]. Interestingly, the greatest atrial enlargement was observed in mice

swimming for 180 and 240 minutes/day relative to sedentary mice. Indeed, there is evidence supporting the relationship between atrial dilation and AF in athletes [133].

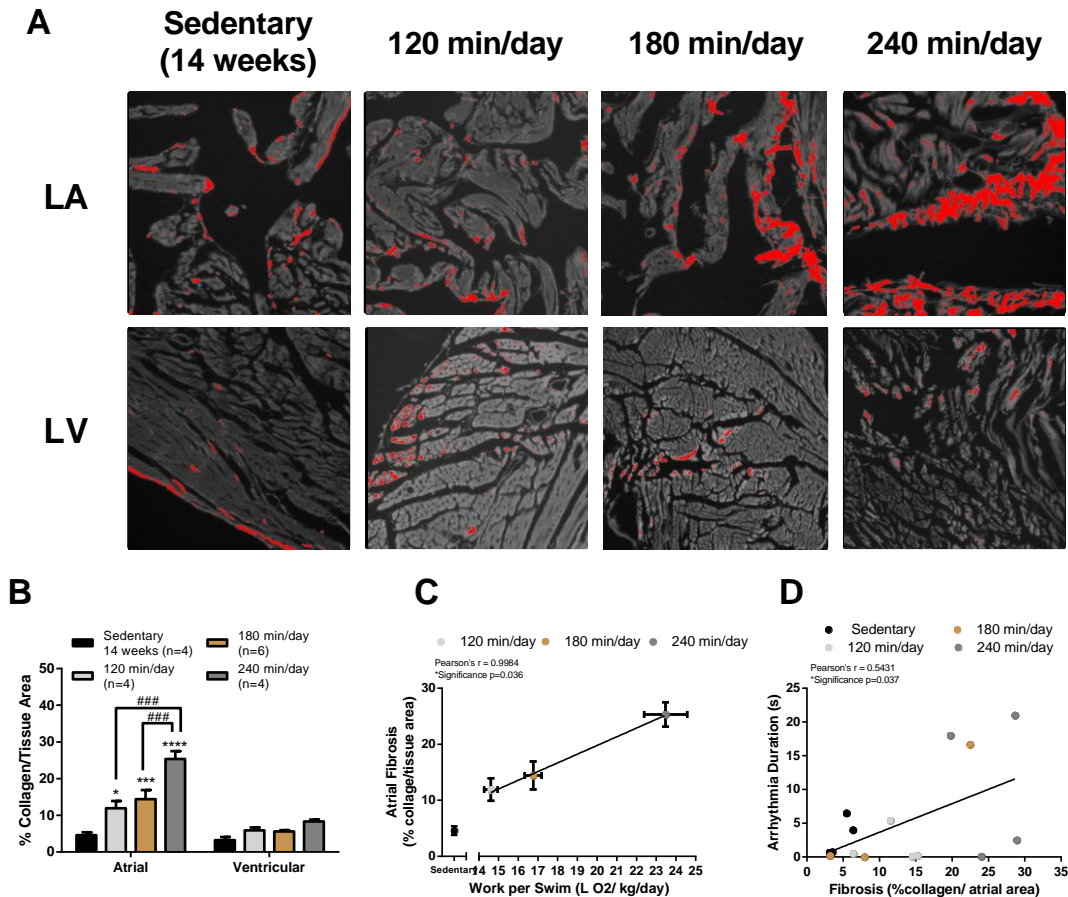


Figure 3-5. Atrial Fibrosis Increases with Swim Dose – To investigate the role of fibrosis on the pathogenesis of AF, paraffin embedded sliced heart tissues were stained with fluorescent Picrosirius red (PSR) dye to visualize collagen. A) Slides were imaged using the EVOS™ FL Auto 2 Imaging System (Thermo Scientific™ AMAFD2000, Waltham, MA, U.S.A) with a Texas Red filter. Exemplary images for the Left Atria Appendages (LAA) and Left Ventricular Wall (LV) are shown. B) Collagen content was quantified with ImageJ software using the threshold method and expressed as percent collagen relative to total tissue area (%collagen). Atrial fibrosis was increased within all exercise groups relative to controls (sedentary 14 weeks old) (two-way ANOVA). No such trend was observed for ventricular fibrosis. C) Atrial collagen content was plotted as a function of swim dose (measured in volume of oxygen consumed per day, normalized by body weight). Pearson’s correlation test was used. D) Fibrosis content was correlated with arrhythmia durations. Data are mean±SEM, sample sizes are shown, significance relative to control indicated by *. *p<0.05, **p<0.01, ***p<0.001, ****p<0.0001. All other significances are indicated by #.

3.4.6 Hemodynamic Changes with Swim Exercise

The results presented thus far, establish that once daily swim duration exceed about 180 minutes per day, atrial hypertrophy and fibrosis as well as P-wave prolongation occur in association with increased AF vulnerability. While the basis for this is unclear, it was noted that as mice swim, their V_{O_2} values decrease progressively with time after the first ~60 minutes. Thus, the exercise intensity during swimming was the highest for mice swimming for 120 minutes per day. Yet the degree of atrial fibrosis and hypertrophy as well as AF inducibility increased as the swim durations per day increased. To assess the hemodynamic factors that underlying these we performed swimming studies in mice with implanted pressure telemetry devices [2]. We found that LV systolic pressure (LVSP), LV end-diastolic pressure (LVEDP) and HR all increase abruptly following the onset of swimming (**Figure 3-6; Table 3-3**), as expected with endurance exercise [163]. Thereafter, the LVSP is maintained throughout the swimming period. By contrast, HR reaches a broad peak (707 ± 103 bpm) during the first ~10 minutes of swimming onset and then declines steadily (to 682 ± 91 bpm after 60 minutes and 644 ± 49 bpm at the end of a 120 minute bout of swimming). Importantly, the LVEDP shows a more complex time course (**Figure 3-6**) characterized by a profound early increase in pressure of 39 ± 5 mmHg at 2 ± 1 minute followed by a nadir in pressure of 25 ± 5 mmHg at 10 ± 2 minutes, which is well-above ($P < 0.045$) the LVEDP prior to swimming (12.7 ± 1.6 mmHg) (**Table 3-3**). Thereafter, the LVEDP slowly rises over time (30.3 ± 3.1 mmHg after 60 minutes and 43.7 ± 0.8 mmHg after 120 minutes of swimming). While the basis for the elevation in LVEDP is unclear, it is noted that it rises with progressive decreases in HR and V_{O_2} , similar to humans during exhaustive exercise [167]. Regardless, the temporal changes in LVEDP during swimming establish that as the time per swim increases the mice experience progressively higher mean

LVEDPs. As discussed below, these findings have important implications since AF risk is strongly linked to conditions with elevated LVEDP.

Table 3-3. Time-Dependent Hemodynamic Changes in Pressure Telemetry-Implanted Mice During an Acute Bout of Swim Exercise

	LVSP (mmHg)	LVEDP (mmHg)	HR (bpm)	dP/dt _{max} (mmHg/s)	dP/dt _{min} (mmHg/s)
Pre-Exercise	116.9±7.5	12.7±1.6	632±83	10894±798	-9204±491
0-10 min *peak value	166.4±4.3	52.4±4.8	707±103	15487±1507	-11439±2280
60 min	153.8±4.5	30.3±3.1	682±91	13574±1380	-10050±1620
90 min	156.5±3.3	39.7±5.0	661±31	13704±1626	-8844±1117
120 min	155.6±1.8	43.7±0.8	644±49	13080±1602	-8037±970

LVSP, Left Ventricular Systolic Pressure (mmHg); LVEDP, Left Ventricular End Diastolic Pressure (mmHg); HR, Heart Rate (bpm); dP/dt max, Maximal Pressure Change over Time (mmHg/s); dP/dt min, Minimal Pressure Change over Time (mmHg/s). Data are mean±SD and collected 30 seconds during the indicated time point, sample size: all time points (n=3) except 120 min time point (n=2).

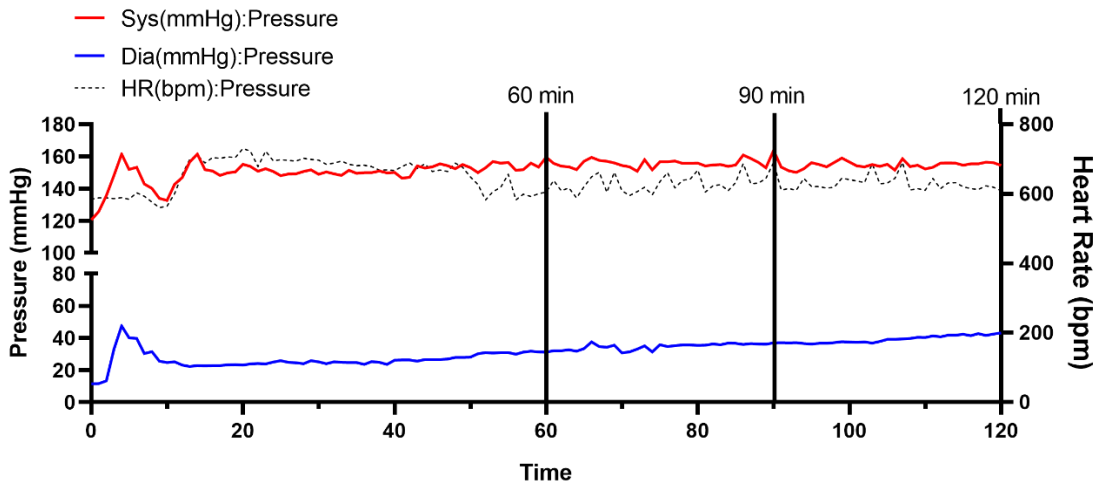


Figure 3-6. Pressure and Heart Rate Changes with Swim Duration – To assess ventricular pressure (systolic and diastolic) and heart rates with the progression of exercise duration, mice were implanted with telemetry units as described in (see Aschar-Sobbi et al. 2015) [2]. A sample tracing during an acute bout of intense swimming exercise is shown with the time points of 60, 90 and 120 minutes marked by vertical lines.

3.5 Discussion

The incidence of AF appears greatest in athletes engaged in endurance sports with the highest intensities measured in METs, and consequently highest V_{O_2} [96]. Therefore, we initially attempted to vary the exercise dose by altering the intensity during swimming by adjusting the velocities of water currents in our swim tanks. This approach failed because we found that mice self-regulate their swimming effort (through intermittent floating and immobility). Specifically, the V_{O_2} did not differ between mice swimming against different water currents, which has been suggested previously [191]. Consequently, we varied exercise dose by altering the daily swim durations (120, 180 or 240 minutes/day divided into 2 swims/day) while ensuring that the total work performed with exercise was similar (i.e. total O_2 consumed with swimming was ~ 500 L O_2 /kg). We found that as the amount of work performed per day with exercise increased (as measured by total O_2 consumed per day with swimming), so did susceptibility to AF. These findings build on reports concluding the incidence of AF correlated with the total cumulative doses of exercise [133], as well as exercise frequency [101, 177], intensity [101, 108, 110, 179, 180, 223, 224] and duration [177] as estimated with self-reporting. Our study is the first study to establish quantitatively that adverse atrial remodeling characterized by atrial hypertrophy and fibrosis, and AF inducibility are increased when daily exercise doses exceed a threshold. We also found that the degree of fibrosis and the duration of the induced AF events correlated with the daily dose of exercise. The association of AF vulnerability in our mice with atrial fibrosis as well as atrial hypertrophy, suggests that the AF arising from excessive daily exercise doses shares common pathogenic mechanisms with that seen in the more typical AF patient (i.e.

patients with poor cardiovascular health) [4]. Thus, our studies have important implication on AF mechanisms in patients other than athletes.

A major outcome of endurance training is ventricular enlargement [112] characterized by eccentric hypertrophy [122] and reduced ejection fractions [225]. We found similar adaptations in our mice, with increased ventricular dilation, ventricular hypertrophy (measured by VW normalized by BW) and reduced resting EFs in the highest daily exercise doses. Consistently, exercise in our mice promoted increases in cardiorespiratory fitness as observed in human athletes [101], which is related to ventricular adaptations [167].

Human athletes also invariably have sinus bradycardia which is linked to autonomic remodelling as well as increased heart rate variability (HRV) [145]. Importantly, the degree of HRV and autonomic remodelling appears to depend on exercise intensity [226, 227], and a speculated threshold of exercise duration for autonomic remodelling was previously hypothesized [141, 228-230]. Our mice showed similar patterns with respects to HR reductions which were only decreased in mice swimming 180 or 240 minutes/day compared to sedentary controls. Thus, our studies are the first of their kind to demonstrate that a threshold level of daily exercise dose is required to induced sinus bradycardia. Furthermore, sinus bradycardia appears to be a risk factor for AF in athletes [9, 148]. In this regard, highest doses of daily exercise (180 and 240 minutes/day) did not only lower resting HRs, but increased AF susceptibility. This observation seems particularly relevant since the bradycardia seen in athletes is linked to increased parasympathetic (PNS) activation which in turn is linked to AF in athletes [138]. The mechanism for this link is that parasympathetic activation causes abbreviated action potential durations (APDs) through activation of $I_{K,Ach}$ and inhibition of I_{Ca} [26] thereby promoting

arrhythmias [4]. Consistent with a role of the PNS in AF [9, 148], we found that parasympathetic nerve blockade reduced the incidence and duration of AF in mice, even though we only observed trends (albeit with $P>0.05$) showing increased PNA with the two higher daily exercise doses.

Another proposed mechanisms driving AF in athletes is atrial enlargement [9, 148], characterized by hypertrophy and dilation which both promote reentry-type arrhythmias [75]. Consistent with a role for atrial hypertrophy in the ability of daily exercise dose to promote AF, mice exercising at 180 and 240 minutes/day presented with atrial enlargement; the possible mechanisms for this are discussed later.

Fibrosis has been also proposed a substrate of AF in athletes [148] and recently quantified using LGE MRI [221]. Direct evidence for a role of fibrosis in AF pathogenesis with endurance exercise has also been identified in several rodent studies [2, 231]. This is highly relevant because fibrosis is considered a hallmark of AF in the general population [4]. Complementary to the proposed mechanism of fibrosis in the pathology of AF in patients and athletes, we observed elevated fibrosis in all exercise groups which was accompanied by decreases in atrial conductivity and P wave prolongation. Nevertheless, our study is the first of its kind to show that fibrosis increased in a dose dependent manner with exercise duration. These outcomes can be explained by the proinflammatory and profibrotic influence of stretch on the atria [4, 134], which invariably occurs with pressure and volume load during exercise. Furthermore, these conclusions are complimented by findings that fibrosis dose influences AF susceptibility and persistence [232-235], and computational models that suggest exercise dose

influences reentry probability [236, 237]. A discussion of how daily dose can directly impact atrial fibrosis is discussed below.

Although our study was limited to an animal model, the influence of exercise duration and dose were suggested from metanalysis and retrospective studies in humans. Multiple studies employ weekly metabolic equivalents (1 MET hours/week equals to 20 minutes of exercise) to assess the dose response relationship with AF with exercise “duration”. For example, >17 MET hours/week was shown associated with AF risk [238]. Interestingly, it was identified that those exercising at vigorous doses had higher AF risk, relative to those that exercise at moderate doses even if both groups exercised for a total 17 MET hours/week [238]. Apart from METs, meta-analyses also employed weekly hour quantities to assess the relationship between exercise dose and cardiovascular outcomes. For example, Schnohr et al. employed a self administrative survey to assess how exercise frequency, weekly duration and pace influence all cause mortality. Here, it was identified that running for 1-2.4 hours/ week showed the lowest hazard risk whereas running for longer periods (2.5-4 and >4 hours/week) showed higher risk of all cause mortality [177]. Interestingly, La Gerche notes that elite athletes, which tend to get AF, exercise 15-40 hours a week and represent the individuals at the upper limits of the studies described above [178]. It is important to note that although we did not identify a role for exercise intensity in the pathogenesis of AF, multiple studies have shown that CRF [96, 181, 239] and exercise intensity [101, 108, 110, 179, 180, 223, 224] also influence cardiovascular outcomes in a dose dependent manner. Nonetheless, no study controlled cumulative exercise dose and daily exercise durations as was done in our study, making it the first of its kind. Undeniably, although we found that swimming mice required a threshold of an exercise dose 15 L O₂/kg per day, such threshold

cannot be ascribed to human capacities as well as metabolic differences between the species are well established [240]. Therefore, such thresholds should be quantified in human studies as well.

3.5.1 Proposed Mechanism

Our findings show for the first time that the average V_{O_2} decreases as swim durations increase beyond ~60 minutes. Thus, even though the degree of atrial fibrosis and hypertrophy as well as AF inducibility increased as a function of daily swim durations, the exercise intensity was the highest for the shorter swims. These results suggest that exercise intensity during the swim (as reflected in the V_{O_2}) is not a primary factor driving remodeling in exercised mice under our experimental conditions. These observations have important implications on the mechanisms for promotion of AF. In particular, we found that, after reaching a broad peak swimming at the outset of swimming, HR declines steadily progressively with time in conjunction with ongoing increases in LVEDP. Similar patterns have previously been shown in humans in response to exhaustive exercise [167]. Regardless, since the atria are highly compliant (compared to ventricles) [2], elevations in LVEDP will cause atrial stretch [75], which is known to activate of pathways involved in adverse remodeling such as hypertrophy and fibrosis (involving TGF β , Angiotensin II and other proinflammatory and profibrotic markers) [4, 134, 241] with elevated influence on the atria compared to the ventricles [4, 241]. Thus, consistent with human studies showing that long-term endurance training promotes electrical and structural changes in atria marked by prolonged P wave durations [212], we observed that there was progressive increases in fibrosis as the daily exercise durations increased.

It is worth to mention that one limitation of employing mice in studying the influence of remodelling on arrhythmia in humans, is the differential impact of fibrosis on susceptibility in

both species [15]. Despite this, fibrosis deposition has been recently shown in human athletes [221], which suggests that the influence of fibrosis dose on AF in athletes should be studied more thoroughly and in conjugation with other pathophysiological substrates and modulators [9, 146, 148].

Collectively, our study is the first of its kind to employ a controlled exercise model to assess the influence of exercise duration on AF pathogenesis, independently of other variables such as integrated total exercise dose, frequency or exercise intensity. We propose that AF susceptibility is increased with elevated exercise durations which is linked to progressive elevations in LVEDP leading to increased atrial stretch as the daily doses of swim exercise are increased (and swim durations are extended). It would be of considerable interest to assess how atria respond when the daily swim times are kept fixed at ~240 minutes/day but divided into larger number of shorter bouts to reduce the extent of LVEDP elevation. Furthermore, our results suggest that although well accepted mechanisms of AF in athletes, such as vagal tone and atrial enlargement, play an important role in AF pathogenesis with extreme endurance exercise – the dose dependent increase of AF to exercise duration is reliant on fibrosis deposition in the atria. The underlying cause for this could be stretch promoted wall stress and remodelling which occurs acutely during exercise [75, 221]. Undeniably, fibrosis behaves as a convergent point to other physiological outcomes resulting from prolonged exposure to intense endurance exercise [241].

3.5.2 Future Directions

It has been previously proposed that workload cannot be varied with swimming exercise in mice [191], supported by progressive increases in immobility with swimming in CD1 mice [187]

and self regulatory behaviours such as bobbing and floating with longer exercise durations in all rodents [19, 193, 194]. Fortunately, this coincides with our observation of progressive decrease in V_{O_2} throughout the swim bout. Therefore, it would be interesting to employ a running model (where incline, speed or resistance are controlled by the researcher) to study the influence of exercise duration of AF and atrial remodelling without allowing for self regulatory behaviours. As such, we are currently investigating the role of exercise in AF with a running model.

We formerly showed that blocking fibrosis deposition through a knockout model or by pharmacological administration of Etanercept [2] or XPRO [68] abolished fibrosis deposition in swimming mice, subsequently eradicating atrial arrhythmias. Observing whether abolishment of fibrosis in this model would eliminate arrhythmogenesis at higher swim doses would support the conclusion that AF pathogenesis is dose dependent on collagen deposition.

Furthermore, atrial stretch is associated with inflammation [134] which is profibrotic in it self. Strachan et al. identified that increases in proinflammatory C-reaction protein (CRP) levels appeared dose dependent in trained athletes running at variable marathon length from 15 to 88 km, with individuals running the longest durations showing pathologically high levels of CRP [242]. Similarly, we previously observed that fibrosis deposition was guided by inflammatory response due to signal transduction mechanisms related to $TNF\alpha$, where macrophages were identified as the primary inflammatory cells. We are currently investigating whether the observed dose response also corresponds with an increase in macrophage infiltration. To this end, we are using immunohistochemistry to stain for macrophages using the F4 80 antibody.

We suspect that a threshold of daily exercise dose (of ~ 15 $LO_2/kg/day$, 180 minutes/day in our mouse model) is required for the pathogenesis of AF. It would be interesting to assess the

much (total exercise dose) swim exercise would be required to exercise at this threshold to promote remodelling which matches that of exercise at longer durations (240 minutes/day). Indeed, research suggests that prolonged increases in cumulative lifetime doses promote adverse autonomic remodelling [138] as well as structural remodelling [133, 138]. To this end, we are investigating whether increasing a swim dose from 6 to 12 weeks for mice swimming at 180 minutes/minute would support these conclusions. Our preliminary results show that a 12-week swim increases AF inducibility to 55%. Nonetheless, we are still investigating the specific underlying pathophysiological mechanisms (**Supplementary Figure 3-9**).

3.6 Supplementary Figures

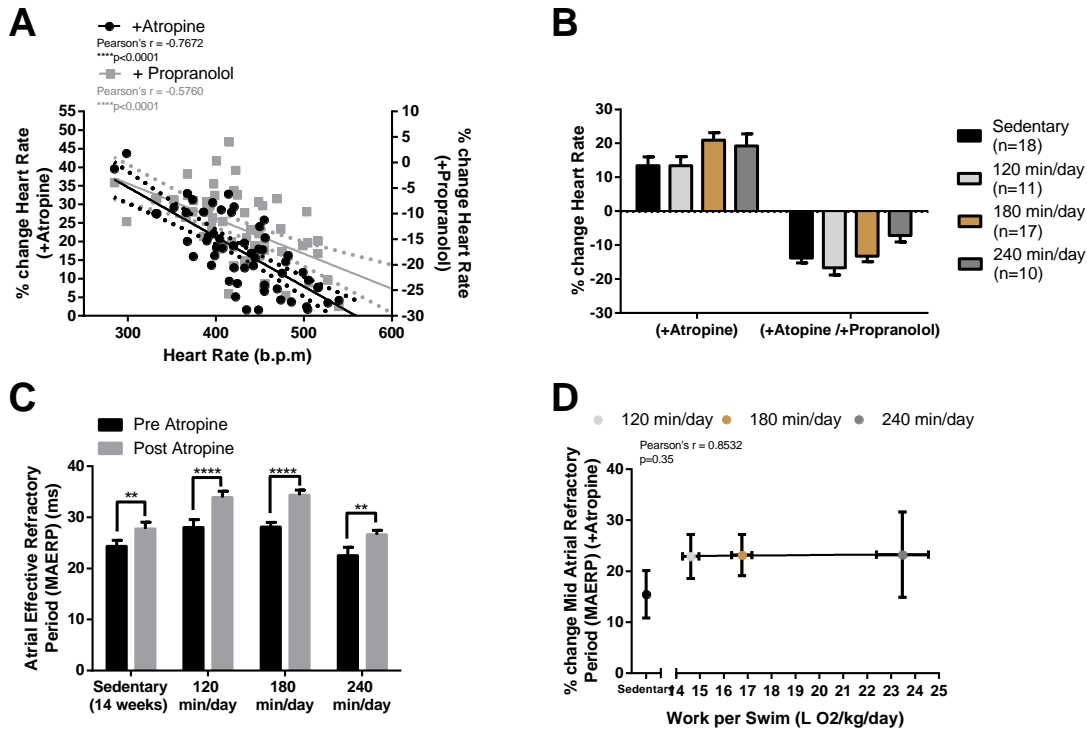


Figure 3-7. Autonomic Remodelling Influences Heart Rates in CD1 Mice – To assess the activity of the Sympathetic and Parasympathetic branches separately, percent change (%) after Atropine injection and after Propranolol injection were plotted, respectively. A) Baseline HRs were significantly correlated with response to atropine and propranolol, suggesting that differences in heart rate are autonomically modulated. B) % change Atropine reflects differences between baseline HR and post Atropine injection, whereas % change Atropine/Propranolol reflects differences between HR post Atropine injection and post Propranolol injection. Parasympathetic remodelling increased proportionally with exercise regime, as observed by an increasing trend. C) AERP in the mid atria was measured before and after atropine injection. MAERP was significantly elevated in all groups after atropine injection (two-way ANOVA). D) there was no association between exercise dose (measure as O₂ volume consumed per swim) and AERP response to atropine. Data are mean±SEM, sample sizes are shown, ** $p < 0.01$, **** $p < 0.0001$.

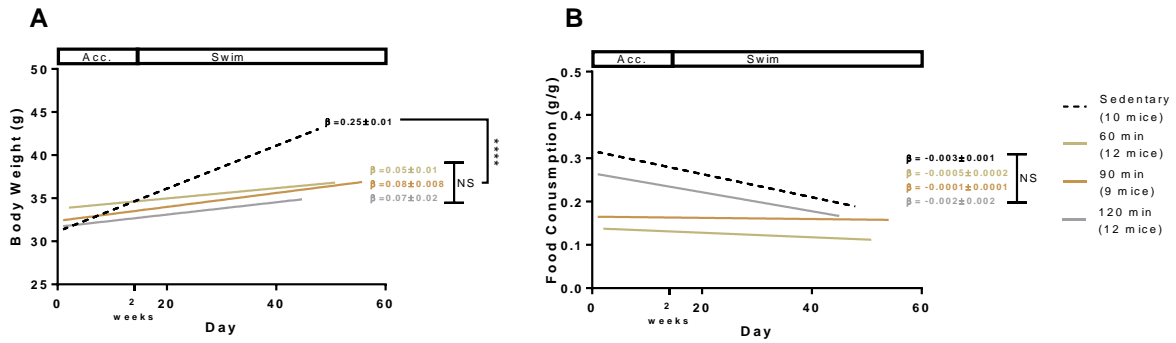


Figure 3-8. Changes in Body Weight and Food Consumption over Exercise Protocol – A)

Body weights of mice in each exercise group were monitored and recorded 2-3 times a week for the whole exercise regime starting the age of 6 weeks. Acclimatization (Acc.) usually lasted ~2 weeks. Mean body weight was identified for each group and plotted as a function of day of protocol. Linear regression analysis was used to find the rate of change (β , slope). Rate of change in body weight was not difference between exercise groups but was significantly lower than sedentary. B) Mice were fed mice chow and water *ad lib*. Every time body weight was measured, changes in food between the previous and current day were noted. To remove bias, food weights were noted at identical times (9 am). Food consumption was quantified as weight of food consumed between the two days, divided by the total body weight of the mice in the cage. Mean food consumption was identified and plotted as a function of day of protocol. Linear regression analysis was used to find the rate of change of food consumption. For simplicity purposes, only the rates of change are shown.

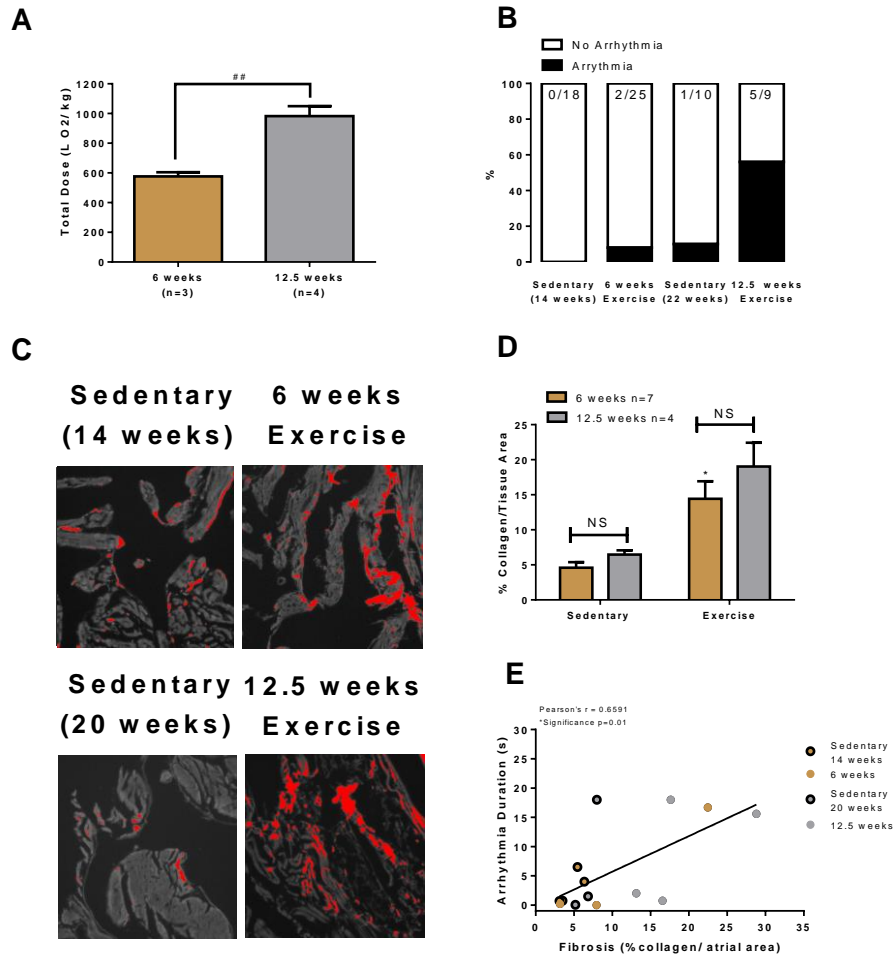


Figure 3-9. Cumulative Exercise Dose and Atrial Fibrillation Preliminary Results – Mice were swam for either 6 weeks or 12.5 weeks (to double the total exercise effort) for 180 minutes/day. Two age matched sedentary groups were employed for comparisons – at 14 weeks of age (for 6-week exercise regimes) and 20 weeks of age (for 12.5-week exercise regimes). These 6-week exercise mice were the ones used for the original study. A) oxygen consumption measurements were employed to quantify cumulative/total exercise dose (i.e the total volume of oxygen consumed over 6 or 12.5 weeks). Mice swimming for 12.5 weeks did double the amount of work as the 6-week mice. B) Doubling the exercise dose, also increased atrial arrhythmia inducibility. Atrial fibrillation was assessed during the intracardiac experiments as previously discussed in the original study. Data analyzed using a contingency table with the χ^2 test. C) Sample images from picrosirius red staining for collagen content. Images were collected as previously described. D) Collagen quantification was completed using the threshold method and was plotted as average fibrosis content. Two-way ANOVA was employed to test differences. E) Fibrosis content and atrial arrhythmia durations were significantly correlated. Data are mean \pm SEM, * $p\leq 0.05$, ** $p<0.01$. * relative to age matched sedentary, # relative to exercise groups

4. References

1. Karunathilake, S.P. and G.U. Ganegoda, *Secondary Prevention of Cardiovascular Diseases and Application of Technology for Early Diagnosis*. Biomed Res Int, 2018. **2018**: p. 5767864.
2. Aschar-Sobbi, R., et al., *Increased atrial arrhythmia susceptibility induced by intense endurance exercise in mice requires TNFalpha*. Nat Commun, 2015. **6**: p. 6018.
3. Wyndham, C.R., *Atrial fibrillation: the most common arrhythmia*. Tex Heart Inst J, 2000. **27**(3): p. 257-67.
4. Schotten, U., et al., *Pathophysiological mechanisms of atrial fibrillation: a translational appraisal*. Physiol Rev, 2011. **91**(1): p. 265-325.
5. Nattel, S., *New ideas about atrial fibrillation 50 years on*. Nature, 2002. **415**(6868): p. 219-26.
6. Lavie, C.J., et al., *Exercise and the cardiovascular system: clinical science and cardiovascular outcomes*. Circ Res, 2015. **117**(2): p. 207-19.
7. O'Keefe, J.H., C.J. Lavie, and M. Guazzi, *Part 1: potential dangers of extreme endurance exercise: how much is too much? Part 2: screening of school-age athletes*. Prog Cardiovasc Dis, 2015. **57**(4): p. 396-405.
8. Garlipp, D.C., et al., *Physical Activity and Incidence of Atrial Fibrillation - Systematic Review and Meta-Analysis*. International Journal of Cardiovascular Sciences, 2019. **32**: p. 384-390.
9. Turagam, M.K., et al., *Atrial Fibrillation In Athletes: Pathophysiology, Clinical Presentation, Evaluation and Management*. J Atr Fibrillation, 2015. **8**(4): p. 1309.
10. Morseth, B., et al., *Physical activity, resting heart rate, and atrial fibrillation: the Tromso Study*. Eur Heart J, 2016. **37**(29): p. 2307-13.
11. Bosomworth, N.J., *Atrial fibrillation and physical activity: Should we exercise caution?* Can Fam Physician, 2015. **61**(12): p. 1061-70.
12. Spach, M.S. and M.E. Josephson, *Initiating reentry: the role of nonuniform anisotropy in small circuits*. J Cardiovasc Electrophysiol, 1994. **5**(2): p. 182-209.
13. Grunnet, M., *Repolarization of the cardiac action potential. Does an increase in repolarization capacity constitute a new anti-arrhythmic principle?* Acta Physiologica, 2010. **198**(s676): p. 1-48.
14. Iwasaki, Y.K., et al., *Atrial fibrillation pathophysiology: implications for management*. Circulation, 2011. **124**(20): p. 2264-74.
15. Kaese, S. and S. Verheule, *Cardiac electrophysiology in mice: a matter of size*. Frontiers in Physiology, 2012. **3**(345).
16. Trépanier-Boulay, V., et al., *Postnatal development of atrial repolarization in the mouse*. Cardiovascular Research, 2004. **64**(1): p. 84-93.
17. Nerbonne, J.M., *Molecular basis of functional voltage-gated K⁺ channel diversity in the mammalian myocardium*. J Physiol, 2000. **525 Pt 2**: p. 285-98.
18. Bootman, M.D., et al., *Calcium signalling during excitation-contraction coupling in mammalian atrial myocytes*. Journal of Cell Science, 2006. **119**(19): p. 3915-3925.
19. Izaddoustdar, F., *Mechanisms Underlying Exercise-induced Atrial Fibrillation in Department of Physiology* 2013, University of Toronto Canada p. 176.

20. Mayer, A.G., *THE CAUSE OF PULSATION* Popular Science Monthly 1908 **73**: p. 481-487.
21. Mines, G.R., *On circulating excitation in heart muscles and their possible relation to tachycardia and fibrillation* Transactions of the Royal Society of Canada, 1914. **4**: p. 43-52.
22. Surawicz, B., *Brief history of cardiac arrhythmias since the end of the nineteenth century: part I.* J Cardiovasc Electrophysiol, 2003. **14**(12): p. 1365-71.
23. Allesie, M.A., F.I. Bonke, and F.J. Schopman, *Circus movement in rabbit atrial muscle as a mechanism of tachycardia. III. The "leading circle" concept: a new model of circus movement in cardiac tissue without the involvement of an anatomical obstacle.* Circulation Research, 1977. **41**(1): p. 9-18.
24. Winfree, A.T., *Spiral waves of chemical activity.* Science, 1972. **175**(4022): p. 634-6.
25. Pandit, S.V. and J. Jalife, *Rotors and the dynamics of cardiac fibrillation.* Circ Res, 2013. **112**(5): p. 849-62.
26. Moe, G.K. and J.A. Abildskov, *Atrial fibrillation as a self-sustaining arrhythmia independent of focal discharge.* American Heart Journal, 1959. **58**(1): p. 59-70.
27. Allesie MA, L.W., Bonke FIM, and Hollen JM. , *Experimental evaluation of Moe's multiple wavelet hypothesis of atrial fibrillation.* . Cardiac Electrophysiology and Arrhythmias., 1985: p. 265-76.
28. Antzelevitch, C. and A. Burashnikov, *Overview of Basic Mechanisms of Cardiac Arrhythmia.* Card Electrophysiol Clin, 2011. **3**(1): p. 23-45.
29. Riley, G., et al., *An introduction to murine models of atrial fibrillation.* Front Physiol, 2012. **3**: p. 296.
30. Lee, A.M., et al., *Importance of atrial surface area and refractory period in sustaining atrial fibrillation: testing the critical mass hypothesis.* J Thorac Cardiovasc Surg, 2013. **146**(3): p. 593-8.
31. Azevedo, P.S., et al., *Cardiac Remodeling: Concepts, Clinical Impact, Pathophysiological Mechanisms and Pharmacologic Treatment.* Arq Bras Cardiol, 2016. **106**(1): p. 62-9.
32. Pellman, J. and F. Sheikh, *Atrial fibrillation: mechanisms, therapeutics, and future directions.* Compr Physiol, 2015. **5**(2): p. 649-65.
33. Stavrakis, S. and S. Po, *Ganglionated Plexi Ablation: Physiology and Clinical Applications.* Arrhythm Electrophysiol Rev, 2017. **6**(4): p. 186-190.
34. Po, S.S., H. Nakagawa, and W.M. Jackman, *Localization of left atrial ganglionated plexi in patients with atrial fibrillation.* J Cardiovasc Electrophysiol, 2009. **20**(10): p. 1186-9.
35. Zheng, S., et al., *Long-term results of a minimally invasive surgical pulmonary vein isolation and ganglionic plexi ablation for atrial fibrillation.* PLoS One, 2013. **8**(11): p. e79755.
36. Kirchhof, C.J. and M.A. Allesie, *Sinus node automaticity during atrial fibrillation in isolated rabbit hearts.* Circulation, 1992. **86**(1): p. 263-271.
37. Nadeau, R.A., F.A. Roberge, and J. Billette, *Role of the Sinus Node in the Mechanism of Cholinergic Atrial Fibrillation.* Circulation Research, 1970. **27**(1): p. 129-138.
38. Page, P.L., *Sinus Node During Atrial Fibrillation To Beat or Not to Beat?* Circulation, 1992. **86**(1): p. 334-336.

39. Volders, P.G.A., et al., *Similarities between early and delayed afterdepolarizations induced by isoproterenol in canine ventricular myocytes I*. Cardiovascular Research, 1997. **34**(2): p. 348-359.
40. Weiss, J.N., et al., *Early afterdepolarizations and cardiac arrhythmias*. Heart Rhythm, 2010. **7**(12): p. 1891-9.
41. Nattel, S., et al., *Arrhythmogenic Ion-Channel Remodeling in the Heart: Heart Failure, Myocardial Infarction, and Atrial Fibrillation*. Physiological Reviews, 2007. **87**(2): p. 425-456.
42. Burashnikov, A. and C. Antzelevitch, *Late-phase 3 EAD. A unique mechanism contributing to initiation of atrial fibrillation*. Pacing Clin Electrophysiol, 2006. **29**(3): p. 290-5.
43. Zhang, H., et al., *Role of up-regulation of IK1 in action potential shortening associated with atrial fibrillation in humans*. Cardiovasc Res, 2005. **66**(3): p. 493-502.
44. Dobrev, D., *Electrical Remodeling in Atrial Fibrillation*. Herz, 2006. **31**(2): p. 108-112.
45. Thomas, S.A., et al., *Disparate effects of deficient expression of connexin43 on atrial and ventricular conduction: evidence for chamber-specific molecular determinants of conduction*. Circulation, 1998. **97**(7): p. 686-91.
46. Allesie, M., J. Ausma, and U. Schotten, *Electrical, contractile and structural remodeling during atrial fibrillation*. Cardiovascular Research, 2002. **54**(2): p. 230-246.
47. Morillo, C.A., et al., *Chronic rapid atrial pacing. Structural, functional, and electrophysiological characteristics of a new model of sustained atrial fibrillation*. Circulation, 1995. **91**(5): p. 1588-95.
48. Wijffels, M.C., et al., *Atrial fibrillation begets atrial fibrillation. A study in awake chronically instrumented goats*. Circulation, 1995. **92**(7): p. 1954-68.
49. Dobrev, D. and U. Ravens, *Remodeling of cardiomyocyte ion channels in human atrial fibrillation*. Basic Research in Cardiology, 2003. **98**(3): p. 137-148.
50. Schotten, U., et al., *Atrial fibrillation-induced atrial contractile dysfunction: a tachycardiomyopathy of a different sort*. Cardiovasc Res, 2002. **53**(1): p. 192-201.
51. Yu, W.C., et al., *Reversal of atrial electrical remodeling following cardioversion of long-standing atrial fibrillation in man*. Cardiovasc Res, 1999. **42**(2): p. 470-6.
52. Hobbs, W.J., et al., *Reversal of atrial electrical remodeling after cardioversion of persistent atrial fibrillation in humans*. Circulation, 2000. **101**(10): p. 1145-51.
53. Verrecchia, F. and A. Mauviel, *TGF- β and TNF- α : antagonistic cytokines controlling type I collagen gene expression*. Cellular Signalling, 2004. **16**(8): p. 873-880.
54. Baudino, T.A., et al., *Cardiac fibroblasts: friend or foe?* American Journal of Physiology-Heart and Circulatory Physiology, 2006. **291**(3): p. H1015-H1026.
55. Nicoletti, A. and J.B. Michel, *Cardiac fibrosis and inflammation: interaction with hemodynamic and hormonal factors*. Cardiovasc Res, 1999. **41**(3): p. 532-43.
56. Clark, D.A. and R. Coker, *Transforming growth factor-beta (TGF-beta)*. Int J Biochem Cell Biol, 1998. **30**(3): p. 293-8.
57. Verrecchia, F. and A. Mauviel, *TGF-beta and TNF-alpha: antagonistic cytokines controlling type I collagen gene expression*. Cell Signal, 2004. **16**(8): p. 873-80.
58. Schnee, J.M. and W.A. Hsueh, *Angiotensin II, adhesion, and cardiac fibrosis*. Cardiovascular Research, 2000. **46**(2): p. 264-268.

59. King, J.H., C.L.H. Huang, and J.A. Fraser, *Determinants of myocardial conduction velocity: implications for arrhythmogenesis*. *Frontiers in physiology*, 2013. **4**: p. 154-154.
60. Spach, M.S., et al., *The discontinuous nature of propagation in normal canine cardiac muscle. Evidence for recurrent discontinuities of intracellular resistance that affect the membrane currents*. *Circ Res*, 1981. **48**(1): p. 39-54.
61. Engelmann, M.D.M. and J.H. Svendsen, *Inflammation in the genesis and perpetuation of atrial fibrillation*. *European Heart Journal*, 2005. **26**(20): p. 2083-2092.
62. Frustaci, A., et al., *Histological substrate of atrial biopsies in patients with lone atrial fibrillation*. *Circulation*, 1997. **96**(4): p. 1180-4.
63. Nakamura, Y., et al., *Tissue factor expression in atrial endothelia associated with nonvalvular atrial fibrillation: possible involvement in intracardiac thrombogenesis*. *Thromb Res*, 2003. **111**(3): p. 137-42.
64. Chung, M.K., et al., *C-Reactive Protein Elevation in Patients With Atrial Arrhythmias*. *Circulation*, 2001. **104**(24): p. 2886-2891.
65. Psychari, S.N., et al., *Relation of elevated C-reactive protein and interleukin-6 levels to left atrial size and duration of episodes in patients with atrial fibrillation*. *American Journal of Cardiology*, 2005. **95**(6): p. 764-767.
66. Aviles, R.J., et al., *Inflammation as a Risk Factor for Atrial Fibrillation*. *Circulation*, 2003. **108**(24): p. 3006-3010.
67. Deng, H., et al., *Role of tumor necrosis factor-alpha in the pathogenesis of atrial fibrillation*. *Chin Med J (Engl)*, 2011. **124**(13): p. 1976-82.
68. Lakin, R., et al., *Inhibition of soluble TNFalpha prevents adverse atrial remodeling and atrial arrhythmia susceptibility induced in mice by endurance exercise*. *J Mol Cell Cardiol*, 2019. **129**: p. 165-173.
69. Saba, S., et al., *Atrial contractile dysfunction, fibrosis, and arrhythmias in a mouse model of cardiomyopathy secondary to cardiac-specific overexpression of tumor necrosis factor- α* . *Am J Physiol Heart Circ Physiol*, 2005. **289**(4): p. H1456-67.
70. Galea, R., et al., *Inflammation and C-reactive protein in atrial fibrillation: cause or effect?* *Tex Heart Inst J*, 2014. **41**(5): p. 461-8.
71. Arora, S., et al., *Atrial fibrillation in a tertiary care multidisciplinary intensive care unit--incidence and risk factors*. *Anaesth Intensive Care*, 2007. **35**(5): p. 707-13.
72. Ho, K.M. and J.A. Tan, *Benefits and risks of corticosteroid prophylaxis in adult cardiac surgery: a dose-response meta-analysis*. *Circulation*, 2009. **119**(14): p. 1853-66.
73. Ito, K., et al., *An immunohistochemical analysis of tissue thrombin expression in the human atria*. *PLoS One*, 2013. **8**(6): p. e65817.
74. Henry, W.L., et al., *Relation between echocardiographically determined left atrial size and atrial fibrillation*. *Circulation*, 1976. **53**(2): p. 273-9.
75. Rosenberg Michael, A. and J. Manning Warren, *Diastolic Dysfunction and Risk of Atrial Fibrillation*. *Circulation*, 2012. **126**(19): p. 2353-2362.
76. Solti, F., et al., *The effect of atrial dilatation on the genesis of atrial arrhythmias*. *Cardiovasc Res*, 1989. **23**(10): p. 882-6.
77. Eijsbouts, S.C., et al., *Effects of acute atrial dilation on heterogeneity in conduction in the isolated rabbit heart*. *J Cardiovasc Electrophysiol*, 2003. **14**(3): p. 269-78.

78. Ravelli, F. and M. Allessie, *Effects of atrial dilatation on refractory period and vulnerability to atrial fibrillation in the isolated Langendorff-perfused rabbit heart.* Circulation, 1997. **96**(5): p. 1686-95.
79. Peyronnet, R., J.M. Nerbonne, and P. Kohl, *Cardiac Mechano-Gated Ion Channels and Arrhythmias.* Circ Res, 2016. **118**(2): p. 311-29.
80. Peter Kohl, F.S., Michael R. Franz *Cardiac mechano-electric coupling and arrhythmias - Second Edition* 2011, New York Oxford University Press.
81. Iribe, G., et al., *Axial stretch of rat single ventricular cardiomyocytes causes an acute and transient increase in Ca²⁺ spark rate.* Circ Res, 2009. **104**(6): p. 787-95.
82. Bode, F., F. Sachs, and M.R. Franz, *Tarantula peptide inhibits atrial fibrillation.* Nature, 2001. **409**(6816): p. 35-6.
83. Bode, F., et al., *Gadolinium decreases stretch-induced vulnerability to atrial fibrillation.* Circulation, 2000. **101**(18): p. 2200-5.
84. Boyden, P.A. and B.F. Hoffman, *The effects on atrial electrophysiology and structure of surgically induced right atrial enlargement in dogs.* Circulation Research, 1981. **49**(6): p. 1319-1331.
85. Verheule, S., et al., *Alterations in atrial electrophysiology and tissue structure in a canine model of chronic atrial dilatation due to mitral regurgitation.* Circulation, 2003. **107**(20): p. 2615-22.
86. Sanfilippo, A.J., et al., *Atrial enlargement as a consequence of atrial fibrillation. A prospective echocardiographic study.* Circulation, 1990. **82**(3): p. 792-7.
87. Haissaguerre, M., et al., *Spontaneous initiation of atrial fibrillation by ectopic beats originating in the pulmonary veins.* N Engl J Med, 1998. **339**(10): p. 659-66.
88. Nguyen, B.L., et al., *Histopathological substrate for chronic atrial fibrillation in humans.* Heart Rhythm, 2009. **6**(4): p. 454-60.
89. Hassink, R.J., et al., *Morphology of atrial myocardium in human pulmonary veins: a postmortem analysis in patients with and without atrial fibrillation.* J Am Coll Cardiol, 2003. **42**(6): p. 1108-14.
90. Verdecchia, P., F. Angeli, and G. Reboldi, *Hypertension and Atrial Fibrillation.* Circulation Research, 2018. **122**(2): p. 352-368.
91. Sopher, S.M. and A.J. Camm, *Atrial fibrillation: Maintenance of sinus rhythm versus rate control.* The American Journal of Cardiology, 1996. **77**(3): p. 24A-37A.
92. Woods, C.E. and J. Olgin, *Atrial Fibrillation Therapy Now and in the Future.* Circulation Research, 2014. **114**(9): p. 1532-1546.
93. Sultan, A., et al., *Predictors of Atrial Fibrillation Recurrence after Catheter Ablation: Data from the German Ablation Registry.* 2017. **7**(1): p. 16678.
94. Shah, S., et al., *Recurrent Atrial Fibrillation After Initial Long-Term Ablation Success.* Circulation: Arrhythmia and Electrophysiology, 2018. **11**(4): p. e005785.
95. Ruegsegger, G.N. and F.W. Booth, *Health Benefits of Exercise.* Cold Spring Harb Perspect Med, 2018. **8**(7).
96. Merghani, A., A. Malhotra, and S. Sharma, *The U-shaped relationship between exercise and cardiac morbidity.* Trends in Cardiovascular Medicine, 2016. **26**(3): p. 232-240.
97. Morris, J.N., et al., *Vigorous exercise in leisure-time: protection against coronary heart disease.* Lancet, 1980. **2**(8206): p. 1207-10.

98. Goraya, T.Y., et al., *Prognostic value of treadmill exercise testing in elderly persons*. Ann Intern Med, 2000. **132**(11): p. 862-70.
99. Kujala, U.M., et al., *Prevalence of diabetes, hypertension, and ischemic heart disease in former elite athletes*. Metabolism, 1994. **43**(10): p. 1255-60.
100. Myers, J., et al., *Exercise Capacity and Mortality among Men Referred for Exercise Testing*. New England Journal of Medicine, 2002. **346**(11): p. 793-801.
101. Lee, D.C., et al., *Leisure-time running reduces all-cause and cardiovascular mortality risk*. J Am Coll Cardiol, 2014. **64**(5): p. 472-81.
102. Furlanello, F., et al., *Atrial fibrillation in elite athletes*. J Cardiovasc Electrophysiol, 1998. **9**(8 Suppl): p. S63-8.
103. Coelho, A., et al., *Tachyarrhythmias in young athletes*. J Am Coll Cardiol, 1986. **7**(1): p. 237-43.
104. Karjalainen, J., et al., *Lone atrial fibrillation in vigorously exercising middle aged men: case-control study*. Bmj, 1998. **316**(7147): p. 1784-5.
105. Mont, L., et al., *Long-lasting sport practice and lone atrial fibrillation*. Eur Heart J, 2002. **23**(6): p. 477-82.
106. Elosua, R., et al., *Sport practice and the risk of lone atrial fibrillation: a case-control study*. Int J Cardiol, 2006. **108**(3): p. 332-7.
107. Vroomen, M. and L. Pison, *Lone Atrial Fibrillation: Risk Factors, Triggers And Ablation Techniques*. J Atr Fibrillation, 2015. **8**(1): p. 1203.
108. Andersen, K., et al., *Risk of arrhythmias in 52 755 long-distance cross-country skiers: a cohort study*. European Heart Journal, 2013. **34**(47): p. 3624-3631.
109. O'Keefe, J.H., et al., *Potential Adverse Cardiovascular Effects From Excessive Endurance Exercise*. Mayo Clinic Proceedings, 2012. **87**(6): p. 587-595.
110. Aizer, A., et al., *Relation of Vigorous Exercise to Risk of Atrial Fibrillation*. American Journal of Cardiology, 2009. **103**(11): p. 1572-1577.
111. Morganroth, J., et al., *Comparative left ventricular dimensions in trained athletes*. Ann Intern Med, 1975. **82**(4): p. 521-4.
112. Fagard, R., *Athlete's heart*. Heart (British Cardiac Society), 2003. **89**(12): p. 1455-1461.
113. Barbier, J., et al., *Sports-specific features of athlete's heart and their relation to echocardiographic parameters*. Herz, 2006. **31**(6): p. 531-43.
114. Baggish, A.L. and M.J. Wood, *Athlete's Heart and Cardiovascular Care of the Athlete*. Circulation, 2011. **123**(23): p. 2723-2735.
115. Hunt, E.A., *Electrocardiographic study of 20 champion swimmers before and after 110-yard sprint swimming competition*. Can Med Assoc J, 1963. **88**: p. 1251-3.
116. Arstila, M. and A. Koivikko, *Electrocardiographic and vectorcardiographic signs of left and right ventricular hypertrophy in endurance athletes*. J Sports Med Phys Fitness, 1966. **6**(3): p. 166-75.
117. Gott, P.H., H.A. Roselle, and R.S. Crampton, *The Athletic Heart Syndrome: Five-Year Cardiac Evaluation of a Champion Athlete*. Archives of Internal Medicine, 1968. **122**(4): p. 340-344.
118. Van Ganse, W., et al., *The electrocardiogram of athletes & Comparison with untrained subjects*. British Heart Journal, 1970. **32**(2): p. 160.

119. Hanne-Paparo, N., M.H. Wendkos, and D. Brunner, *T wave abnormalities in the electrocardiograms of top-ranking athletes without demonstrable organic heart disease*. American Heart Journal, 1971. **81**(6): p. 743-747.
120. Katritsis, G.D. and D.G. Katritsis, *The Electrocardiogram in Athletes Revisited*. Arrhythm Electrophysiol Rev, 2013. **2**(2): p. 99-104.
121. Maron, B.J., J.M. Isner, and W.J. McKenna, *Task force 3: Hypertrophic cardiomyopathy, myocarditis and other myopericardial diseases and mitral valve prolapse*. Journal of the American College of Cardiology, 1994. **24**(4): p. 880-885.
122. Muhl, C., W.R. Dassen, and H. Kuipers, *Cardiac remodelling: concentric versus eccentric hypertrophy in strength and endurance athletes*. Neth Heart J, 2008. **16**(4): p. 129-33.
123. Fagard, R., C. Van Den Broeke, and A. Amery, *Left ventricular dynamics during exercise in elite marathon runners*. Journal of the American College of Cardiology, 1989. **14**(1): p. 112-118.
124. Bar-Shlomo, B.Z., et al., *Left ventricular function in trained and untrained healthy subjects*. Circulation, 1982. **65**(3): p. 484-8.
125. Fulghum, K. and B.G. Hill, *Metabolic Mechanisms of Exercise-Induced Cardiac Remodeling*. Frontiers in Cardiovascular Medicine, 2018. **5**(127).
126. Wood, A.L.B.a.M.J., *Athlete's Heart and Cardiovascular Care of the Athlete*. Circulation, 2011. **123**: p. 2723–2735.
127. Fagard, R., et al., *Noninvasive assessment of seasonal variations in cardiac structure and function in cyclists*. Circulation, 1983. **67**(4): p. 896-901.
128. Pelliccia, A., et al., *Remodeling of left ventricular hypertrophy in elite athletes after long-term deconditioning*. Circulation, 2002. **105**(8): p. 944-9.
129. Bulwer, B.E., S.D. Solomon, and R. Janardhanan, *Echocardiographic Assessment of Ventricular Systolic Function*, in *Essential Echocardiography: A Practical Handbook With DVD*, S.D. Solomon and B. Bulwer, Editors. 2007, Humana Press: Totowa, NJ. p. 89-117.
130. Fagard, R., et al., *Cardiac structure and function in cyclists and runners. Comparative echocardiographic study*. Br Heart J, 1984. **52**(2): p. 124-9.
131. Lakin, R., et al., *Changes in Heart Rate and Its Regulation by the Autonomic Nervous System Do Not Differ Between Forced and Voluntary Exercise in Mice*. Front Physiol, 2018. **9**: p. 841.
132. Pelliccia, A., et al., *Prevalence and clinical significance of left atrial remodeling in competitive athletes*. J Am Coll Cardiol, 2005. **46**(4): p. 690-6.
133. Brugger, N., et al., *Effect of lifetime endurance training on left atrial mechanical function and on the risk of atrial fibrillation*. Int J Cardiol, 2014. **170**(3): p. 419-25.
134. De Jong, A.M., et al., *Mechanisms of atrial structural changes caused by stretch occurring before and during early atrial fibrillation*. Cardiovascular Research, 2010. **89**(4): p. 754-765.
135. La Gerche, A. and G. Claessen, *Increased Flow, Dam Walls, and Upstream Pressure: The Physiological Challenges and Atrial Consequences of Intense Exercise**. JACC: Cardiovascular Imaging, 2016. **9**(12): p. 1389-1391.
136. Erol, M.K. and S. Karakelleoglu, *Assessment of right heart function in the athlete's heart*. Heart Vessels, 2002. **16**(5): p. 175-80.

137. Nishimura, T., Y. Yamada, and C. Kawai, *Echocardiographic evaluation of long-term effects of exercise on left ventricular hypertrophy and function in professional bicyclists*. *Circulation*, 1980. **61**(4): p. 832-40.
138. Wilhelm, M., et al., *Atrial Remodeling, Autonomic Tone, and Lifetime Training Hours in Nonelite Athletes*. *American Journal of Cardiology*, 2011. **108**(4): p. 580-585.
139. Wilhelm, M., et al., *Comparison of Pro-Atrial Natriuretic Peptide and Atrial Remodeling in Marathon Versus Non-Marathon Runners*. *American Journal of Cardiology*, 2012. **109**(7): p. 1060-1065.
140. Colazzo, F., et al., *Murine left atrium and left atrial appendage structure and function: echocardiographic and morphologic evaluation*. *PLoS One*, 2015. **10**(4): p. e0125541.
141. Michael, S., K.S. Graham, and G.M. Davis, *Cardiac Autonomic Responses during Exercise and Post-exercise Recovery Using Heart Rate Variability and Systolic Time Intervals—A Review*. *Frontiers in Physiology*, 2017. **8**(301).
142. Blomqvist, C.G. and B. Saltin, *Cardiovascular adaptations to physical training*. *Annu Rev Physiol*, 1983. **45**: p. 169-89.
143. White, P.D., *BRADYCARDIA (BELOW RATE OF 40) IN ATHLETES, ESPECIALLY IN LONG DISTANCE RUNNERS*. *Journal of the American Medical Association*, 1942. **120**(8): p. 642-642.
144. Estes, N.A.M., et al., *ECG Findings in Active Patients*. *The Physician and Sportsmedicine*, 2001. **29**(3): p. 67-74.
145. Carter, J.B., E.W. Banister, and A.P. Blaber, *Effect of Endurance Exercise on Autonomic Control of Heart Rate*. *Sports Medicine*, 2003. **33**(1): p. 33-46.
146. Flannery, M.D., et al., *State of the Art Review: Atrial Fibrillation in Athletes*. *Heart Lung Circ*, 2017. **26**(9): p. 983-989.
147. Bahrainy, S., et al., *Exercise training bradycardia is largely explained by reduced intrinsic heart rate*. *Int J Cardiol*, 2016. **222**: p. 213-216.
148. Estes, N.A.M. and C. Madias, *Atrial Fibrillation in Athletes: A Lesson in the Virtue of Moderation*. *JACC: Clinical Electrophysiology*, 2017. **3**(9): p. 921-928.
149. Fragakis, N., G. Vicedomini, and C. Pappone, *Endurance Sport Activity and Risk of Atrial Fibrillation - Epidemiology, Proposed Mechanisms and Management*. *Arrhythm Electrophysiol Rev*, 2014. **3**(1): p. 15-9.
150. Wernhart, S. and M. Halle, *Atrial fibrillation and long-term sports practice: epidemiology and mechanisms*. *Clinical Research in Cardiology*, 2015. **104**(5): p. 369-379.
151. Gabrielli, L., et al., *Potential adverse cardiac remodelling in highly trained athletes: still unknown clinical significance*. *European Journal of Sport Science*, 2018. **18**(9): p. 1288-1297.
152. Liew, R., et al., *Role of tumor necrosis factor-alpha in the pathogenesis of atrial fibrosis and development of an arrhythmogenic substrate*. *Circ J*, 2013. **77**(5): p. 1171-9.
153. Wilson, M., et al., *Diverse patterns of myocardial fibrosis in lifelong, veteran endurance athletes*. *J Appl Physiol (1985)*, 2011. **110**(6): p. 1622-6.
154. La Gerche, A., et al., *Exercise-induced right ventricular dysfunction and structural remodelling in endurance athletes*. *Eur Heart J*, 2012. **33**(8): p. 998-1006.
155. McMullen, C.W., M.A. Harrast, and A.L. Baggish, *Optimal Running Dose and Cardiovascular Risk*. *Current Sports Medicine Reports*, 2018. **17**(6).

156. Swanson, D.R., *Atrial fibrillation in athletes: implicit literature-based connections suggest that overtraining and subsequent inflammation may be a contributory mechanism*. Med Hypotheses, 2006. **66**(6): p. 1085-92.
157. Kasapis, C. and P.D. Thompson, *The Effects of Physical Activity on Serum C-Reactive Protein and Inflammatory Markers: A Systematic Review*. Journal of the American College of Cardiology, 2005. **45**(10): p. 1563-1569.
158. Cannon, J.G. and B.A. St Pierre, *Cytokines in exertion-induced skeletal muscle injury*. Mol Cell Biochem, 1998. **179**(1-2): p. 159-67.
159. Francis Stuart, S.D., et al., *The crossroads of inflammation, fibrosis, and arrhythmia following myocardial infarction*. Journal of molecular and cellular cardiology, 2016. **91**: p. 114-122.
160. Mujika, I., *Quantification of Training and Competition Loads in Endurance Sports: Methods and Applications*. 2017. **12**(s2): p. S2-9.
161. Pollock, M.L., *The Quantification of Endurance Training Programs*. Exercise and Sport Sciences Reviews, 1973. **1**(1): p. 155-188.
162. Speakman, J.R., *Measuring energy metabolism in the mouse - theoretical, practical, and analytical considerations*. Front Physiol, 2013. **4**: p. 34.
163. Xu, F. and E.C. Rhodes, *Oxygen uptake kinetics during exercise*. Sports Med, 1999. **27**(5): p. 313-27.
164. Wasserman, K., *The anaerobic threshold: definition, physiological significance and identification*. Adv Cardiol, 1986. **35**: p. 1-23.
165. Veigl, V.L., *Chapter 5 - Exercise Physiology*, in *Orthopaedic Physical Therapy Secrets (Second Edition)*, J.D. Placzek and D.A. Boyce, Editors. 2006, Mosby: Saint Louis. p. 37-46.
166. Hughson, R.L. and J.M. Kowalchuk, *Beta-blockade and oxygen delivery to muscle during exercise*. Can J Physiol Pharmacol, 1991. **69**(2): p. 285-9.
167. Reeves, J.T., et al., *Operation Everest II: Cardiac filling pressures during cycle exercise at sea level*. Respiration Physiology, 1990. **80**(2): p. 147-154.
168. Jette, M., K. Sidney, and G. Blumchen, *Metabolic equivalents (METs) in exercise testing, exercise prescription, and evaluation of functional capacity*. Clin Cardiol, 1990. **13**(8): p. 555-65.
169. Bouchard C, G.G., Landry F. Shephard R, Skinner J, *Multiplies of the Resting Metabolic Rate (METs) of Physical Activities*. 1983, Canada Fitness Survey: Ottawa, Canada
170. Lee, M.G., et al., *Resting metabolic rate after endurance exercise training*. Med Sci Sports Exerc, 2009. **41**(7): p. 1444-51.
171. Gilliat-Wimberly, M., et al., *Effects of habitual physical activity on the resting metabolic rates and body compositions of women aged 35 to 50 years*. J Am Diet Assoc, 2001. **101**(10): p. 1181-8.
172. Sullo, A., et al., *Resting metabolic rate and post-prandial thermogenesis by level of aerobic power in older athletes*. Clin Exp Pharmacol Physiol, 2004. **31**(4): p. 202-6.
173. Byrne, H.K. and J.H. Wilmore, *The relationship of mode and intensity of training on resting metabolic rate in women*. Int J Sport Nutr Exerc Metab, 2001. **11**(1): p. 1-14.
174. Burkhard-Jagodzinska, K., et al., *Resting metabolic rate and thermogenic effect of glucose in trained and untrained girls age 11-15 years*. Int J Sport Nutr, 1999. **9**(4): p. 378-90.

175. Franklin, B.A., et al., *Using Metabolic Equivalents in Clinical Practice*. Am J Cardiol, 2018. **121**(3): p. 382-387.
176. Tremblay, M.S., et al., *New Canadian physical activity guidelines*. Applied physiology, nutrition, and metabolism, 2011. **36**(1): p. 36-46.
177. Schnohr, P., et al., *Dose of Jogging and Long-Term Mortality*. Journal of the American College of Cardiology, 2015. **65**(5): p. 411.
178. La Gerche, A. and H. Heidbuchel, *Can intensive exercise harm the heart? You can get too much of a good thing*. Circulation, 2014. **130**(12): p. 992-1002.
179. Gerche, A.L. and C.M. Schmied, *Atrial fibrillation in athletes and the interplay between exercise and health*. European Heart Journal, 2013. **34**(47): p. 3599-3602.
180. Mozaffarian, D., et al., *Physical Activity and Incidence of Atrial Fibrillation in Older Adults*. Circulation, 2008. **118**(8): p. 800-807.
181. Khan, H., et al., *Cardiorespiratory Fitness and Atrial Fibrillation: A population-based follow-up study*. Vol. 12. 2015.
182. Hawkins, M.N., et al., *Maximal oxygen uptake as a parametric measure of cardiorespiratory capacity*. Med Sci Sports Exerc, 2007. **39**(1): p. 103-7.
183. Lieber, D.C., R.L. Lieber, and W.C. Adams, *Effects of run-training and swim-training at similar absolute intensities on treadmill VO₂max*. Med Sci Sports Exerc, 1989. **21**(6): p. 655-61.
184. Scribbans, T.D., et al., *The Effect of Training Intensity on VO₂max in Young Healthy Adults: A Meta-Regression and Meta-Analysis*. Int J Exerc Sci, 2016. **9**(2): p. 230-247.
185. Swift, D.L., et al., *Physical activity, cardiorespiratory fitness, and exercise training in primary and secondary coronary prevention*. Circ J, 2013. **77**(2): p. 281-92.
186. Feng, R., et al., *A systematic comparison of exercise training protocols on animal models of cardiovascular capacity*. Life Sci, 2019. **217**: p. 128-140.
187. Valencia, S., et al., *Comparative Behavioral Correlation of High and Low-Performing Mice in the Forced Swim Test*. Biomol Ther (Seoul), 2019. **27**(4): p. 349-356.
188. Gall, G.A. and W.H. Kyle, *Growth of the laboratory mouse*. Theor Appl Genet, 1968. **38**(7): p. 304-8.
189. Chappell, M.A., E.L. Rezende, and K.A. Hammond, *Age and aerobic performance in deer mice*. Journal of Experimental Biology, 2003. **206**(7): p. 1221-1231.
190. Schefer, V. and M.I. Talan, *Oxygen consumption in adult and AGED C57BL/6J mice during acute treadmill exercise of different intensity*. Exp Gerontol, 1996. **31**(3): p. 387-92.
191. Bernstein, D., *Exercise assessment of transgenic models of human cardiovascular disease*. Physiological Genomics, 2003. **13**(3): p. 217-226.
192. Lakin, R., *Exercise-induced right ventricular impairment and arrhythmia susceptibility in mice* in Exercise Sciences 2018, University of Toronto Toronto, Ontario. p. 249.
193. Evangelista, F.S., P.C. Brum, and J.E. Krieger, *Duration-controlled swimming exercise training induces cardiac hypertrophy in mice*. Braz J Med Biol Res, 2003. **36**(12): p. 1751-9.
194. dos Reis, I.G.M., et al., *Forced Swim Reliability for Exercise Testing in Rats by a Tethered Swimming Apparatus*. Frontiers in Physiology, 2018. **9**(1839).
195. Kaplan, M.L., et al., *Cardiac adaptations to chronic exercise in mice*. American Journal of Physiology-Heart and Circulatory Physiology, 1994. **267**(3): p. H1167-H1173.

196. Burnett, C.M. and J.L. Grobe, *Direct calorimetry identifies deficiencies in respirometry for the determination of resting metabolic rate in C57Bl/6 and FVB mice*. Am J Physiol Endocrinol Metab, 2013. **305**(7): p. E916-24.
197. Patel, H., et al., *Aerobic vs anaerobic exercise training effects on the cardiovascular system*. World J Cardiol, 2017. **9**(2): p. 134-138.
198. Even, P.C., A. Mokhtarian, and A. Pele, *Practical aspects of indirect calorimetry in laboratory animals*. Neuroscience & Biobehavioral Reviews, 1994. **18**(3): p. 435-447.
199. Even, P.C. and N.A. Nadkarni, *Indirect calorimetry in laboratory mice and rats: principles, practical considerations, interpretation and perspectives*. American Journal of Physiology-Regulatory, Integrative and Comparative Physiology, 2012. **303**(5): p. R459-R476.
200. Brouwer, E., *On simple formulae for calculating the heat expenditure and the quantities of carbohydrate and fat oxidized in metabolism of men and animals, from gaseous exchange (Oxygen intake and carbonic acid output) and urine-N*. Acta Physiol Pharmacol Neerl, 1957. **6**: p. 795-802.
201. Elia, M. and G. Livesey, *Energy expenditure and fuel selection in biological systems: the theory and practice of calculations based on indirect calorimetry and tracer methods*. World Rev Nutr Diet, 1992. **70**: p. 68-131.
202. Lusk, G., *The elements of the science of nutrition*. 1917: WB Saunders Company.
203. Weir, J.B., *New methods for calculating metabolic rate with special reference to protein metabolism*. J Physiol, 1949. **109**(1-2): p. 1-9.
204. Chappell, M.A., *Maximum oxygen consumption during exercise and cold exposure in deer mice, Peromyscus maniculatus*. Respir Physiol, 1984. **55**(3): p. 367-77.
205. Desai, K.H., et al., *Cardiovascular indexes in the mouse at rest and with exercise: new tools to study models of cardiac disease*. Am J Physiol, 1997. **272**(2 Pt 2): p. H1053-61.
206. Chappell, M.A., et al., *Voluntary running in deer mice: speed, distance, energy costs and temperature effects*. J Exp Biol, 2004. **207**(Pt 22): p. 3839-54.
207. Tschop, M.H., et al., *A guide to analysis of mouse energy metabolism*. Nat Methods, 2011. **9**(1): p. 57-63.
208. Simon, A., G. Veress, and I. Berényi, *Oxygen Deficit During Exercise Testing*. CHEST, 1997. **112**(2): p. 567-568.
209. Elia, M., *Organ and tissue contribution to metabolic rate*. Energy Metabolism, Tissue Determinants and Cellular Corollaries, 1992: p. 61-80.
210. Van Klinken, J.B., et al., *Estimation of activity related energy expenditure and resting metabolic rate in freely moving mice from indirect calorimetry data*. PLoS One, 2012. **7**(5): p. e36162.
211. La Gerche, A. and D.L. Prior, *Exercise--is it possible to have too much of a good thing?* Heart Lung Circ, 2007. **16 Suppl 3**: p. S102-4.
212. Opondo, M.A., et al., *Does High-Intensity Endurance Training Increase the Risk of Atrial Fibrillation?* Circulation: Arrhythmia and Electrophysiology, 2018. **11**(5): p. e005598.
213. Li, N. and X.H. Wehrens, *Programmed electrical stimulation in mice*. J Vis Exp, 2010(39).
214. Conti, C.R., *Electrophysiology, pacing, and arrhythmia*. Clin Cardiol, 1989. **12**(6): p. 306.

215. Laughner, J.I., et al., *Processing and analysis of cardiac optical mapping data obtained with potentiometric dyes*. American Journal of Physiology-Heart and Circulatory Physiology, 2012. **303**(7): p. H753-H765.
216. Fluhler, E., V.G. Burnham, and L.M. Loew, *Spectra, membrane binding, and potentiometric responses of new charge shift probes*. Biochemistry, 1985. **24**(21): p. 5749-5755.
217. Umapathy, K., et al., *Phase Mapping of Cardiac Fibrillation*. Circulation: Arrhythmia and Electrophysiology, 2010. **3**(1): p. 105-114.
218. Wegner, K.A., et al., *Fluorescence of Picosirius Red Multiplexed With Immunohistochemistry for the Quantitative Assessment of Collagen in Tissue Sections*. J Histochem Cytochem, 2017. **65**(8): p. 479-490.
219. Kinoshita, N., et al., *Automating measurements of fluorescent signals in freely moving plant leaf specimens*. Plant Biotechnol (Tokyo), 2019. **36**(1): p. 7-11.
220. Hadi, A.M., et al., *Rapid quantification of myocardial fibrosis: a new macro-based automated analysis*. Cellular Oncology, 2011. **34**(4): p. 343-354.
221. Peritz, D.C., et al., *High-intensity endurance training is associated with left atrial fibrosis*. American Heart Journal, 2020. **226**: p. 206-213.
222. van Deel, E.D., et al., *Exercise training does not improve cardiac function in compensated or decompensated left ventricular hypertrophy induced by aortic stenosis*. J Mol Cell Cardiol, 2011. **50**(6): p. 1017-25.
223. Williams, P.T. and P.D. Thompson, *Increased cardiovascular disease mortality associated with excessive exercise in heart attack survivors*. Mayo Clin Proc, 2014. **89**(9): p. 1187-94.
224. O'Keefe, J.H., B. Franklin, and C.J. Lavie, *Exercising for Health and Longevity vs Peak Performance: Different Regimens for Different Goals*. Mayo Clinic Proceedings, 2014. **89**(9): p. 1171-1175.
225. Baggish, A.L., et al., *The impact of endurance exercise training on left ventricular systolic mechanics*. American Journal of Physiology-Heart and Circulatory Physiology, 2008. **295**(3): p. H1109-H1116.
226. Perini, R., et al., *The influence of exercise intensity on the power spectrum of heart rate variability*. Eur J Appl Physiol Occup Physiol, 1990. **61**(1-2): p. 143-8.
227. Gregoire, J., et al., *Heart Rate Variability at Rest and Exercise: Influence of Age, Gender, and Physical Training*. Canadian Journal of Applied Physiology, 1996. **21**(6): p. 455-470.
228. Kaikkonen, P., A. Nummela, and H. Rusko, *Heart rate variability dynamics during early recovery after different endurance exercises*. European journal of applied physiology, 2008. **102**: p. 79-86.
229. Seiler, S., O. Haugen, and E. Kuffel, *Autonomic recovery after exercise in trained athletes: intensity and duration effects*. Med Sci Sports Exerc, 2007. **39**(8): p. 1366-73.
230. Kaikkonen, P., et al., *Can HRV be used to evaluate training load in constant load exercises?* European journal of applied physiology, 2009. **108**: p. 435-42.
231. Benito, B., et al., *Cardiac Arrhythmogenic Remodeling in a Rat Model of Long-Term Intensive Exercise Training*. Circulation, 2011. **123**(1): p. 13-22.
232. Nattel, S., *How does fibrosis promote atrial fibrillation persistence: in silico findings, clinical observations, and experimental data*. Cardiovascular research, 2016. **110**(3): p. 295-297.

233. Zahid, S., et al., *Patient-derived models link re-entrant driver localization in atrial fibrillation to fibrosis spatial pattern*. Cardiovasc Res, 2016. **110**(3): p. 443-54.
234. Goette, A., et al., *Determinants and consequences of atrial fibrosis in patients undergoing open heart surgery*. Cardiovascular Research, 2002. **54**(2): p. 390-396.
235. Xu, J., et al., *Atrial Extracellular Matrix Remodeling and the Maintenance of Atrial Fibrillation*. Circulation, 2004. **109**(3): p. 363-368.
236. Balaban, G., et al., *Fibrosis Microstructure Modulates Reentry in Non-ischemic Dilated Cardiomyopathy: Insights From Imaged Guided 2D Computational Modeling*. Frontiers in Physiology, 2018. **9**(1832).
237. Kazbanov, I.V., K.H.W.J. ten Tusscher, and A.V. Panfilov, *Effects of Heterogeneous Diffuse Fibrosis on Arrhythmia Dynamics and Mechanism*. Scientific reports, 2016. **6**: p. 20835-20835.
238. Jin, M.-N., et al., *Physical Activity and Risk of Atrial Fibrillation: A Nationwide Cohort Study in General Population*. Scientific Reports, 2019. **9**(1): p. 13270.
239. Blair, S.N., et al., *Physical fitness and all-cause mortality. A prospective study of healthy men and women*. Jama, 1989. **262**(17): p. 2395-401.
240. Garland, T., et al., *The biological control of voluntary exercise, spontaneous physical activity and daily energy expenditure in relation to obesity: human and rodent perspectives*. The Journal of Experimental Biology, 2011. **214**(2): p. 206-229.
241. Burstein, B. and S. Nattel, *Atrial fibrosis: mechanisms and clinical relevance in atrial fibrillation*. J Am Coll Cardiol, 2008. **51**(8): p. 802-9.
242. Strachan, A.F., et al., *C reactive protein concentrations during long distance running*. Br Med J (Clin Res Ed), 1984. **289**(6454): p. 1249-51.
243. Wei, Y., et al., *Review of Dissolved Oxygen Detection Technology: From Laboratory Analysis to Online Intelligent Detection*. Sensors (Basel, Switzerland), 2019. **19**(18): p. 3995.

Appendices

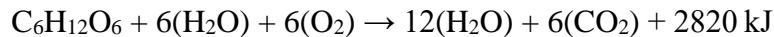
5.1 Appendix A – Oxygen Consumption Quantification

Introductory Notes

The means of data collection will be discussed starting from raw data of one swim to large scale estimations of oxygen consumption, as well as oxygen volume consumptions per swim and in total integrated effort.

Theoretical Framework of Oxygen Consumption

Energy production processes ultimately begin by the breakdown of glucose into energy, and carbon dioxide (CO₂), water and by products. As such, indirect calorimetry is often employed to estimate energy production according to the following chemical reaction:



It can, therefore, be assumed that for every 6 moles of oxygen (O₂), 2820kJ of energy are produced and used by the mouse – the theoretical framework behind indirect calorimetry/respirometry. The ratio between energy expenditure and O₂ consumed is variable and depends on multiple conditions including dietary factors. Such differences are often corrected by simultaneous measurements of CO₂ production given that carbon atoms originate from the foodstuffs consumed. This is done by calculation of a ratio termed respiratory exchange ratio (RER) [162]. Nonetheless, RER was not quantified here as discussed in the **Introduction**. Often, indirect calorimetry estimates energy expenditure with oxygen consumption (V_{O₂}) rate (mLs of O₂/kg/min). Here, a modified Oxymax system (Oxymax, Columbus Instruments,

Columbus, OH, U.S.A) was used (**Figure 2-1 and 2-2**), which reports O₂ measurements as relative O₂ content in the sampled air, or a percentage (%O₂), as a function of time. There were two means of calculating V_{O₂} during swims – the “integral method” and the “average method”. Only the average method will be described here. The integral method was theoretical and lengthy, as well as treats %O₂ as a function of time, and can therefore be found in **Appendix B**. Nonetheless, it is an important framework which forms the basis for the shorter, average method, and is essential for understanding the calculations introduced here.

The Average Method – Practical Means of Calculating Oxygen Consumption

As previously mentioned, Oxymax records oxygen content as %O₂ over time. The data is collected at a frequency of 1 data point per 5 seconds. Theoretically, changes in O₂ content are only attributed to O₂ consumed by the mice exercising. Because percentages are simply fractions, the difference fraction in O₂ consumed can be calculated according to:

$$\frac{\%O_2 \text{ consumed}}{100} = \frac{\%O_2 \text{ in}}{100} - \frac{\%O_2 \text{ out}}{100} = \frac{\%O_2 \text{ in} - \%O_2 \text{ out}}{100}$$

Where %O₂in is the %O₂ in the atmospheric air entering the swimming apparatus (inflow air) and %O₂out is the %O₂ leaving the swimming apparatus (outflow air)

Atmospheric %O₂ was assumed unchanging and 20.95%. Therefore, the calculation for every data point can be converted to:

$$\frac{20.95\% - \%O_2 \text{ out}}{100}$$

To find the real volume of O₂ in the sampled air, the fractions calculated above were multiplied by the inflow and outflow rates (units: L/min). *Theoretically*, all air entering the swimming

apparatus is also leaving it, making inflow and outflow rates equivalent. As such the differences in O₂ contents between inflow and outflow rates can be calculated according to:

$$O_2 \text{ consumed (volume)} = \frac{\%O_2in}{100} * F1 - \frac{\%O_2out}{100} * F2$$

Where, F₁=F₂, F₁ is the inflow rate in L/min and F₂ is the outflow rate in L/min. Therefore,

$$O_2 \text{ consumed (L/min)} = \frac{\%O_2in}{100} * F - \frac{\%O_2out}{100} * F = \frac{\%O_2in - \%O_2out}{100} * F$$

As previously mentioned, indirect calorimetry estimates energy expenditure with V_{O₂} which has the units of mLs of O₂/kg/min. Thus, the final calculation of V_{O₂} can be shortly modeled as (with the correct unit conversions):

$$VO_2 \left(\frac{mL O_2}{kg \text{ min}} \right) = \frac{\frac{\%O_2in - \%O_2out}{100} * F}{\text{animal mass}}$$

Of course, this V_{O₂} is momentary and is only represented from 1 data point. The means of converting this data to large scale data will be discussed further in the Appendix. However, V_{O₂} from each data point must first be corrected for multiple factors – which will be discussed now. This will be done by a stepwise description of how the above calculation of V_{O₂} changes with each correction.

Values Calibration

As with every technology – observed values are not always those expected. Calibration is employed for these purposes. O₂ flow into the bucket was adjusted using a simple flow regulator and kept at a constant rate of a premeasured 4.0L/min to assure O₂ air concentrations (%O₂) was

within the range of the oxygen sensor (minimum: 19.3%, maximum: 21.5%). Rate of air out flow was not measured as it does not affect oxygen consumption calculations (**Figure 5.1-1**).

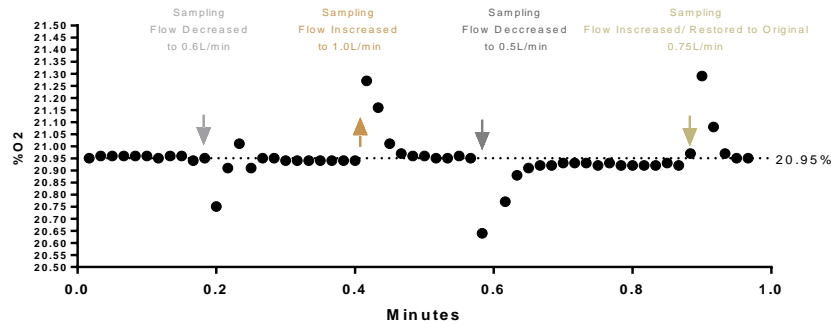


Figure 5.1-1. Oxygen Levels Do Not Depend on Sampling Rate – Sampling rate is defined as the rate at which gas is sampled from the swimming apparatus by the oxygen sensor – or out-flow rate. The oxygen sensor was calibrated to 20.95% O₂ atmospheric air and the flow of gas entering the sensor was adjusted with a flow regulator, as indicated in the figure above. Despite momentary changes in % O₂, the measured % O₂ from the atmosphere did not change. This empirical data suggested there was no requirements to regulate out-flow rate from the swimming apparatus.

The Oxymax system was calibrated according to the manual to set dry room air as 20.95% O₂.

Due to the nature of the sensor (Fuel Cell/Electrochemical Oxygen Sensor) an expected 0% O₂ is registered as 0V, and therefore an observed value of 0% O₂. Despite this, the sensor used here had a higher, lower limit of 19.3% O₂. A two-point calibration was completed using a 20% O₂ N₂ balance (Custom, Praxair, Inc., CT, U.S.A) and dried room air assumed as 20.95% O₂. These gases were chosen because:

- 1) The oxygen content was within the range of the Oxymax unit (minimum: 19.3%, maximum: 21.5%) and,
- 2) Oxygen levels were never observed to drop below 20% O₂ when 3 mice were exercising in the swimming apparatus at 4.0L/min inflow (**Figure 5.1-2**)

- 3) >20% O₂ represents non hypoxic conditions, assuring our swim model appropriately represented normal exercise conditions.

Calibration gases were passed throughout the whole apparatus (**Figure 2-3**) during calibration to simulate experimental conditions. The measured %O₂ were allowed to equilibrate for a minimum of 2 minutes and an average %O₂ over 1 minute was registered as observed %O₂, where data point were recorded every 5 seconds. The calibration curve was plotted (**Figure 5.1-3**) as Expected %O₂ vs. Observed %O₂. A standard curve was generated such that:

$$y_i = m * x_i + c$$

Where y_i is the observed %O₂, x_i is the expected %O₂, m is the gain of the calibration curve and c is the offset of the calibration curve.

Each data point (%O₂) collected during the swims was then calibrated using the generated standard curve. Therefore, each calibrated data point can be named x_i . The equation previously derived can now be rewritten as:

$$VO_2 = \frac{(20.95 - x_i)}{100} * F$$

mass animals

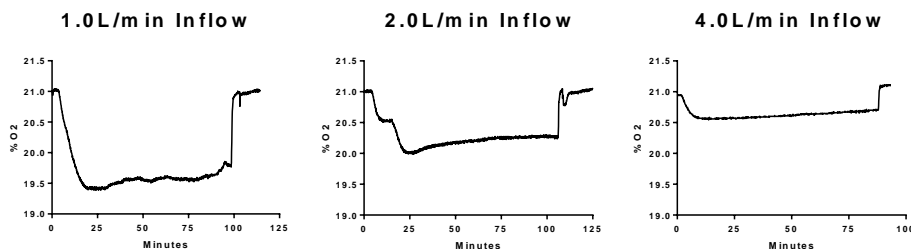


Figure 5.1-2. Measured Oxygen Concentration Depends on Inflow Rate – Three (n=3) mice were swam for 90 minute bouts at 3 different inflow rates into the swimming apparatus. Changes in %O₂ are attributed to dilution of gas in the swimming apparatus as opposed to behavioural differences.

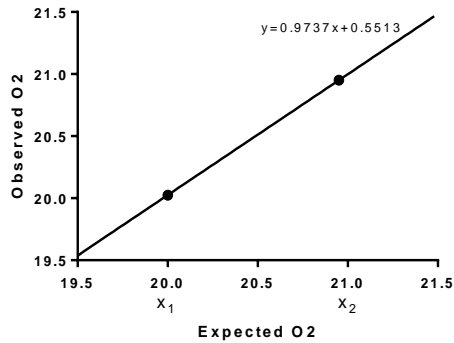


Figure 5.1-3. Two Point Calibration Curve for the Oxymax System – Observed Oxygen content (%O₂ observed) was set as “y” and expected %O₂ was set as “x”. The following data points were used to generate the calibration curve above: y₁= 20.025 and x₁= 20, y₂= 20.95 and x₂= 20.95.

Pressure Compensation

Fuel cell oxygen sensors/ electrochemical oxygen sensors measure O₂ content using reduction chemical reactions whereby the produced electricity is directly proportional to the O₂ content in the sampled gas [243]. These cells depend on the diffusion of gas and are therefore intrinsically dependent on the partial pressure of O₂ (i.e concentration of O₂ in the atmosphere relative to the sensor cell) in the sampled gas, according to Fick’s Law of Diffusion.

To empirically validate the dependence of measured %O₂ on pressure, room air gas and atmospheric pressure (P_{atm}) were recorded over ~48 hours (**Figure 5.1-4A**). Pressure was measured directly in-line with air inflow into the sensor, using a pressure sensor (Adafruit BME280 I2C or SPI Temperature Humidity Pressure Sensor, Bosch Sensortec, Kusterdingen, Germany) connected to a custom designed beagle board (Texas Instruments Incorporate, TX, U.S.A) and Python software. P_{atm} was assumed directly proportional to the partial pressure of oxygen (P_{O₂}) according to Dalton’s Law. The relationship between %O₂ and P_{atm} revealed a

direct relationship with a strong correlation – empirically indicating the requirement for a pressure compensation (**Figure 5.1-4B**).

To correct for changes in %O2 related to fluctuations in Patm (and therefore P_{O2}), Patm was recorded upon calibration as well as for each %O2 data point. The pressure correction was completed according to:

$$x_{i,p} = x_i * \frac{Patm_i}{P_{atm_c}}$$

Where, x_i = calibrated %O2, Patm_i = atmospheric pressure at point i, Patm_c = atmospheric pressure at calibration and x_{i,p} = calibrated, pressure compensated %O2. The V_{O2} equation can now be defined as:

$$VO_2 = \frac{(20.95 - x_{i,p})}{100} * F$$

mass animals

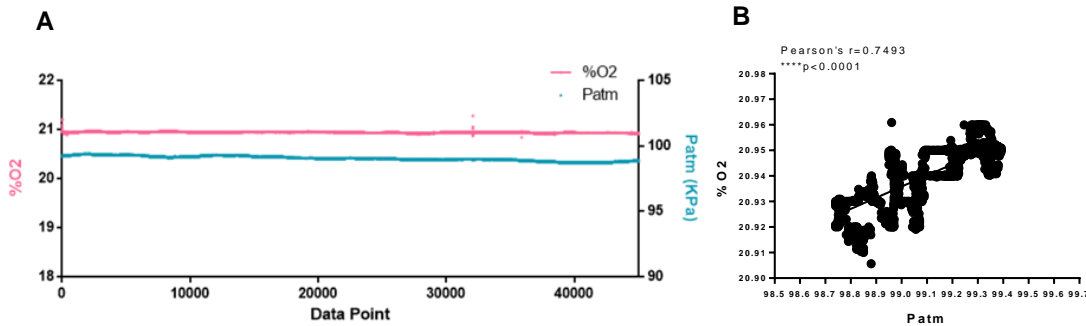


Figure 5.1-4. Oxygen Measured by the Oxymax Unit is Intrinsically Dependent on Atmospheric and Partial Oxygen Pressures –A) The raw data used to find panel A. Atmospheric pressure (Patm) and %O2 were recorded over ~48 hours. Each data point represents 5 seconds. B) %O2 and Patm are intrinsically correlated. Correlation was assessed using Pearson’s correlation test.

Baselining

Intrinsic to the oxygen sensor is fluctuation in recorded %O₂ value despite lack in real changes of oxygen content. These fluctuations are easily corrected through baselining – adjusting the recorded value relatively to an anticipated/expected value. For example, atmospheric O₂ concentration is a never concentration of 20.95%. Despite this, atmospheric %O₂ recorded pre- and post-swim changes. An example of such swim bout is shown in **Figure 5.1-5**.

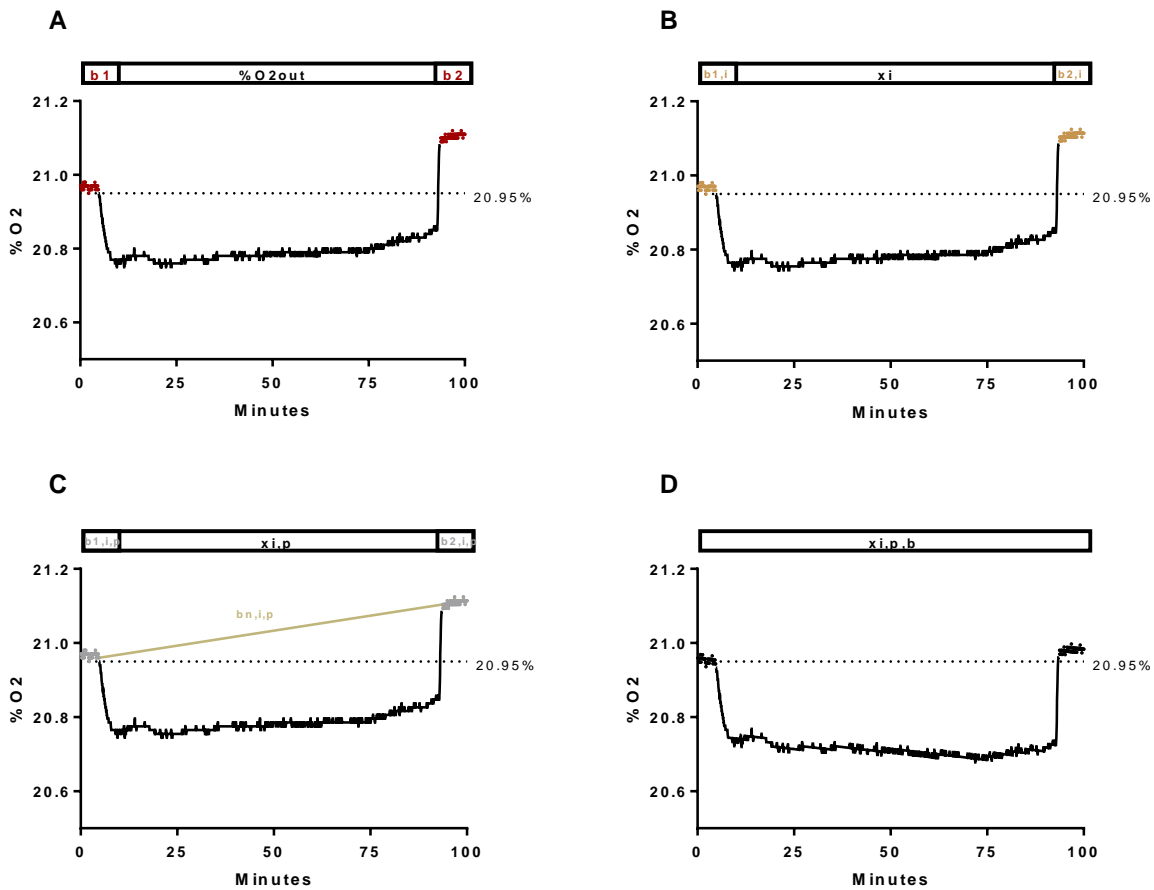


Figure 5.1-5. Raw Swim Recording without Baselining – Mice (n=3) were swam for 90 minutes and atmospheric %O₂ was recorded before and after the swim ended. Atmospheric %O₂ also denotes the air which flows into the bucket. Note the increase of %O₂ recorded after the swim to 21.10%. For visual purposes, a horizontal line has been drawn at 20.95%O₂. A-D represent a step wise correction towards baselining.

A simple correction is to adjust all recorded values based on fluctuations occurring in recorded value of a known calibration gas. This was modeled according to the following equation:

$$x_{i,b} = x_i + (\%O2_{known,expected} - \%O2_{known,observed})$$

Where, x_i = raw %O2 at point i, $\%O2_{known,expected}$ = %O2 content of a known gas (calibration gas), $\%O2_{known,observed}$ = the measured %O2 content of the known gas (calibration gas) and $x_{i,b}$ = baselined %O2. It is important to note that fluctuations occurred in both directions – as such the difference between $\%O2_{known,expected}$ and $\%O2_{known,observed}$ could be either negative or positive. If the difference was positive, x_i was increased to account for a decreased fluctuation; if the difference was negative, x_i was decreased to account for an increased fluctuation (**Figure 5.1-6**). Given one of the calibration points is dried room air (20.95%O2), it was easily used as $\%O2_{known,expected}$ by measuring oxygen content before and after swim completion (**Figure 5.1-5A**).

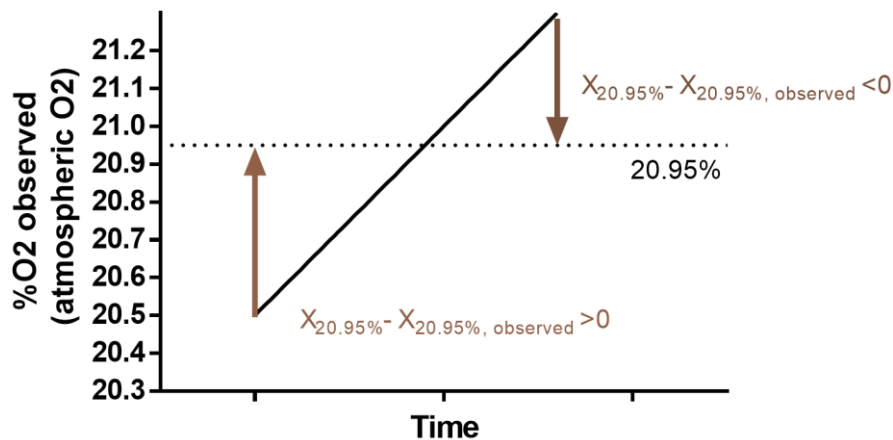


Figure 5.1-6. Purpose of Baselining Data – When baselining, fluctuations relative to dried atmospheric O2 concentrations were used. These were expected to be 20.95%O2, as indicated by the horizontal line. Arrows point to the direction of the baselining correction. For example, if the difference between %O2 20.95%, expected and %O2 20.95%, observed was positive, x_i was increased to account for a decreased fluctuation.

Baselining values are also impacted by 1) calibration and 2) pressure fluctuations. Therefore, the baselining data points were also calibrated, and pressure compensated. Consequently, baselining points can be corrected according to the following equations:

- 1) Calibrating baselining points is completed using the previously derived standard curve:

$$y_i = m * x_i + c$$

Here, we plug the baselining points b_1 and b_2 for y_i , to get the calibrated points. Instead of x_i , these points can be named as: $b_{1,i}$ and $b_{2,i}$, - the calibrated b_1 and b_2 (**Figure 5.1-5B**):

$$b_1 = m * b_{1,i} + c$$

- 2) Pressure compensating baseline points was completed using the previously derived equation:

$$x_{i,p} = x_i * \frac{P_{atm} i}{P_{atm} c}$$

Here, we plug the calibrated baselining points $b_{1,i}$ and $b_{2,i}$ to get $b_{1,i,p}$ and $b_{2,i,p}$ (**Figure 5.1-5C**):

$$b_{1,i,p} = b_{1,i} * \frac{P_{atm} i}{P_{atm} c}$$

We found that a linear relationship can be used to estimate baseline values not recorded before and after swim completion. These can be named $b_{n,i,p}$ and calculated according to a linear standard curve derived from the two baseline points - $b_{1,i,p}$ and $b_{2,i,p}$. This can be modeled according to the following equation:

$$b_{n,i,p} = \left(\frac{b_{2,i,p} - b_{1,i,p}}{t_2 - t_1} \right) * t_i + c_1 = m_1 * t_n + c_1$$

Where, $b_{n,i,p}$ is the estimated, calibrated, pressure compensated baseline point at time n , $b_{1,i,p}$, and $b_{2,i,p}$ are the two baseline points recorded before (t_1) and after (t_2) the swim, m_1 is the empirically identified slope of the linear curve and c_1 is the empirically identified offset of the linear curve (Figure 5.1-7).

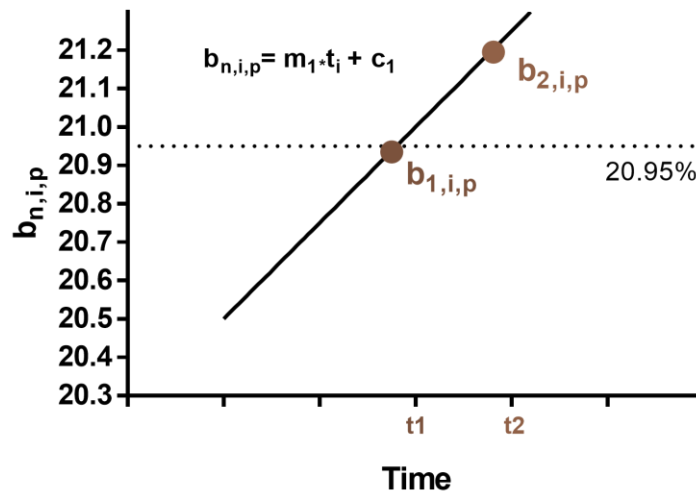


Figure 5.1-7. Calculating Baseline Points – Ideally, baseline points could be measured using a two-sensor system. Nonetheless, baseline points can be estimated using empirical data using two points measured periodically. These two points were chosen as before and after the swim was completed. These values were pressure compensated and calibrated to yield $b_{1,i,p}$, and $b_{2,i,p}$ which were used to find a linear model to estimate any value of $b_{n,i,p}$ – the baseline point at any time n .

Finally, to complete baselining the calibrated and pressure compensated %O₂ was adjusted according to the following equation (Figure 5.1-5D):

$$x_{i,p,b} = x_{i,p} + (20.95\% - b_{n,i,p})$$

Where, $x_{i,p,b}$ is the calibrated, pressure compensated and baselined observed %O₂ during swim, $x_{i,p}$ is the value prior to baselining, and $b_{n,i,b}$ is the estimated baseline point at time i. Note that the expected 20.95%O₂ is unchanged because the value is intrinsically calibrated and pressure compensated as it was used during the initial calibration process.

V_{O_2} at this point can be rewritten as:

$$VO_2 = \frac{(20.95 - x_{i,p,b}) * F}{100 \text{ mass animals}}$$

Conversion to Molarity and Volume

V_{O_2} is often presented at STP (Standard Conditions of Pressure and Temperature) which are a standard set of conditions to allow experimental data to be easily compared across various studies. At STP, P_{atm} is 1atm (or 101.325kPa) and Temperature is 0°C (or 273.15K).

Alternatively, V_{O_2} can be expressed in molarity (mol O₂/kg/min) as molarity does not fluctuate with environmental conditions. To achieve V_{O_2} at STP we must first convert to molar V_{O_2} .

To start this correction, the ideal gas law must be examined:

$$PV = nRT$$

Where, P=pressure, V=volume, n=moles of gas, R=gas constant and T=temperature. If the formula is rearranged a molar concentration is emerged (mol/L):

$$\frac{n}{V} \left(\frac{mol}{L} \right) = \frac{P}{RT}$$

Because pressure is inherent to the V_{O_2} calculation, the equation above can be directly applied to the calculation of molar V_{O_2} . This is shown below:

$$\text{molar } VO_2 = \frac{\left(\frac{20.95\% - x_{i,p,b}}{100}\right) * \frac{(P)}{RT} * F}{\text{mass animals}}$$

Where the new variables R and T are the gas constant and temperature. Nonetheless, P, R and T are variable for inflow and outflow air. Therefore, the above equation should be rewritten as:

$$\begin{aligned} VO_2 &= \frac{\frac{\%O_2in}{100} * \frac{(P_{atm})}{RTin} * F - \frac{\%O_2out}{100} * \frac{(P_{atm})}{RTout} * F}{\text{mass animals}} \\ &= \frac{\frac{20.95\%}{100} * \frac{(P_{atm})}{RTin} * F - \frac{x_{i,p,b}}{100} * \frac{(P_{atm})}{RTout} * F}{\text{mass animals}} \end{aligned}$$

Therefore, a correction to STP can be easily modeled according to the following equation, where the units are converted back to V_{O_2} measured as volume:

$$VO_{2STP} = \frac{\frac{20.95\%}{100} * \frac{(P_{atm})}{RTin} * F - \frac{x_{i,p,b}}{100} * \frac{(P_{atm})}{RTout} * F}{\text{mass animals}} * \frac{RT_{STP}}{P_{STP}}$$

Nonetheless, there is a final correction we need to complete – that of pressure of water vapour (i.e humidity).

Humidity Compensation

To begin the humidity compensation, it is important to note that the values recorded experimentally are desiccated and are therefore lacking the the effects of humidity (water content in the air). Nonetheless, humidity effects the concentration of O₂ in the inflow and outflow air. The real concentration of %O₂ can be estimated according to Dalton's Law, meaning that the relative %O₂ content in the air is actually *lower* than that measured by the oxygen sensor:

$$P_{atm} = P_{O_2} + P_{H_2O} + P_{other\ gases}$$

Where, P_{atm} = the atmospheric pressure at any point, P_{O_2} = the partial pressure of oxygen, P_{H_2O} = the partial pressure of water in the air and $P_{other\ gases}$ = the sum partial pressure exerted by other gases in atmospheric air. Therefore, when the air is dried, P_{atm} becomes:

$$P_{atm} = P_{O_2} + P_{other\ gases}$$

As such, $x_{i,p,b}$ must be corrected for the lack of water (H₂O) upon recording. To do this, we calculate the following value:

$$P_{bucket} = P_{atm} - P_{H_2O}$$

And we can correct %O₂ values according to:

$$\%O_2 * \frac{P_{atm} - P_{H_2O}}{RT}$$

And rewrite the previous equation for V_{O_2} as:

$$VO_{2STP} = \frac{\frac{20.95\%}{100} * \frac{(P_{atm} - P_{H_2O\ in})}{RT_{in}} * F - \frac{x_{i,p,b}}{100} * \frac{(P_{atm} - P_{H_2O\ out})}{RT_{out}} * F}{mass\ animals} * \frac{RT_{STP}}{P_{STP}}$$

The value of ($P_{atm} - P_{H_2O}$) is always smaller than P_{atm} , and therefore decreases the value of %O₂ (i.e inflow 20.95% and outflow $x_{i,p,b}$) to that of wet air.

Despite this, V_{O_2} is calculated using both the inflow and outflow air, each having different water contents. Water in the atmosphere fluctuates greatly and quickly, whereas the water content in the swimming apparatus is always at 100%, as a result of water vapour from the swimming water. As such corrections of V_{O_2} become more complicated and depend on the temperature and

its effect on the water content in the air. Nonetheless, there is no need to correct the outflow rate for humidity influences because excess water simply leaves the apparatus as excess [198].

It is easy to start this correction by assuming there are no mice in the swimming apparatus, in which case following assumption must hold true because there are no animals consuming O₂:

$$\%O_2inflow\ dry = \%O_2outflow\ dry$$

If the following previous assumptions are considered:

- 1) Patm is unchanging for both inflow and outflow air,
- 2) Humidity differs between inflow and outflow air, and
- 3) Inflow and outflow rates are equivalent

Nonetheless, upon careful consideration an inherent flaw is observed in this equation – if there are no animals in the unit, V_{O₂} must be 0mL O₂ hr⁻¹kg⁻¹, and the equation becomes:

$$\frac{\frac{20.95\%}{100} * \frac{(P_{atm} - P_{H_2O\ in})}{RT_{in}} * F}{mass\ animals} * \frac{RT_{STP}}{P_{STP}} = \frac{\frac{x_{i,p,b}}{100} * \frac{(P_{atm} - P_{H_2O\ out})}{RT_{out}} * F}{mass\ animals} * \frac{RT_{STP}}{P_{STP}}$$

Using the previous assumption that %O₂inflow dry=%O₂outflow dry with no mice and therefore

20.95% = x_{i,p,b}, the equation can be further modified to:

$$\frac{\frac{20.95\%}{100} * \frac{(P_{atm} - P_{H_2O\ in})}{RT_{in}} * F}{mass\ animals} * \frac{RT_{STP}}{P_{STP}} = \frac{\frac{20.95\%}{100} * \frac{(P_{atm} - P_{H_2O\ out})}{RT_{out}} * F}{mass\ animals} * \frac{RT_{STP}}{P_{STP}}$$

$$\frac{(P_{atm} - P_{H_2O\ in})}{RT_{in}} = \frac{(P_{atm} - P_{H_2O\ out})}{RT_{out}}$$

This is a false statement because humidity within the swimming apparatus is always 100% and humidity in the inflow air is variable, meaning the partial pressure of water in each these two

gases *cannot* be equivalent. Given $P_{H_2O\ in} < P_{H_2O\ out}$, excess water pressure must exist within the bucket intrinsically. This water *must exit the bucket*, meaning the outflow rate *cannot* be equal to inflow rate. If we name inflow rate F1 and outflow rate F2:

$$F1 < F2$$

As such the previous equation can be changed to:

$$VO_{2\ STP} = \frac{\frac{20.95\%}{100} * \frac{(P_{atm} - P_{H_2O\ in})}{RT_{in}} * F1 - \frac{x_{i,p,b}}{100} * \frac{(P_{atm} - P_{H_2O\ out})}{RT_{out}} * F2}{mass\ animals} * \frac{RT_{STP}}{P_{STP}}$$

There are no means to measure F2. Therefore, it must be calculated. We can drive the following equation, to isolate for F2 according to (if we maintain our assumptions that no mice are in the bucket and $V_{O_2}=0$):

$$F2 = \frac{20.95\%}{x_{i,p,b}} * \left(\frac{\left(\frac{(P_{atm} - P_{H_2O\ in})}{RT_{in}} \right)}{\left(\frac{(P_{atm} - P_{H_2O\ out})}{RT_{out}} \right)} * F1 \right)$$

Since we assumed there are no mice in the bucket, %O₂inflow dry=%O₂outflow and therefore, $x_{i,p,b}=20.95\%$. The above equation becomes:

$$F2 = \left(\frac{\left(\frac{(P_{atm} - P_{H_2O\ in})}{RT_{in}} \right)}{\left(\frac{(P_{atm} - P_{H_2O\ out})}{RT_{out}} \right)} * F1 \right)$$

Using the derived F2, V_{O_2} now becomes:

$$VO_{2\ STP} = \frac{\frac{20.95\%}{100} * \frac{(P_{atm} - P_{H_2O\ in})}{RT_{in}} * F1 - \frac{x_{i,p,b}}{100} * \frac{(P_{atm} - P_{H_2O\ out})}{RT_{out}} * \left(\frac{\left(\frac{(P_{atm} - P_{H_2O\ in})}{RT_{in}} \right)}{\left(\frac{(P_{atm} - P_{H_2O\ out})}{RT_{out}} \right)} * F1 \right)}{mass\ animals} * \frac{RT_{STP}}{P_{STP}}$$

Which simply becomes:

$$VO_{2STP} = \frac{\frac{20.95\%}{100} * \frac{(P_{atm} - P_{H_2O\ in})}{RT_{in}} * F1 - \frac{x_{i,p,b}}{100} * \frac{(P_{atm} - P_{H_2O\ in})}{RT_{in}} * F1}{mass\ animals} * \frac{RT_{STP}}{P_{STP}}$$

$$= \frac{\left(\frac{20.95\%}{100} - \frac{x_{i,p,b}}{100}\right) * \frac{(P_{atm} - P_{H_2O\ in})}{RT_{in}} * F1}{mass\ animals} * \frac{RT_{STP}}{P_{STP}}$$

All of the above values were empirically measured. To find $P_{H_2O\ in}$, atmospheric %H₂O was measured using the BME280 pressure and humidity sensor. Humidity pressure/ pressure of water vapour was modeled previously for various conditions. Here, we used the Magnus equation:

$$P_{H_2O} = \frac{\%H_2O}{100} * 6.1094 * \frac{\left(e^{\frac{17.625 * temp\ c}{temp\ c + 243.04}}\right)}{10}$$

Where “temp c” is the temperature of inflow air in Celsius and is also measured using the BME280 pressure and humidity sensor. This is the same temperature as used in the V_{O_2} calculation.

Oxygen Consumption Calculations and Experimental Design

Oxygen Consumption Grand Calculation

Calculating V_{O_2} at each data point i is not enough to estimate the final V_{O_2} of the whole swim bout. The final V_{O_2} was initially calculated according to the steps outlined in **Appendix B** (the integral method). The integral method is useful in understanding how data from the whole swim can be used to find a grand value theoretically. Nonetheless, a simplified way arises when the equations are carefully examined (to understand this equation refer to **Appendix B**):

$$estimated \%O2_{exercise} = avg \%O2_{exercise} = \frac{\sum_i^N \%O2_{swim\ i}}{N}$$

As such, the estimated $\%O2_{exercise}$ (can also be referred to as $estimatedX_i$) is simply the average of all x_i values collected during the swim. Nonetheless it is important to note that all the corrections discussed above still hold for each data point separately, and therefore each separate VO_2 calculation. As such the following steps were used to find the estimated V_{O_2} for each swim bout:

- 1) Each $\%O2_{swim}$ observed was calibrated, pressure compensated, baselined and humidity corrected to yield the previously derived equation of V_{O_2} :

$$VO2_{STP\ i} = \frac{\left(\frac{20.95\%}{100} - \frac{x_{i,p,b}}{100}\right) * \frac{(P_{atm} - P_{H2O\ in})}{RT_{in}} * F1}{mass\ animals} * \frac{RT_{STP}}{P_{STP}}$$

- 2) The grand V_{O_2} of the swim bout was then calculated as:

$$avgVO2 = \frac{\sum_i^N VO2_{STP\ i}}{N}$$

Where N is the number of data points selected to analyze from the data collected for each swim bout (**Figure 5.2-1**).

Experimental Design

V_{O_2} s from swim where mice were swam in open air cages were estimated. To do this the mice were divided into groups. There were 3 exercise regimes – 120, 180 and 240 minutes/day swimming at 60-, 90- and 120-minute bout durations twice daily. Each exercise regime was composed of a variable number of mice, divided into subgroups of 3 mice. As such, V_{O_2} was measured once in the morning (9am swim) and once in the afternoon (3pm swim) for a group of 3 mice, which differed each day. This way all mice were swam twice daily, and the V_{O_2} of each subgroup (n=3 mice) was recorded in alternating orders to assure V_{O_2} was quantified for each exercise regime.

Total Dose of Exercise Calculations

Total exercise dose was defined as the total volume of O₂ consumed over the course of exercise regime. Because of self regulatory behaviour (i.e variable V_{O₂} values during swim), total exercise dose could not be hypothetically structured (i.e just by external planning of the time swam and proportionally varying the number of days) and was therefore was empirically determined by monitoring O₂ consumption *daily*. Previously, experiments were conducted on mice swam for 6 weeks, twice daily at 90-minute bouts. As such, this group was swam first, and its exercise dose was determined. All other doses were titrated relative to this value (**Figure 2-2**). To do this, V_{O₂} of swim bouts where V_{O₂} was not monitored (and instead mice were swam in regular, open air tanks) (**Figure 2-1**), was instead either interpolated and extrapolated (depending on the swim bout number) from the line of best fit from the swims up to that point in time (**Figure 5.1-8a and 5.1-8b**) for each exercise regime *subgroup* (**Figure 5.1-8c**). Finally, the average V_{O₂} for each exercise regime (120, 180 or 240 minutes/day) was calculated from mean of its *subgroups* (**Figure 5.1-8d**). This was done primarily to assure appropriate swim titration on a daily basis – as it was not possible to quantify V_{O₂} with every swim. To achieve this titration, we had to estimate an average work conducted per swim (measured as volume of O₂ consumed per swim) according to:

$$\text{approximate Work per bout} = VO_2 \text{ estimated} * \text{time}$$

Total exercise dose was calculated using this value (i.e volume of O₂ consumed per swim bout) for each subgroup. Simply:

$$\text{Dose so Far} \left(\frac{\text{mLO}_2}{\text{kg}} \right) = \text{approximate Work per bout} \left(\frac{\text{mLO}_2}{\text{kg swim bout}} \right) * \text{Total Number of Swims Already Swum}$$

Finally, the following quick calculation was completed *daily* in order to accurately titrate swim numbers:

$$\frac{(\text{Required Exercise Dose} - \text{Dose so Far})}{\text{approximate Work Bout}} = \text{number of swims needed}$$

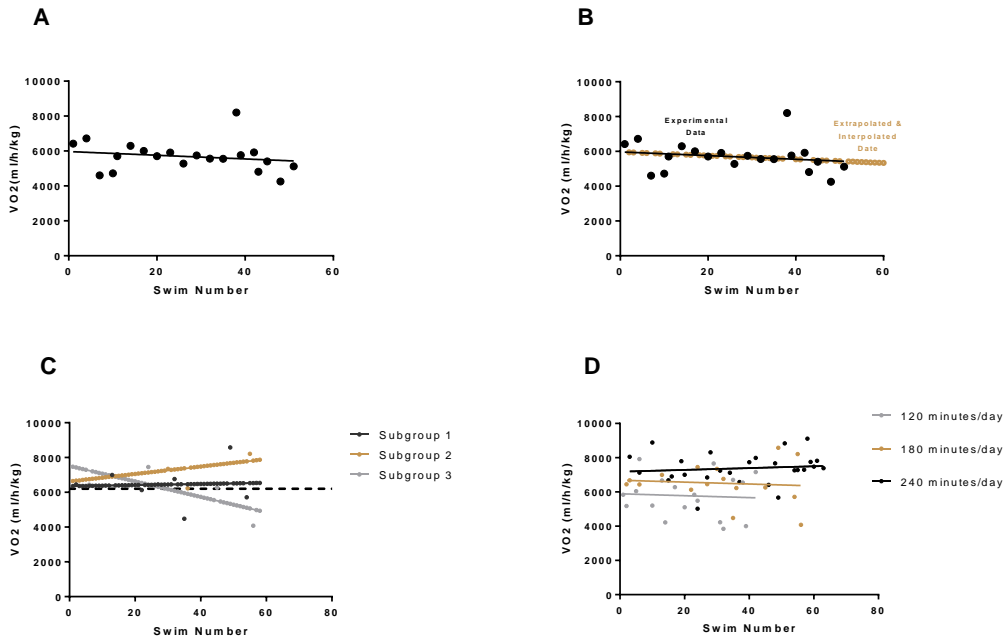


Figure 5.1-8. Oxygen Consumption Raw Data and Data Extrapolation– A) V_{O_2} data was plotted over the course of exercise regime as a function of swim number. The bold line indicates the line of best fit used to calculate interpolated and extrapolated V_{O_2} of bouts where oxygen consumption was not recorded, and mice were swam in open air tanks (seen in B). C) extrapolated and interpolated V_{O_2} data for 4 swim subgroups swimming for 6 weeks, at 60-minute bouts. Average V_{O_2} found from all the subgroups is indicated by the horizontal line. D) average V_{O_2} for each exercise regime group plotted as a function of swim number. For simplicity purposes only measured data is shown, extrapolated and interpolated data was omitted.

Swim bout Dose of O₂ Calculation

Here, we quantified the exercise volume per bout (work per bout) as the amount (volume) of oxygen consumed per swim bout per mass animal. This value was derived from V_{O_2} which has the units of mLs of O₂/kg/min. Simply, for each swim where V_{O_2} was empirically quantified the following calculation was completed:

$$\textit{Work per bout} = V_{O_2} * \textit{time}$$

The average exercise dose per swim per subgroup (n=3 mice) was found by calculating the mean work per bout according to:

$$\textit{mean Work per Bout} = \frac{\sum_z \textit{Work per Bout}}{z}$$

Where z is the number of swims for which V_{O_2} was empirically quantified for each *subgroup*.

Finally, because there were multiple subgroups in each exercise regime, the mean work per bout was calculated from the values of its subgroups for that swim.

5.2 Appendix B - The Integral Method, Theoretical Means of Calculating Oxygen Consumption

Introductory Notes

The integral method was a theoretical framework and therefore was not used to calculate V_{O_2} for each swim. Thus, Appendix C lacks the corrections discussed in **Appendix B**. Nonetheless, it is important to understand how calculations were initially derived from the collected raw data. This method treats %O₂ as a function of time. Here, a hypothetical calculation is completed for a 90-minute swim. Adjustments can be made according to the swim bout length.

The Integral Method

Integrals are areas and the area under a figure with y-axis %O₂ and x-axis of time should have the units of (%time). To find the integral in the data collected here, the sum of all %O₂ was found according to:

$$\sum_i^N \%O_{2_{swim\ i}}$$

where N is the number of points we have selected from our data set as shown in **Figure 5.2-1**.

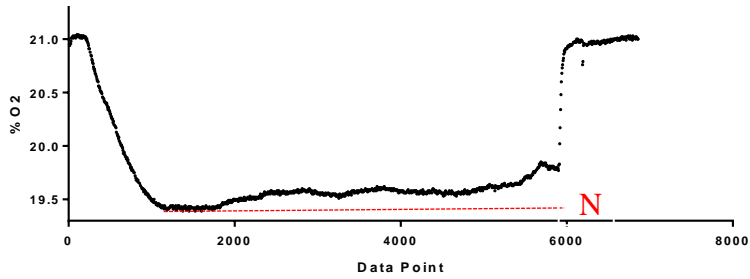


Figure 5.2-1. Raw Data from a Singular 90 Minute Swim – Three (n=3) were swam for a 90-minute swim bout with an inflow rate of 1.0L/min. The data was plotted as %O₂ as a function of data point collected – as data was sampled at a frequency of 1 data point/ 5 seconds. N represents the data points manually selected for V_{O₂} estimation.

To account for the units of time, it is important to understand the frequency of data collection occurs every 5 seconds. Thus:

$$\int Sum\%O_2 = \frac{\sum_i^N \%O_{2_{swim\ i}}}{\left(\frac{1}{5s}\right)} = \sum_i^N \%O_{2_{swim\ i}} * 0.2s$$

$\int Sum\%O_2$ varies with each swim given that

- 1) the number of data points selected (N) for each data set varied, because
- 2) the rate constant for the rate of dilution of atmospheric air with the air within the bucket during swims varied with each swim.

This data was used to estimate the integral that would have been calculated if the whole 90 minute swim bout was measured without any time constant variations – this integral can be

termed $\int_{estimated} Sum\%O_2$. This was done by using the following ratio:

$$\frac{\int Sum\%O_2}{N \times 5 \text{ seconds}} = \frac{\int_{estimated} Sum\%O_2}{5400 \text{ seconds}}$$

For example, because a 90-minute swim contains 5400 seconds. This ratio should be adjusted depending on the swim bout length (i.e for 60 or 120 minutes). This integral can be used to calculate various other parameters as will be discussed now.

- 1) **Total oxygen consumption - $totVO2_{exercise}$.** The total O₂ consumed during swims depends on the content of O₂ in the atmospheric air flowing into the cage - $\%O2_{in}$. The difference between this value and the $\%O2$ registered at exercise gives us a difference of how much oxygen was consumed, in the units of % (**Figure 5.2-2**)

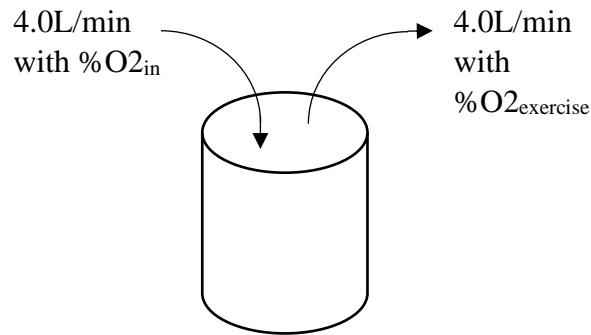


Figure 5.2-2. Hypothetical Framework of Oxygen Content Changes during Exercise – Air flows into the bucket at a constant rate (here, this rate was shown as 4.0L/min as it was the final inflow rate used for experimental purposes). Outflow rate must be theoretically equivalent. The difference in the content of O₂ in the inflow air ($\%O2_{in}$) and the outflow air ($\%O2_{exercise}$) only occurs as the mice swimming consume oxygen for the purposes of oxygen expenditure.

Because $\int_{estimated} Sum\%O2$ includes the sum of all $\%O2_{exercise}$ over the course of a hypothetical 5400 seconds, we need to compare it to the same number of points of $\%O2_{in}$ (i.e over the course of the hypothetical 5400 seconds). We therefore calculate

$\int Sum_{avg} O2_{in} :$

$$\int Sum_{avg} O2_{in} = \%O2_{in} \times 5400seconds$$

Furthermore, this allows conversion of the units of % in %O_{2in} to %time, as in

$\int_{estimated} Sum\%O_2$. Simply, this value represents the area (integral) underneath the

%O₂ data collected from atmospheric air. The total oxygen difference

(*totDO_{2exercise}*) can be found according to the following equation (i.e the area between

%O_{2in} and %O_{2exercise}) (**Figure 5.3-3**):

$$totDO_{2exercise} = \int Sum_{avg} O_{2in} - \int_{estimated} Sum\%O_2$$

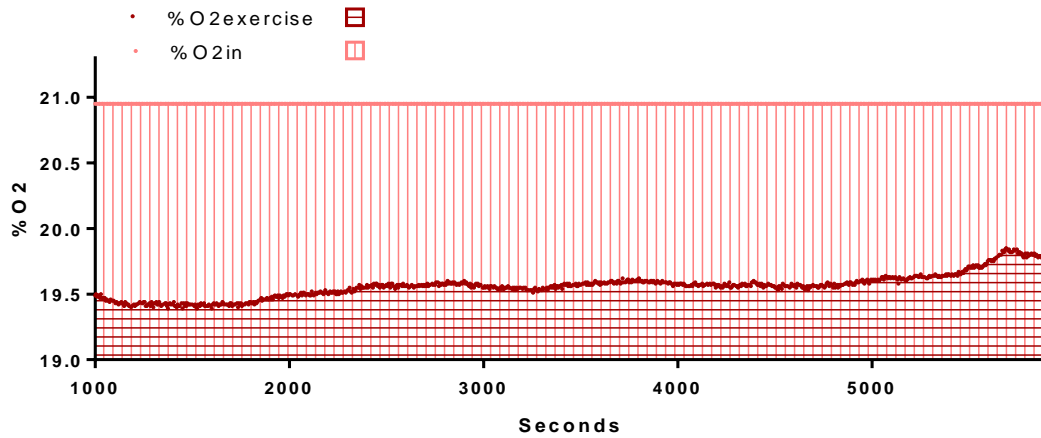


Figure 5.2-3. Oxygen Consumption as an Integral - %O_{2exercise} was plotted only for the values used for V_{O₂} estimation, over time. %O_{2in} was plotted as an estimated value of 20.95%O₂ over the course of the whole swim. The area under each curve is color coded. Note the area with no overlap between the two curves symbolizes the integral difference $\int_0^{5400} Sum_{avg} O_{2in} - \int_0^{5400} estimated Sum\%O_2$ where, the two curves are estimations from the above selected data points.

This value is still an integral with the units of %time and therefore requires conversion to consumed volume of O₂. Given that percentage is really a fraction, *totDO_{2exercise}* was divided by 100. This value was termed *fraction totDO_{2exercise}* and has the units of time. *totVO_{2exercise}* consumed was then calculated using the inflow rate, which gives us

a unit of volume. At this step it is important to make sure the time units of inflow rate and $totDO2_{exercise}$ are the same:

$$totVO2_{exercise} = fraction \cdot totDO2_{exercise} \times F \left(\frac{L}{min} \right)$$

This value is the total volume of oxygen (i.e has units of volume) consumed per a hypothetical 90-minute swim, given the data we have collected for the swim with our system.

- 2) **Calculating oxygen consumption rate - $VO2_{exercise}$.** To find this value the fraction of O2 consumed by the mice ($DO2_{exercise}$) was found.

$\int_{estimated} Sum\%O2$ is an integral and represents the area under a hypothetical 90 minute swim. It has units of time which are not part of $DO2_{exercise}$. Moreover, it represents the total difference in oxygen consumed over the course of 90 minutes, not over the course of 1 data point - as explained in 1). Thus, $\int_{estimated} Sum\%O2$ was converted back to % units and only per 1 data point. $estimated\%O2_{exercise}$ was found according to:

$$estimated\%O2_{exercise} = \frac{\int_{estimated} Sum\%O2}{5400 \text{ seconds}}$$

Shortly, $estimated\%O2_{exercise}$ is actually equal to $avg\%O2_{exercise}$:

$$estimated\%O2_{exercise} = avg\%O2_{exercise} = \frac{\sum_i^N \%O2_{swim\ i}}{N}$$

Assuming that $\%O2_{in}$ is unchanging (room air always contains 20.95%O2) and therefore can be used for a calculation for any data point – whether measured, or in between measured points, $DO2_{exercise}$ is actually equal to:

$$DO2_{exercise} = \%O2_{in} - \text{estimated}\%O2_{exercise}$$

$DO2_{exercise}$ actually has the units of %, and should be converted to a fraction by dividing by 100%. This value can be termed $\text{fraction}DO2_{exercise}$. To find $VO2_{exercise}$, this fraction is converted to units of volume per unit time, per unit mass. This was done by multiplying by the inflow rate and dividing by the mass of the subjects. This $VO2_{exercise}$ is the same value calculate in 3):

$$VO2_{exercise} = \frac{\text{fraction}DO2_{exercise} \times F \left(\frac{L}{min} \right)}{mass}$$

The units of $VO2_{exercise}$ would be mL/h/kg or any other unit conversion.

3) **Exercise Work per Bout.** This value was termed: $totVO2_{per\ minute}$ by:

$$totVO2_{per\ minute} = \frac{totVO2_{exercise}}{minutes\ per\ swim\ bout}$$

To find oxygen consumption ($VO2_{exercise}$) from this, $totVO2_{per\ minute}$ was divided by the mass of the subjects. The units of $VO2_{exercise}$ would be mL/h/kg or any other unit conversion, and is the *equivalent* value to the one calculated in 2).